Finite Element Model of a Two-cell Contact and Separation Experiment

by

Simon Tsui

A thesis
presented to the University of Waterloo
in fulfillment of the
thesis requirement for the degree of
Master of Applied Science
in
Civil Engineering

Waterloo, Ontario, Canada, 2008

Author's Declaration

I hereby declare that I am the sole author of this thesis. This is a true copy of the thesis, including any required final revisions, as accepted by my examiners. I understand that my thesis may be made electronically available to the public.

Simon Tsui

Abstract

Cell-cell adhesion is important to understanding the mechanics of cell-cell interactions. A recent study of cell adhesion was conducted by others using an Atomic Force Microscopy to measure forces when two cells are brought together and then pulled apart. When the two cells come in contact, the adhesion molecules of one cell bind to molecules of the other cell throughout the contact region. When the two cells are then pulled apart, some of these bonds break off while others lead to the formation of tethers which also eventually also break. These phenomena create a force-time curve, which is difficult to interpret.

In order to model this experiment and understand details of the experiments, a series of modules were added to a 2D finite element model used previously to model cells and their mechanical interactions. These new modules were designed to replicate mechanical processes associated with molecular detachments at the cell-cell interface. The enhanced model includes several new types of elements including an InterfaceTruss, which characterizes individual adhesion bonds between two cells.

Parametric studies carried out using the new finite element model showed that cytoplasmic viscosity, actin cortex stiffness, and the lifetime of the molecular attachments at the cell-cell interface all affect one or more portions of the force time curve. The model was able to model virtually all of the significant features of the experimental force-time curve, and when suitable parameter values are chosen, the model closely approximates the observed features of the experimental curves.

The new finite element model provides an effective tool for investigating features of the cell-cell interface. It also provides a powerful tool for learning about the mechanical properties of the cells and their bonds and tethers and for the design of new cell adhesion experiments.

Acknowledgements

To my supervisor, Dr. G. Wayne Brodland, for his time and effort in helping me understand the mechanics and structure of cells. His passion for discovering knowledge has been a profound inspiration on me both in the present and as I look toward the future. This work would not be possible without his support and guidance. I would like to share a quote which is very meaningful to me:

> *"Call to me and I will answer you and tell you great and unsearchable things you do not know" – Jeremiah 33:3*

To my father and mother, my siblings, and all my friends for their support and unsurpassed love. I would like to thank them for believing in whatever paths I chose in my career.

To my colleague Jim Veldhuis, for his software and technical assistance. Without him, this project would not have succeeded.

To my colleagues Paul Groh, Justina Yang, Graham Cranston, Abby Li, Tony Leung, Caleb Horst, Xiaoguang Chen, and Oscar Ariza, for making my Master's program at the University of Waterloo an enjoyable and exciting experience.

Finally, special thanks to my friend Ivan Lee.

Table of Contents

List of Figures

List of Tables

Chapter 1 Introduction

1.1 Cell Mechanics

Mechanical interactions between cells are of fundamental importance to embryogenesis, cancer metastases, and tissue engineering (Bell, 1978; Ward, 1995; Evans, 1995). A variety of experimental techniques are available to study these interactions (Evans, 1991; Raucher, 1999; Sun, 2005; Krieg, 2008).

Here, focus is given to experiments in which two cells are brought in contact with each other and are then pulled apart. In experiments carried out by others (Puech, 2005), an Atomic Force Microscope (AFM) is used as a force spectroscopy to measure force-displacement relationships, making it possible to observe the time-dependent dynamic behaviours of the molecular interactions at the cell-cell interface. Figure 1.1 presents the layout of an adhesion experiment.
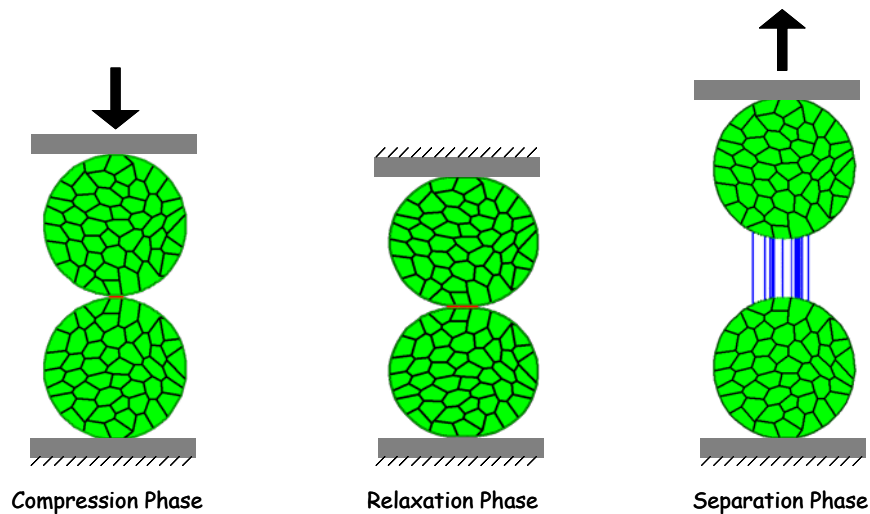
Figure 1.1 – Atomic Force Microscopy Adhesion Experiment

When the two cells approach each other, the receptors on the cell surface will stochastically link to the ligands on the surface of the other cell, creating a network of attachment bonds across the cell-cell interface. As the cells are separated, individual or a group of molecular attachments at the cell-cell interface layer must be broken. Some of these bonds give rise to

formation of tethers. Figure 1.2 shows a force-time curve from a typical contact and separation experiment. The curve has many complex features and it is difficult to interpret them (Bell, 1978) without a suitable computational model.
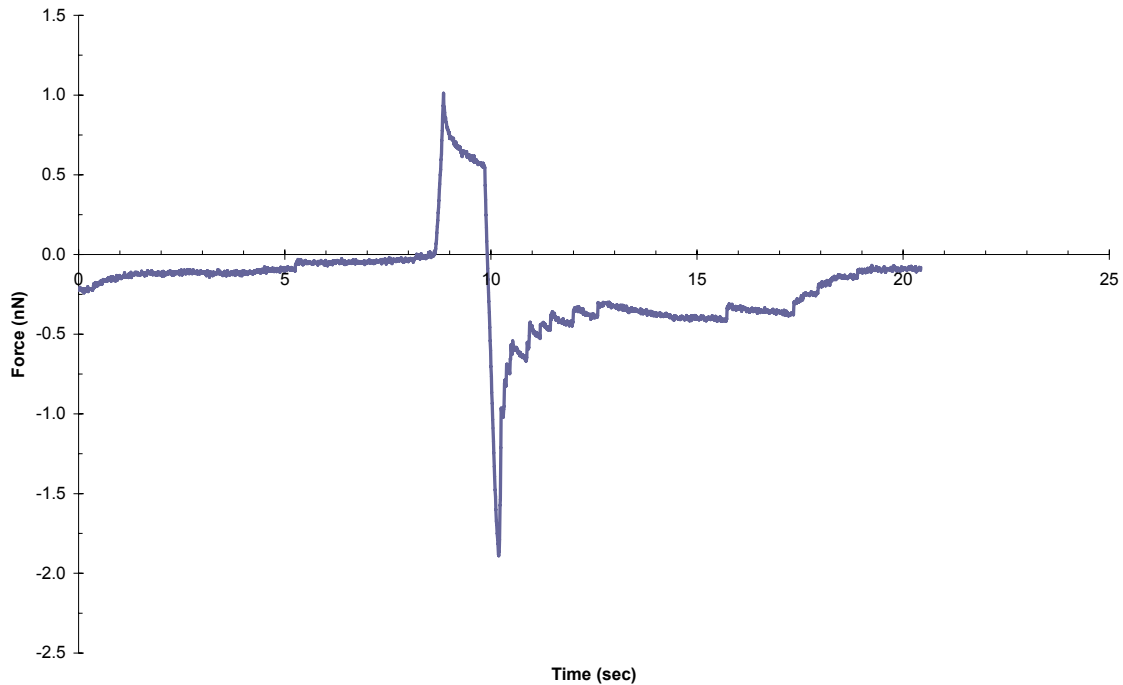
Figure 1.2 – AFM Experimental Force-Time Curve

In this thesis, a new FE model is developed and used to investigate the following questions:

1) Can a finite element (FE) model explain the significant features of the force-displacement curves?

2) What are the key physical components and mechanical properties of the two-cell system that give the force-displacement curves its general shape?

3) How do the curves change when specific parameters are adjusted?

4) Can specific experimental curves be matched by choosing suitable parameter values?

The answers to these questions will lead to a more fundamental understanding of the cell-cell adhesion system. Also, a computer model would enable scientists to simulate and make predictions about what would actually happen to the system when subject to changes. Finally, the FE model can be used to improve the design of future laboratory experiments.

1.2 The Importance of Cell-Cell Interactions

Cell-cell adhesion is a crucial driving mechanism for the construction and maintenance of multi-cellular structures (Evans, 1995). These complex processes are associated with the tethering of cells, cell-cell communication, tissue formation, as well as cell migration (Puech et al., 2006). In many situations, it also influences other cellular processes during the development of mature tissues in an embryo (Ruoslahti, 1996). Some of these processes are proliferation, differentiation, and apoptosis.

The formation of an embryo begins with a single original cell called the fertilized egg (Alberts, 1989). Within several hours after fertilization, this single cell would undergo cleavage, subdividing itself into smaller blastomere cells by repeated mitosis. In the gastrulation stage, the adhesion and detachment of the physical bonds and interfacial tension on these blastomeres would initiate cell migration, forming and assembling the blastomeres into distinct germ layers. These germ layers provide a base for the formation of certain bodily systems.

Therefore, the study of cell-cell adhesions and interactions would lead to an improved understanding in the cause of failure in embryo development. In doing so, this study can help advance the fields of tissue reconstruction, treatment for cancer metastases and other diseases, and prevention of congenital malformation.

1.3 Approach

To address the questions in Section 1.1, it is imperative to analyze the mechanics of the cell using a reverse-engineering approach. Experimental data has provided the forces needed to deform the two-cell system in a certain way, yet the internal driving mechanisms and interactions of the different components remain unknown. With the growth of advanced computer technology and engineering analysis tools, FE analysis was proposed to approach this particular problem.

A computer finite element (FE) model was developed to simulate the actual AFM experiments. With the availability of geometric data and other information regarding the experiments, realistic computer simulations can be carried out. These simulations then provide force-time curves, which can be compared to experimental results.

Changing the governing parameters within the FE model affects the shape of the force-time curves. Thus, if given a FE model that correctly represents the two-cell system, a set of parameters should exist such that the simulated curves closely match the experimental curves. Using these parameters and their corresponding force-time curves, one can then answer the important questions about the mechanical properties of the cells and their cell-cell interface.

1.4 Main Results

This study showed that finite element modeling is an effective way to investigate the mechanical properties of the cell and their tethers. For the first time, the cell-cell interface was studied using non-linear finite element analysis. The computer simulations explained the significant details in the force-time curves, and provided estimations for the parameters that govern these curves for the actual cell adhesion experiments.

The model shows that parameters such as surface tension, cytoplasmic viscosity, actin cortex stiffness, and the lifetime of the molecular attachments at the cell-cell interface significantly affect the shape of the force-time curves. Finally, the algorithm for the rupture of adhesion

bonds along with the existing finite element model can provide new insights and assistance to researchers for their design of future cell adhesion experiments.

Chapter 2 Cell Structure

2.1 Cell Micromechanics

All living creatures are made up of small membrane-bounded vesicles, called cells, filled with a concentrated aqueous solution of chemicals (Alberts, 1989). Cells have typical dimensions of 10-20µm. Each of these vesicles is formed by a sophisticated system of internal sub-cellular structures and peripheral components, which gives the cells their mechanical properties and functions. These components often interact with each other to perform cellular processes, some of which are specifically for embryo morphogenesis. Figure 2.1 illustrates some major sub-cellular structures found in a cell.
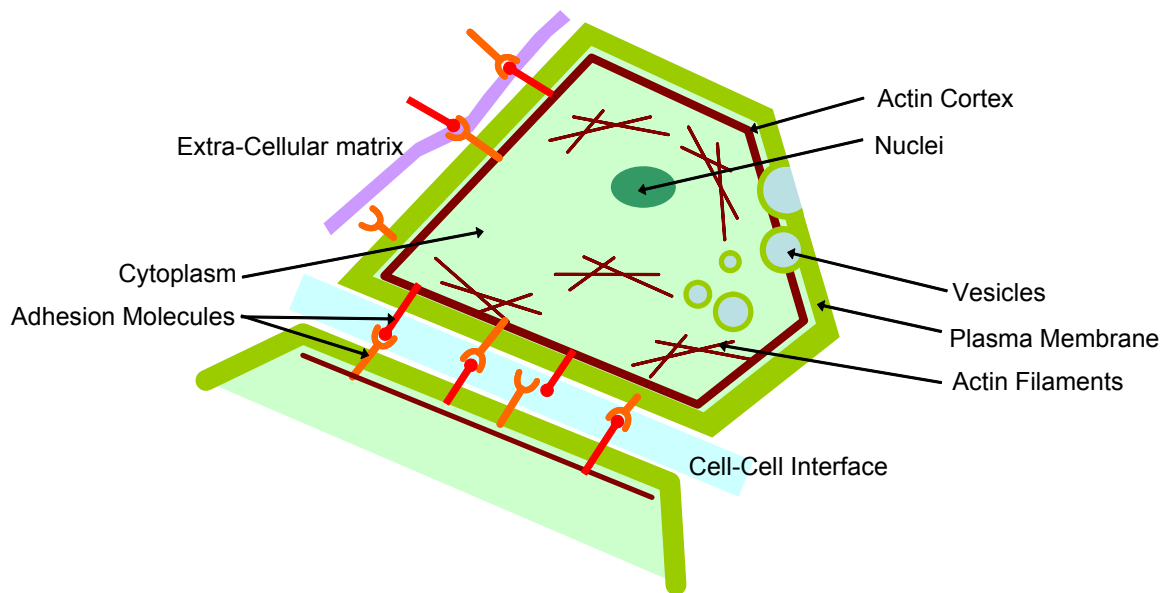
Figure 2.1 – Sub-cellular Components and Cell Structure

These complex systems contain: the plasma membrane, membrane proteins, the cytoplasm, networks of filaments in the cytoskeleton and the actin cortex, and multiple junctions and subsystems of cell-cell adhesion molecules located on the plasma membrane. Interactions of these components and systems give rise to complex mechanical responses, which have not been fully studied. Although many adhesion experiments have been done in the past, they

primarily focused on only one or several of these adhesion subsystems, isolating all other factors. A good example would be measuring the pulling force of a single molecular-point attachment between two macroscopically smooth-membrane capsules (Evans, 1991).

Recent studies have been done to measure the mechanical properties of these cell structures. For example, the rupture force of a single membrane tether and the viscosity of the cytosol in white blood cells (Sheetz, 1999; Zhu, 2000). Before looking in depth at the cell's structural system and the adhesion system, it is necessary to study each sub-structure of the cell individually.

2.2 Plasma Membrane

The cell's plasma membrane is a two-layered structure that encloses the cell's cytoplasmic components. Not only does the plasma membrane act as a selective impermeable barrier against the external environment, it also gives the cell its shape (Alberts, 1989). Each of the two layers is made up of phospholipid molecules, along with dissolved protein molecules that mediate biological processes. Figure 2.2 shows the structure of the plasma membrane.
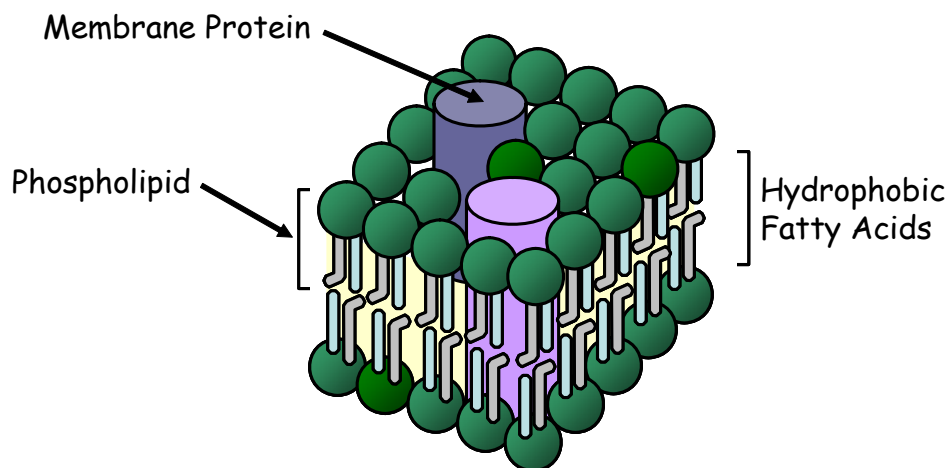
Figure 2.2 – Three-dimensional Representation of the Plasma Membrane

Each phospholipid contains a hydrophilic head group and two hydrophobic fatty-acid tails. The amphipathic nature of these molecules causes the bi-layers to be arranged in such a way

that both surfaces of the plasma membrane are the hydrophilic head group. Another property of the phospholipids is that they can exchange places with their neighbour laterally at high diffusion rates, enabling the lipid layers to reseal itself if torn and permitting some membrane proteins to diffuse across the membrane if necessary.

The total surface area of the plasma membrane is approximately 1000μm² (Sun, 2005). Depending on the excess of membrane in the membrane reservoir, the area can be subject to changes. Modification to the membrane area is by means of unfolding parts of the membrane folds (Raucher, 1999), or by membrane transport processes such as exocytosis and endocytosis. Exocytosis is the process where vesicles in the cell fuse with the membrane, releasing particles to the extra-cellular space. Endosytosis is the process where parts of the plasma membrane enclose substances in the extra-cellular space, and pinch off into the cytoplasm. Therefore, membrane is added to the plasma membrane by endocytosis, and subtracted by exocytosis. The size of the reservoir is also vital to the number of membrane tethers that could be formed during the separation phase of the two-cell adhesion experiment.

Since the plasma membrane holds the cytoplasmic fluid and the filament networks inside it, these components exert an internal pressure on the plasma membrane and create a surface tension on the membrane. This surface tension, namely the membrane tension, is one of the contractile forces that drive morphogenetic processes (Brodland, 2002). In addition to direct contributions to the net interfacial tension, the membrane also acts as an embedment for the adhesion molecules that link to external mechanisms. These external mechanisms are can also exert an adhesive force on the membrane, reducing interfacial tensions.

2.3 Membrane Proteins

Membrane proteins are organic compounds that are associated with the cell's plasma membrane. They made up approximately 50% of the plasma's membrane total mass, and they carry out specific functions of the biological membrane, including cell signalling and cell adhesion. For example, some glycoproteins are mediators for the binding of cells (Evans, 1995). Membrane proteins also provide linkage to the oligosaccharides chains at the

extracellular side of the membrane that covers the cell, namely, the glycocalyx cell coat (Alberts, 1989).

There are five ways in which membrane proteins can associate with the lipid bilayer: 1) transmembrane protein that extend across the bi-layer as a single α-helix or multiple passes of α-helix; 2) transmembrane protein with a covalently attached fatty acid chain inserted into the cytoplasmic monolayer; 3) attached solely by a covalently attached fatty acid chain into the cytoplasmic monolayer; 4) attached via oligosaccharides to minor phospholipids at the outer monolayer, and 5) non-covalent attachment to another membrane protein (Alberts, 1989). Figure 2.3 shows the five ways in which membrane proteins are associated with the plasma membrane.
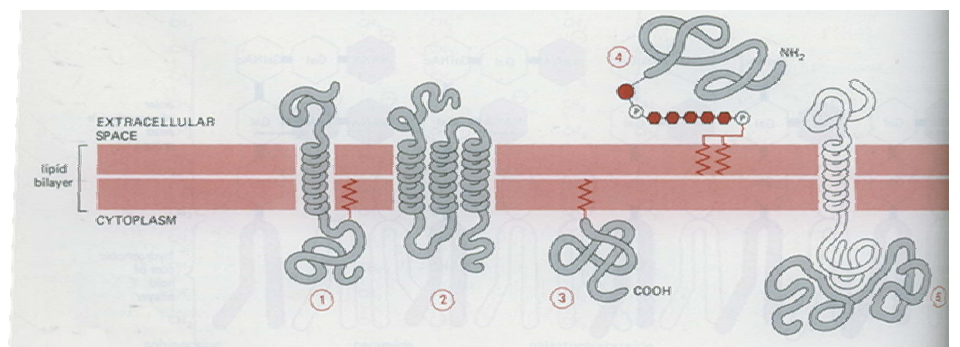
Figure 2.3 – Association of Membrane Proteins with the Plasma Membrane (from Alberts, 1989)

An example of a membrane protein is the spectrin protein, located on the intracellular side of the membrane. Spectrin proteins form a structural network adjacent to the membrane, maintaining the structural integrity and bioconcave shape of the cell. Furthermore, this meshwork anchors itself to the plasma membrane through ankryn and "Band 3" membrane proteins, and connects itself to the actin proteins of the cytoskeleton. Figure 2.4 shows a schematic drawing of the spectrin cytoskeleton network.
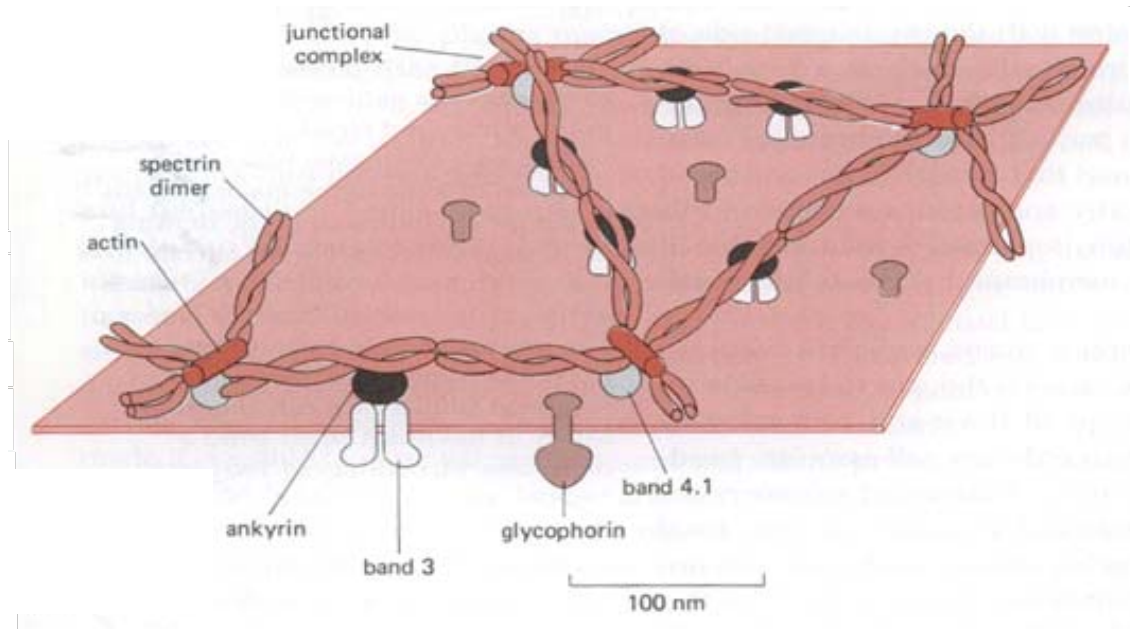
Figure 2.4 – Spectrin Structural Network and Components (from Alberts, 1989)

2.4 Cytoplasm

The cytoplasm of the cell is all of the elements bounded by the plasma membrane, excluding the nucleus. There are three major elements in the cytoplasm: the cytosol, the organelles, and the inclusions. Cytosol is the fluid which fills up the space between the organelles within the cytoplasm (Alberts, 1989). The cytoplasm is comprised of mainly water and molecules, and accounts for approximately 50% of the cell's total volume. The cytoplasm is also the site for cellular activities such as protein synthesis.

Furthermore, the cytoplasm houses the cytoskeleton of the cell, providing the cell its viscoelastic behaviour. Previously, methods have been introduced to measure the bulk viscosity of the cytoplasm. For example, total internal reflection-flourescence recovery after photobleaching (TIR-FRAP) was previously applied to measure solute translational diffusion in membrane-adjacent cytoplasm (Swaminathan et al., 1996). In that study, Swaminathan found that the dense network of the cytoskeleton near the plasma membrane significantly retards the translational diffusion of solute. From his result, it was found that the cell viscosity near the cytoplasmic membrane is 6-10 times greater than the viscosity of water.

2.5 Cytoskeleton and the Cell Cortex

The cytoskeleton is a structural framework that enables a cell to adopt a variety of shapes. It also allows the cell to carry out coordinated movements, such as in morphogenesis. Diverse activities of the cytoskeleton are mainly dependent on three principle types of protein filaments: 1) Actin Filament, 2) Microtubules, and 3) Intermediate Filaments. Figure 2.5 shows a freeze-etch electron micrograph of an intestinal epithelial cell.
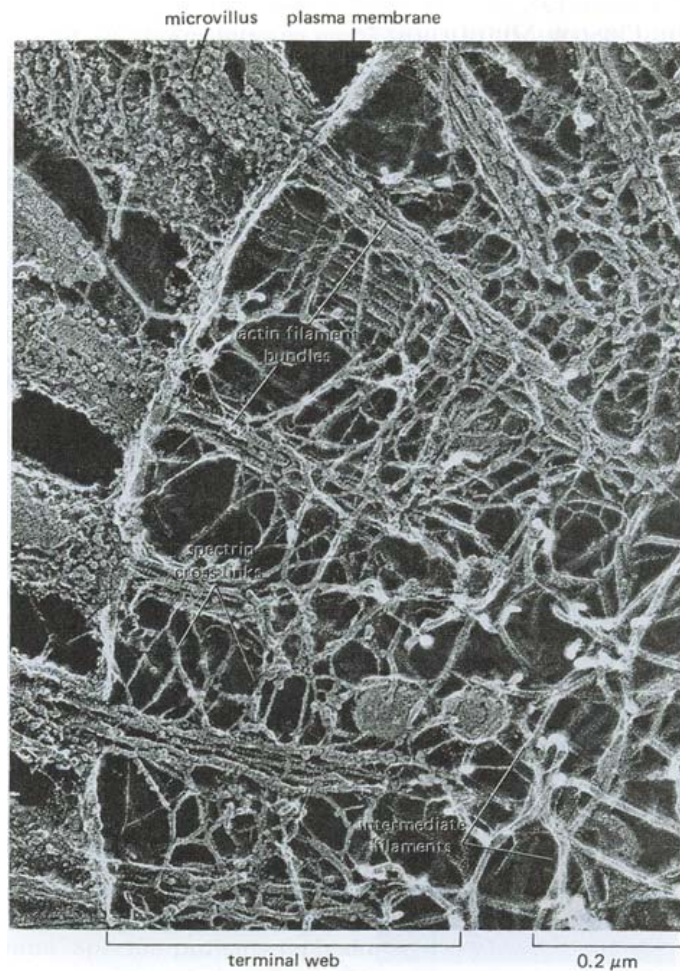
Figure 2.5 – The Cytoskeleton (from Alberts, 1989)

Actin filaments are most abundant protein found in eukaryotic cells. They are approximately 8nm in diameter. These actin filaments constitute about 5% of the total proteins found in cell and are distributed throughout the cytoplasm. Actin filaments are formed by individual actin

monomers. When energy is provided by Adenosine Tri-Phosphate (ATP) hydrolysis, these monomers can form the chains of actin filaments, a process called polymerization (Alberts, 1989). Polymerization and de-polymerization of the actin filament chains enables themselves to retract and extend, and thus play an important role in the reshaping of the cell.

Two filaments can be linked together by cross-linking proteins called filamin. With these filamins, actin filaments form a dense network called the cell cortex, just beneath the plasma membrane. The viscoelastic nature of the actin cortex gives the cell mechanical strength against external loads as well as enabling the cell to change shape and migrate. These filaments also allow cell-surface extension and anchor the organelles in place.

Unlike the actin filaments, the microtubules usually exist as single filaments. They are tubular structures formed by tubulin molecules, with a diameter of approximately 25 nm. They are spread out throughout the cytoplasm from a position near the nucleus. Due to their combination of α-tubulin and β-tubulin, microtubules induce a polarity to the cell, providing instructions and directions for cell division and migration.

Finally, the intermediate filaments are tough durable protein fibres in the cytoplasm that are approximately 8-10 nm in diameter. Together they form a network of overlapping arrays, which results in high tensile strength (Alberts, 1989). Their primary function is to provide mechanical support and structural integrity of the cell and the nucleus. Moreover, they resist the compression loads that are exerted on the microtubules.

2.6 Intracellular Junctions

Multi-cellular animals are composed of cooperative assemblies of various tissues. Subsequently, these tissues are combinations of the extracellular matrix (ECM) and cells. ECM is a complex network of secreted extracellular macromolecules that provides important functions, such as a structural support for cells in tissues. In places where these elements contact, junctions are formed for specific functions. These junctions could either be intercellular junction, regions of the plasma membrane where cells are directly contacting

with neighbouring cells, or cell-matrix junction, regions of the plasma membrane where the cell attaches to the ECM. Intracellular junctions are classified into 3 functional groups: 1) occluding or tight junctions; 2) communicating or gap junctions; and 3) anchoring junctions. Figure 2.6 shows a graphical representation of these three types of junctions in an epithelial cell sheet.
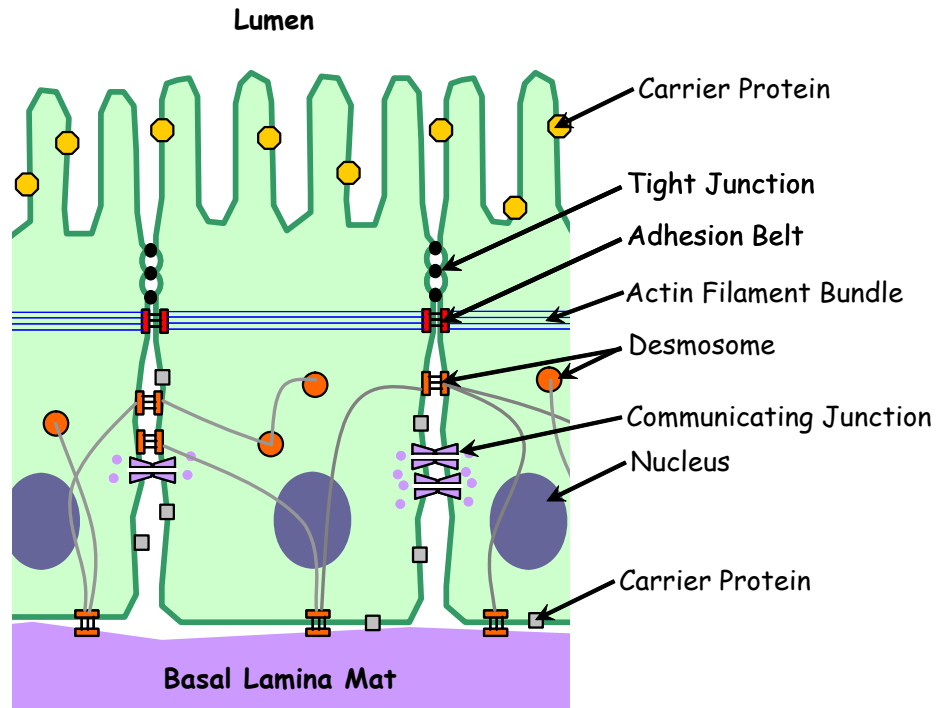
Figure 2.6 – Cell Junctions in Epithelial Cell Sheet (After Alberts, 1989)

Occluding junctions can be found in both surfaces of the epithelial cell sheet. Their primary functions are to act as a selective permeability barriers against water-soluble molecules and to block membrane-bound carrier proteins from migrating between the apical and the basolateral surfaces. Communicating junctions are constructed by transmembrane proteins called connexon. Two connexons would connect at the junction, and leave a 3 nm wide gap between the two cell surfaces. Its primary function is to allow inorganic ions and small intracellular signalling molecules to freely pass between cells. They also play an important role in embryogenesis, where they coordinate the coupling and decoupling of different cells types.

Anchoring junctions are structural units that link the cytoskeletal elements in a cell to those of the neighbouring cells or to the ECM. Anchoring junctions are composed of two classes of proteins: 1) the intracellular attachment protein, which connect junctional complex to cytoskeletal elements; and 2) the transmembrane linker proteins, which bind intracellular attachment proteins to the extracellular domain of other linker glycoproteins.

One example of anchoring junctions is the desmosomes, a structure specialized for cell-cell adhesions. Demosomes are intercellular contacts that rivet cells together. They also provide anchoring sites for a type of intermediate filaments called keratin. Figure 2.7 shows the connections of the components in a desmosome complex.
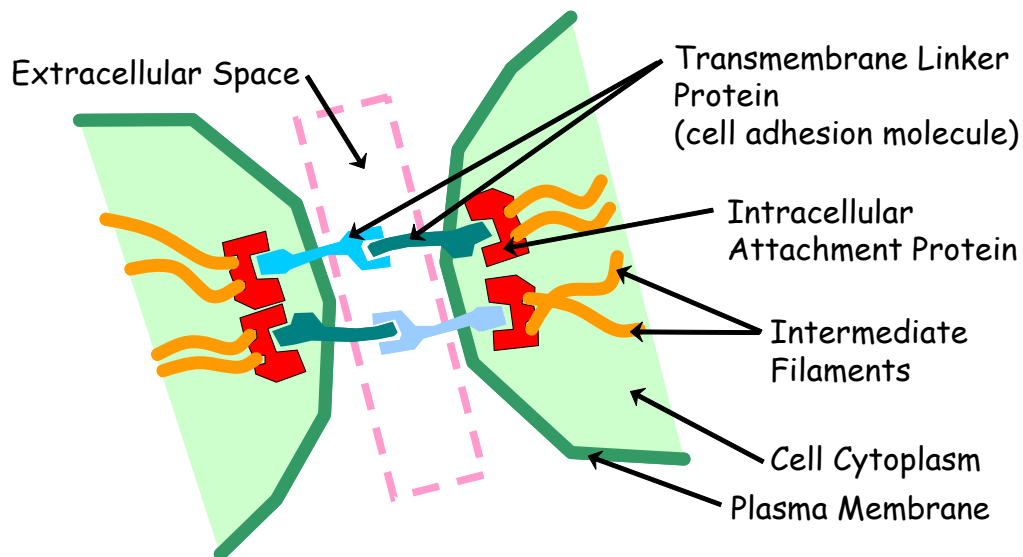
Figure 2.7 – Receptor-Ligand Connection of Desmosome Complex

In the extracellular space, cadherin adhesion protein links the adhesion molecule on the other cell to the intracellular attachment protein inside the cell. The intracellular attachment protein subsequently provides an attachment for the filaments. Together, they form a structural network which provides tensile strength to the cytoplasm.

2.7 Cell Adhesion Molecules

Cells within aggregates and tissues do not move independently. Rather, their displacements and deformations depend on complex interactions of cell adhesion molecules and tissue properties, such as cell-cell adhesion (Rieu, 2000). For example, migration of cells either as a coherent group or as individual is controlled by the attachment strength of the cell adhesion molecules (Evans, 1995). Cell adhesion molecules (CAM) are transmembrane proteins that could be found on the cell surface. Acting as ligands and receptors, they enable themselves to bind to other proteins and molecules on neighbouring cell.

CAMs can classified into four groups: 1) integrin, which are membrane glycoproteins that bind the cell to the ECM; 2) selectins, which are calcium-dependent membrane proteins found only in circulating cells and endothelium; 3) immunogoblin (Ig) family, which are plasma membrane glycoproteins for cell-cell adhesion; and 4) cadherin, which are cell-surface glycoproteins that are involved in Ca2+ dependent cell-cell adhesion found in developing tissues of vertebrates.

These adhesion proteins could exhibit one of two binding modes: homophilic and heterophilic. Cadherin and Ig family molecules are of homophilic self-association mode, and bind to other molecules of the same type. In contrast, integrin and selectins are of heterophilic mode, binding themselves to CAMs of another type (Alberts, 1989). The distinction between the two different modes is somewhat arbitrary. An example would be that integrin can bind to the fibronectin fibres in the ECM, yet it can also serve as a ligand, mediating cell-cell adhesion. Besides these two binding mechanisms, CAMs could also bind together by multivalent linker molecules within the extracellular space. Figure 2.8 shows the three mechanisms in which cell adhesion molecules could bind.
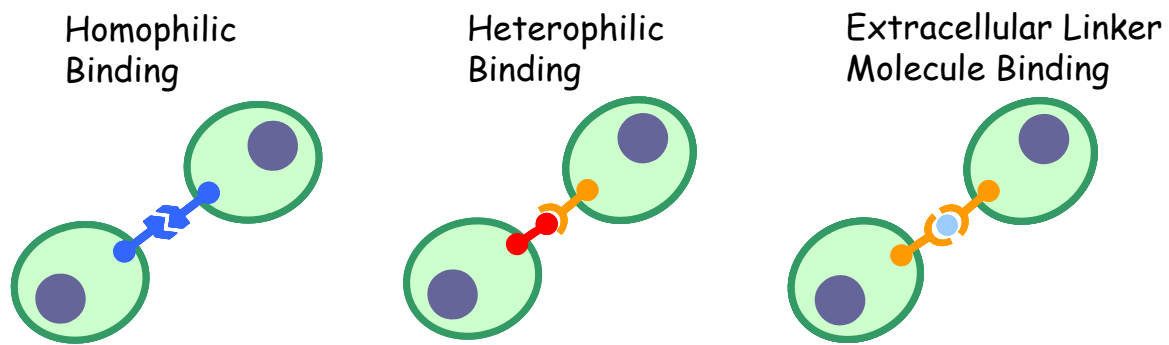
Figure 2.8 – Three Types of Binding Mechanisms (After Alberts, 1989)

Not only do these proteins have different binding modes, they also attach to the cell by different mechanisms. Cadherin and integrin proteins are associated with the actin filament system, connecting to the cytoskeleton of the cell (Evans, 1995). However, Ig family molecules are only linked to the cell membrane, mediating weaker adhesive interactions. Strong adhesion molecules serve as connected plaques, whereas weaker adhesion molecules serve as fine-tuning devices, respectively. Together, they coordinate the movements in cell migration (Alberts, 1989).

Adhesive strength is also dependent on the lifetime of the bond (Ohmori, 1986 and Krieg, 2008). Experiments showed that as contact time increases, formed bonds become more likely to dissociate (Zhu, 2000). However, as this probability of bonds dissociation increases, equilibrium will eventually be reached and this probability will balance the opportunity for new bonds to form. As such, the adhesion probability of the cells will approach equilibrium in time, as shown in Figure 2.9.
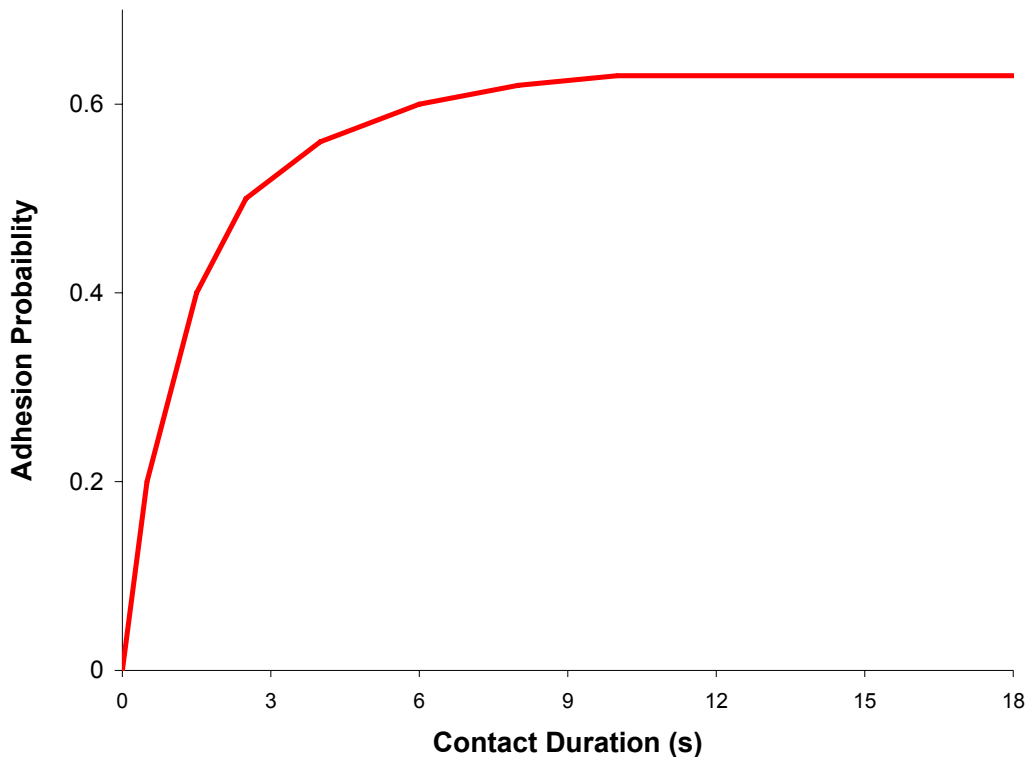
Figure 2.9 – Plot of Adhesion Probability versus Contact Duration (After Zhu, 2000)

Once two cells are in contact, the adhesion molecules on the surface of both cells bind to each other, forming a contact region on the cell-cell interface. The contact region is approximately 10-100 nm thick, which is estimated from the receptor-ligand bond length (Ward, 1995). The likelihood for a bond to form in the interface is partly affected by the position of the molecules on the surface, as well as the diffusive rate for these molecules to become close to each other for binding (Bell, 1978). Mechanically speaking, bonds can be unbound at two specific locations: at the binding site in the extracellular space, or in the cytoplasm where the molecule attaches to the cytoskeletal elements (Evans, 1991).

2.8 Membrane Reservoir and Tether

As mentioned in earlier sections, the plasma membrane contains a membrane reservoir that can provide the cell with additional membranes. During morphological events, the cell may

experience rapid osmotic pressure changes, causing the plasma membrane to stretch and result in high tensile stress. Since the maximum elastic stretching is only about 4% (Raucher, 1999), it is important for the cell to have a membrane reservoir, which regulates the membrane tension. Recently, membrane reservoir was studied in AFM tether length experiments, as shown in Figure 2.10.
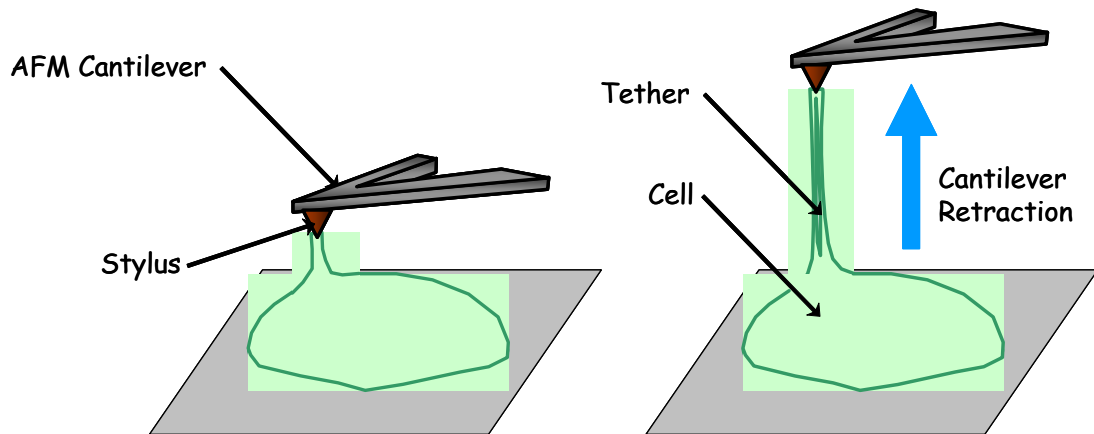
Figure 2.10 – Tether Length Experiment

In a typical tether length experiment, a cell is placed on top of a glass cover slip, inside a petri dish. The AFM cantilever is lowered until the stylus of the cantilever touches the cell and maintains contact with the membrane for a time period. With the cell surface still attached to the stylus, the cantilever pulls the membrane upward, forming multiple membrane tubes called tethers between the cell and the AFM cantilever. As the cantilever continues to retract, these membrane tubes begins to rupture, recycling themselves back to the membrane reservoir for the elongation of the remaining tubes (Sun, 2005). Once all the tethers are ruptured, the tether lengths can be used to estimate the size of the membrane reservoir (Sun, 2005). From these experiments, it was found that the actual membrane area extracted to form tethers was approximately 3-10 μm^2, compared to ~1000 μm^2 of plasma membrane in a typical cell (Raucher, 1999).

Tethers are hollow tubular structures composed of the phospholipid bi-layer, as shown in Figure 2.11. These nano-tubes are highly viscous and ductile and can withstand large

elongation prior to rupture. The formation of tethers begins with the decoupling of the adhesion bond from the cytoskeleton when a certain force is reached. Meanwhile, the transmembrane linker proteins from both cells remain linked in the extracellular space, and portions of the plasma membrane is extracted, forming the tether tubes, as shown in Figure 2.11.
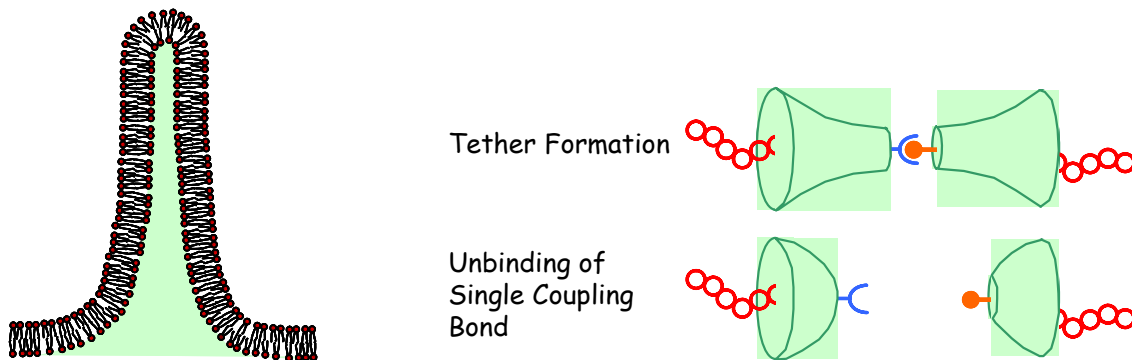
Figure 2.11 – Extraction of Tether and Bond Dissociation

Experiments have shown that tethers are approximately 0.2 μm wide in diameter (Hochmuth, 1996), and their maximum tether length can range from 5 μm to 10 μm depending on the speed of pulling. The pulling speed also affects the probability of tether forming (Heinrich, 2005). For example, the slower the pulling speed, the less likely a tether would form between the cell interfaces. Moreover, AFM experiments have also shown that tethers begin to rupture when they have reached a certain length or there is a depletion in the membrane reservoir (Sun, 2005). However, the mechanical behaviours of tethers are not well understood. For example, some theories suggest that tethers behave as visco-elastic materials (Schmitz, 2007), while others thought tethers as visco-plastic membrane tubes (Evans, 1976).

Chapter 3 Experiments and Mechanical Models for Living Cells

3.1 Cell-Cell Adhesion Experiments

Biological functions and processes are governed by the mechanical properties and interactions of cellular components. Some of these properties and interactions have been studied through adhesion experiments both qualitatively and quantitatively, such as in micropipette manipulator experiments (Evans, 1991) and in atomic force microscopy experiments (Krieg, 2008). These experimental results and observations provided significant insights for the development of a finite element model for the cell-cell interface.

3.2 Micropipette Manipulator

In Evan's experiment, two red blood cells were manoeuvred by micropipettes. Figure 3.1 shows the sequence of the assembly and detachment of red bloods cells. The micropipettes exert suction to the red blood cells, holding the cell in position. The pipettes further pressurize the cell membrane, controlling their bending rigidity and stiffness (Evans, 1991). As the micropipettes assemble or separate the cell capsule, a video recorder captures the geometry of the cells in real time, and the pipette pressure is recorded. This raw data is then used to calculate the force required to rupture the molecular attachments at the interface.
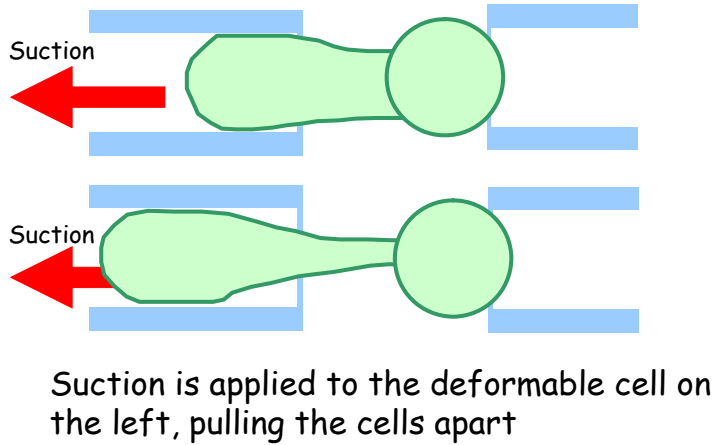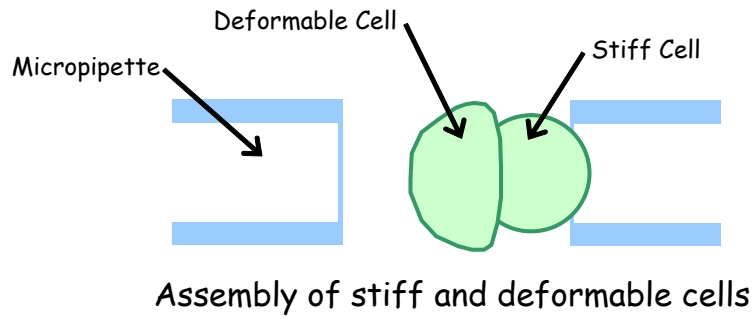
Figure 3.1 – Experimental Set-up for Micropipette Experiment (Evans, 1991)

Evans observed the rapid detachment force is not a single value. Rather, the rupture force is based on a probability distribution dependent on the contact duration (Evans, 1991). Evans measured these forces for different agglutinin adhesion molecules, which are summarized in Table 3.1. The rapid detachment forces were found to be ~20 pN.

Table 3.1 – Force for rapid detachment of different agglutinin (Evans, 1991)

Agglutinin	Average Force (pN)	Standard Deviation (pN)
Anti-A Serum	20	± 7
HPA	20	± 8
R10 MAb	21	± 10

Based on the captured images, Evans concluded that when pushing the cells together, large flat contact regions will form between the cells. The contact region contains the adhesion bonds, which are the rupture sites for cell detachment (Evans, 1991). Evans also suggested that the tension force needed to separate the cells and reduce the contact is not constant throughout the experiment. The force increases linearly as the cells separate, until a critical tension force is reached. Moreover, Evan's experiments further led to a significant finding of tether formation, which is crucial to the study of the cell-cell interface.

3.3 Atomic Force Microscopy

Recently, cell-cell adhesion and other functions of biological molecules have been studied by atomic force microscopy (AFM). AFM is not an instrument for viewing objects like an ordinary optical microscope. Instead, AFM scans a biological specimen by contacting its surface with a stylus probe, and then reconstructs a topographic image of that specimen (Engel, 2008).

Besides being a high-resolution imaging device for biological specimen, the AFM can be used in force spectroscopy, such as recording force-displacement curves in adhesion experiments and measuring the dynamic viscoelastic properties of bio-molecules (Engel, 2008). Recently, AFM was used to quantitatively measure the adhesion properties of a single cell, such as the adhesion properties of primary gastrulating cells from zebrafish embryo and other coated substrates. Examples include measuring the pulling force for the formations of multiple membrane tethers in a single cell (Sun, 2005).

AFM is a powerful application in studying biological processes because it captures images in real time, as much as 200 images per second. In addition, during experiments, the setup of the AFM device allows specimens to remain in its in vivo environments, permitting the study of live specimens. Figure 3.2 shows a schematic of the AFM microscope.
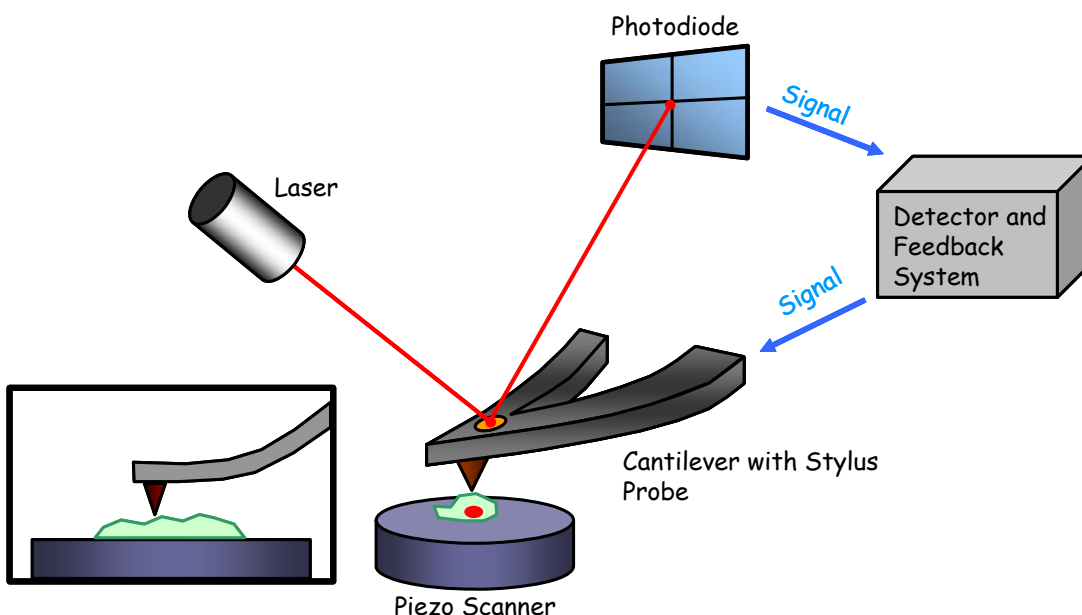
Figure 3.2 – AFM Instrument Components and Imaging Set-up

Other research has been done using AFM. In earlier studies, diffusion of single membrane proteins within an assembly of membrane proteins was observed using AFM imaging, providing new insights as to how bio-molecular interaction drives proteins to move across the membrane and assemble (Mueller, 2003). Recently, the unfolding of a single protein was analyzed with an AFM nanotweezer, by observing the folding steps and kinetics of a single membrane protein (Engel, 2008).

Besides the biochemical processes and structure of membrane protein studies, AFM was also used to study the plasma membrane, such as the formation of tethers in blebbing cells (Dai, 1999). Raucher also studied the effects of membrane reservoir on membrane tension using AFM (Raucher, 1999). Yet, questions as to how membrane tension affects the cell's total surface area and volume, and what are the intermediate steps and mechanisms associated the increased membrane area are still not well understood (Dai, 1998).

Another study done by AFM involved measuring the adhesion and cell-cortex tension of germ-layer progenitors. The study concluded that cell adhesion and membrane tension

correlate with the sorting of germ-layer during gastrulation (Krieg, 2008). However, it is yet to be determined whether other factors, such as directed cell migration and extracellular matrix disposition, are involved. Furthermore, in the study of integrin-mediated adhesion to collagen, rupture forces for single-integrin-collagenbonds are measured by AFM. Nevertheless, adhesion molecules tend to form groups of cooperatively binding clusters that yield larger detachment forces. From these AFM experiments, no conclusion can be made concerning the number of adhesive bonds within the receptor complexes (Taubenberger, 2007).

3.4 Two-Cell AFM Adhesion Experiments

The two-cell pressing and retracting experiments associated with this thesis are discussed in this section. Zebrafish blastoderm cells of ~20 μm in diameter were used in the experiments. Figure 3.3 shows the diagram of the experiment procedure.
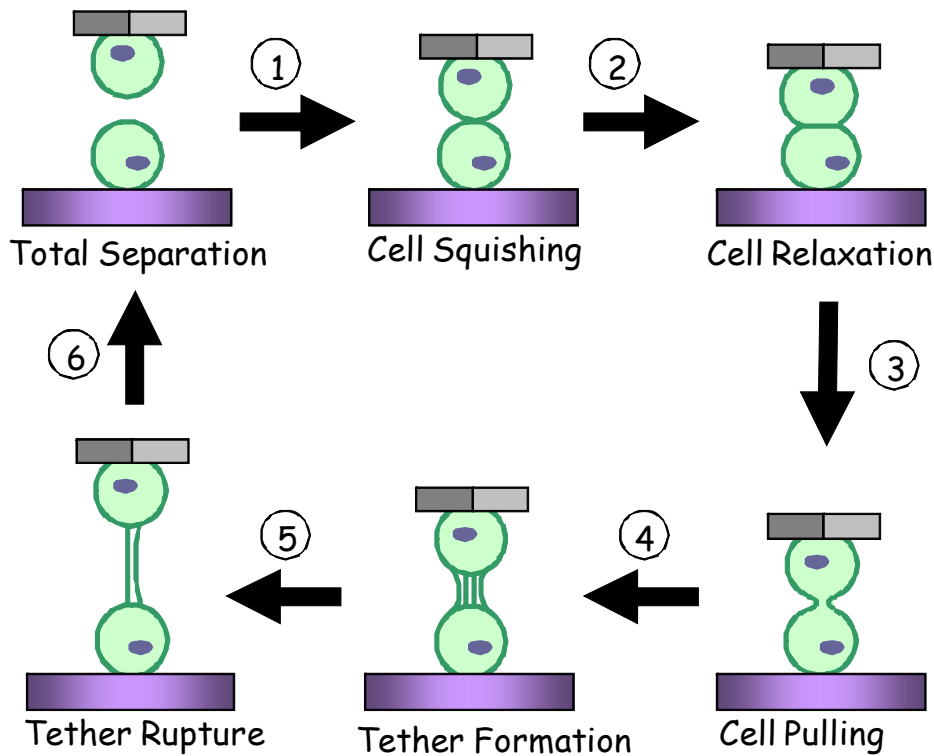
Figure 3.3 – Procedure for Two-Cell Adhesion Experiments

Prior to these experiments, the cantilever probe is coated with lectin Concanavalin A, a sugar-binding protein that strongly adheres to zebrafish cells. In the experiment, the probe is gently pressed on the 'probe cell' with 1 nN of force for 1 second, causing the probe cell to be firmly attached to the cantilever tip.

The adhesion experiment begins by moving the probe cell on the cantilever tip towards the target cell at 10 µm/second. When the probe cell and the target cell are in contact, and cantilever continues to compress the cells together until ~1 nN of force is reached. Then, the entire system is held for a period of contact time, varying from 1 to 60 seconds.

The probe cell and the cantilever are then retracted upward, separating the two cells 50 µm apart at a speed of 10 µm/second. The whole process is repeated three times, with a resting period of 30 seconds between each cycle.

The piezo position and the static deflection of the cantilever are recorded during the experiments. These measurements along with the mechanical properties of the cantilever enable the calculation of the approach and retract forces required to deform the cell, using the equation for cantilever beams shown below (Hibbeler, 1995):

$$v = \frac{PL^3}{3EI} \ ,$$

(3.1)

where v is the deflection of the cantilever, P is the force acting on the cell by the cantilever tip, L is the cantilever length, E is the Young's modulus of the cantilever material, and I is the moment of inertia of the cross-sectional area. Figures 3.4 and 3.5 shows the layout of the two cells during contact and when tethers were formed.

Plasma Membrane

Actin Cortex

Unbonded Adhesion
Molecules

Bonded Adhesion
Molecules

Actin Filament

Microtubule

Nucleus
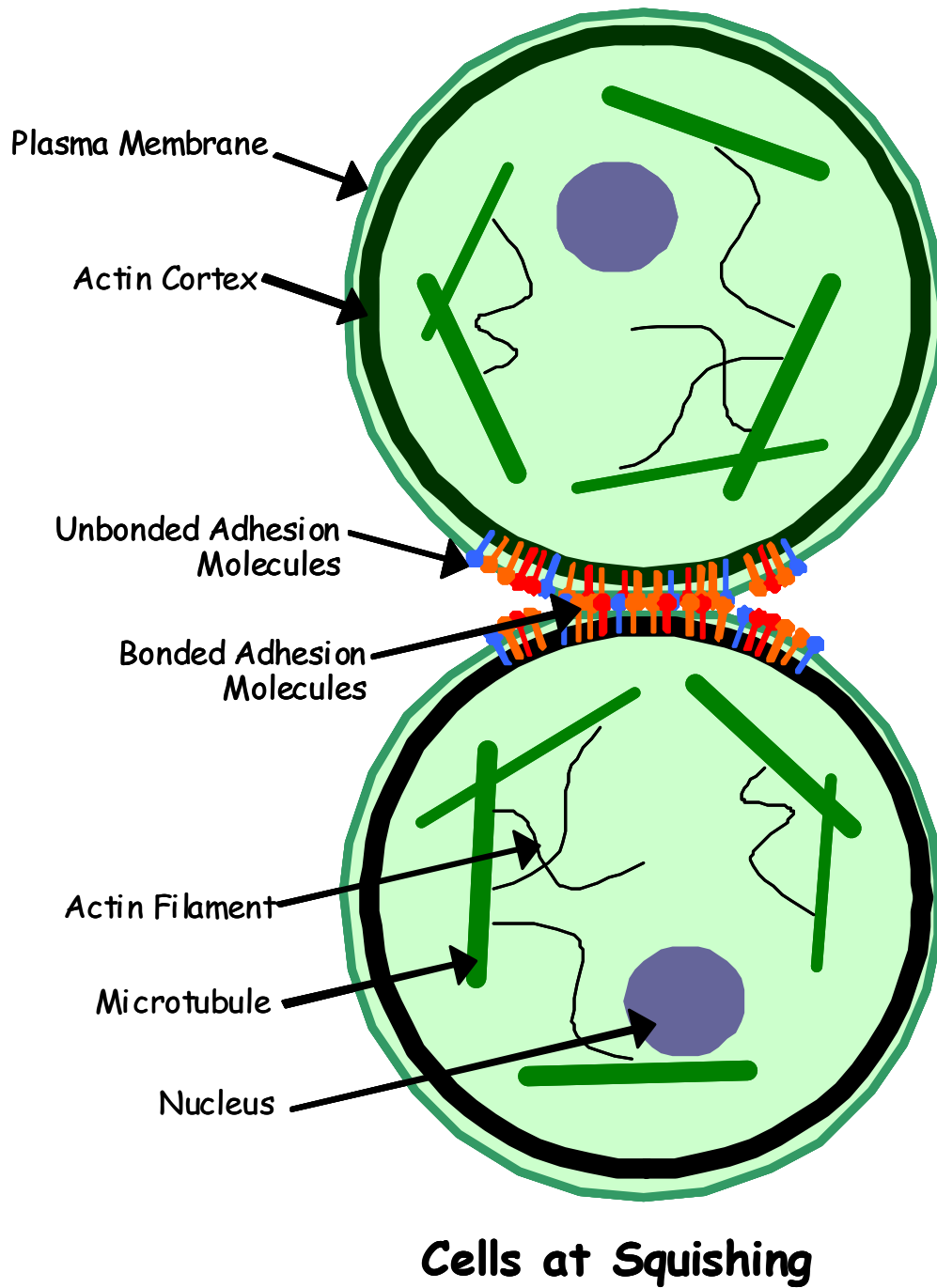
Cells at Squishing

Figure 3.4 – Major Biological Components Considered in Cell Squishing

Tether Tube

Bonded Adhesion Molecules

Unbonded Adhesion Molecules

Cells at Separating
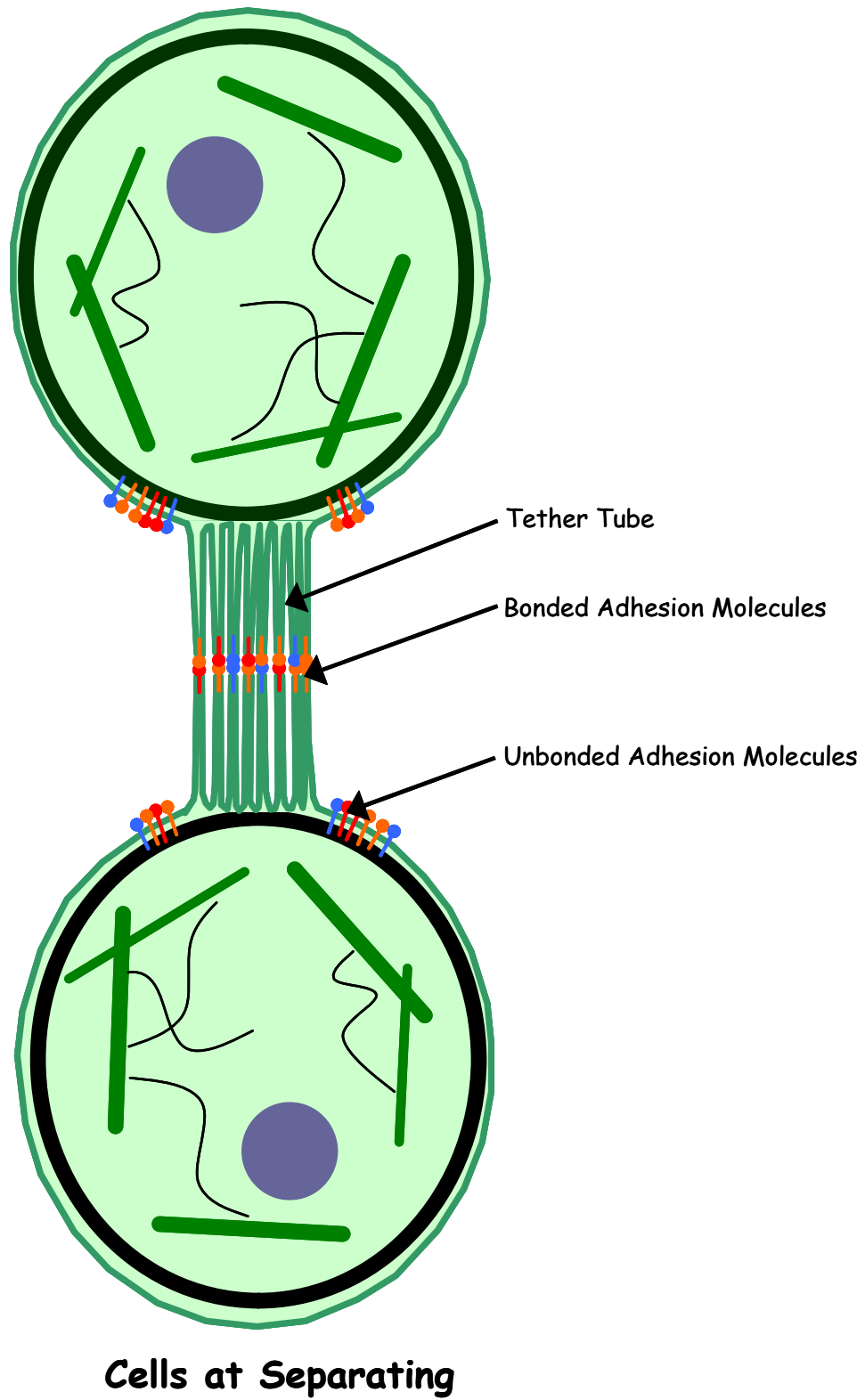
Figure 3.5 – Major Biological Components Considered in Cell Pulling

The resulting forces are then plotted against piezo positions and time to generate force-distance curves as well as force-time curves. Figure 3.6 shows a force-time curve obtained from an AFM experiment. Furthermore, plotting piezo positions against time will display the distance-time curve for each experiment. Figures 3.7 and 3.8 show the force-distance curve and distance-time curve respectively.
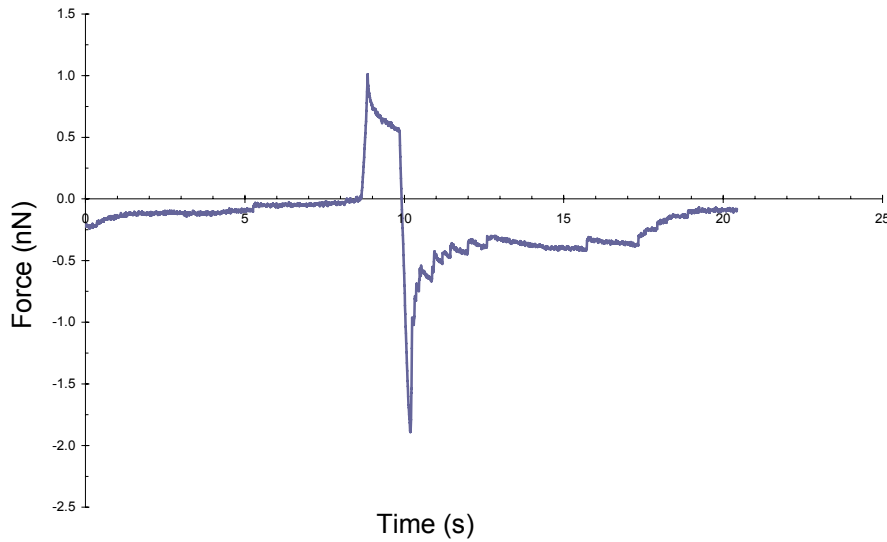
Figure 3.6 – AFM Experimental Force-Time Curve
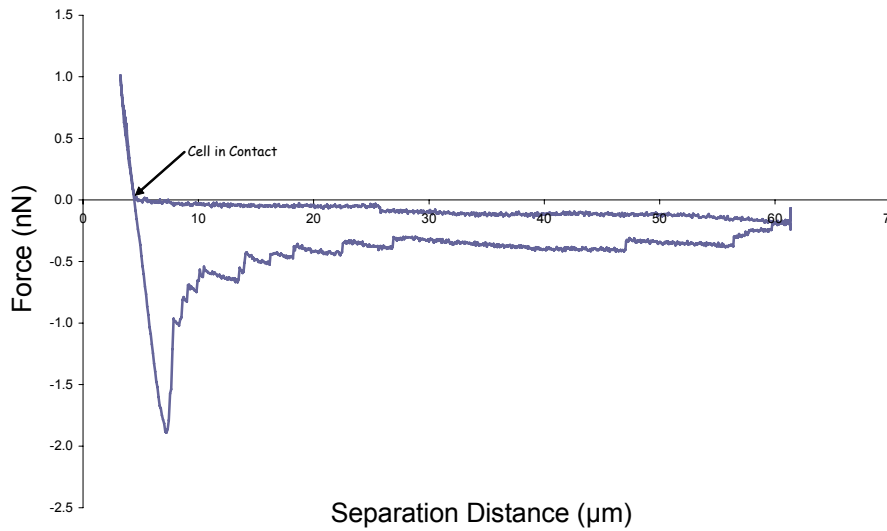
Figure 3.7 – AFM Experimental Force-Distance Curve
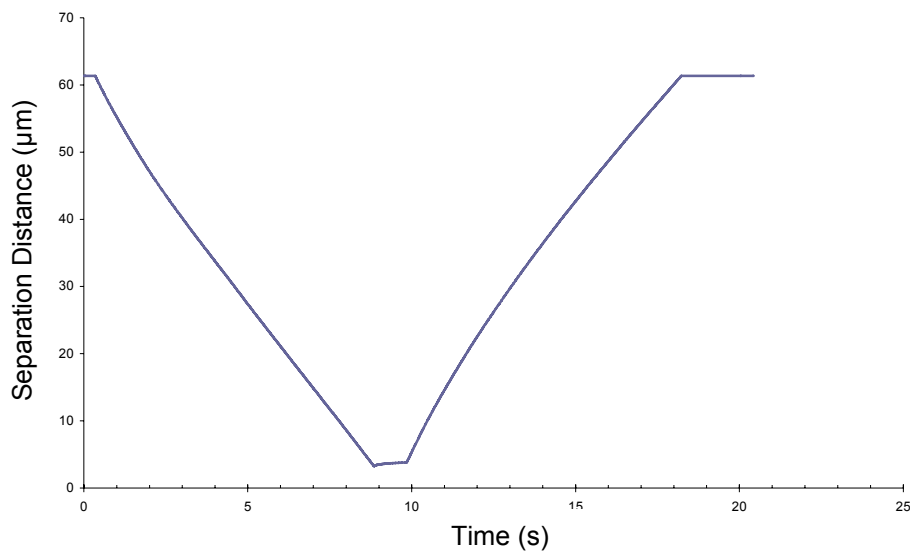
Figure 3.8 – AFM Experimental Distance-Time Curve

In this experiment, the cells contact each other at time 8.6 s, until the compressive force reached 1.0 pN at time 8.8 s. Subsequently, the cells are relaxed for 1 second and retraction of the probe cell begins at time 9.8 s. During retraction, the force initially declines very quickly until it reaches a peak at time 10.2 s. As separation continues, step patterns and force plateaus were observed in the force-time curve starting at 10.2 s and beyond. The applied force gradually reduces towards zero force.

These step patterns during the separation phase are thought to be the detachment of bonds coupled to the cytoskeleton and the rupture of membrane tethers. However, these tether extrusion observations are only descriptive, and without a theoretical model, it is impossible to further quantify the measurements and determine the origin of these force steps. Tether experiments suggested that a tether can divide into two thinner tubes to reduce membrane tension, or fuse with another tether to increase tension (Cuvelier, 2005). The opinion has lead to the unanswered question of whether the force steps are due to tether unbinds at the receptors or ruptures somewhere along its length, or even the fusion of them. Again, a theoretical model is lacking to explain these phenomena. Other important questions also arise about the curve:

1) What parameters govern the shape of the curve during squishing, relaxation, and separation?

2) Does contact time affect the strength of the adhesion bonds, which leads to a higher de-adhesion peak?

3) What biological processes cause the step-like patterns in the curve, and the height of them?

4) What factors control the length of individual plateau, namely, the length of the tethers?

Theoretical models have been previously developed by researchers in hopes of answering these underlying questions of cell-cell adhesion. They provide the fundamental framework to the study of cell-cell interface using finite element analysis. The following sections briefly present the mechanical and mathematical models that describe the cell and the cell-cell interface.

3.5 Mechanical Model for the Cell

Advances in nanotechnology have provided new and innovative experimental techniques to measure the mechanics of cells. However, the diverse techniques and experimental setup have made the mechanical responses very different. Therefore, it is necessary to use adequate theoretical models for different experiments. Taking such approaches will then give us better and more accurate understanding of living cells.

3.6 Cortical Shell-Liquid Core Models for a Single Cell

The cortical shell-liquid model is one of the continuum mechanical models developed to model living cells. Continuum mechanical models are advantageous because it groups the mechanical components and structures into only a few continuum mechanical properties

(Lim, 2006). These mechanical properties can be easily obtained through experimental observations, and in turn they facilitate the development of nano-scale structural models for sub-cellular components. In this thesis, interest is shown in the cortical shell-liquid core models, first introduced to study the rheology of white blood cells in micro-pipette experiments (Lim, 2006).
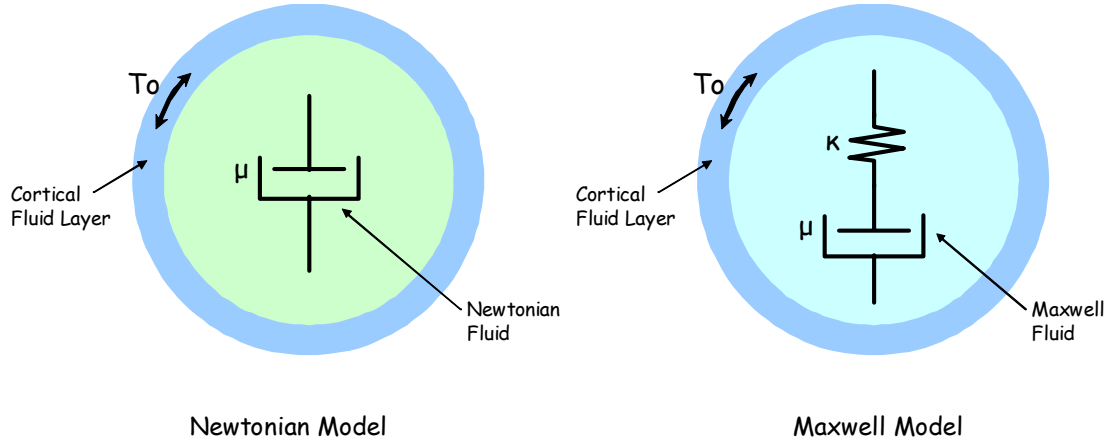
Figure 3.9 – Newtonian and Maxwell Cortical Shell-Liquid Models

In the Newtonian cortical shell-liquid model, a cell is thought to have a cortical shell surrounding a Newtonian fluid in its cytoplasm. The outer shell is of anisotropic viscous material along with a constant tension. Figure 3.9 illustrates this model. The constitutive relations for the Newtonian fluid are given by Equations 3.2, 3.3, and 3.4.

$$\tau_{ij} = \mu \dot{\gamma}_{ij} \tag{3.2}$$

$$\tau_{ij} = \sigma_{ij} - \frac{1}{3} \delta_{ij} \sigma_{kk} \tag{3.3}$$

$$\dot{\gamma}_{ij} = \frac{\partial v_i}{\partial x_j} + \frac{\partial v_j}{\partial x_i} , \tag{3.4}$$

where σ_{ij} and τ_{ij} are the whole and deviatoric stress components, δ_{ij} is the Kronecker delta, μ is the apparent Newtonian viscosity, $\dot{\gamma}_{ij}$ is the strain rate, and v_i is the velocity in the *i*-axis. The subscripts *i* and *j* correspond to the two axes in the Cartesian coordinate system. The constitutive relations of the cortical shell can be found in the review literature by Lim (2006).

The Maxwell cortical shell-liquid model is similar to the latter model in that it also comprises of a liquid core and a cortical shell as shown in Figure 3.9. Yet, the fluid in the Maxwell model is composed of a dashpot and a spring in series. This gives the elastic behaviour of cells. Equation 3.5 shows the constitutive equation for the Maxwell fluid. μ and κ are the dashpot viscous constant and the spring elastic constant respectively, and $\dot{\tau}_{ij}$ is the change in deviatoric stress with respect to time.

$$\tau_{ij} + \frac{\mu}{\kappa}\dot{\tau}_{ij} = \mu\dot{\gamma}_{ij}$$

(3.5)

From the equation, it can be seen that as κ increases, the fluid would behave more like a Newtonian fluid. Because of its elastic element, the Maxwell cortical shell-liquid model is good for cells with small deformations and initial rapid loadings. However, if deformation is large and loading time is long, the spring constant in the Maxwell model must be altered to become more Newtonian fluid like (Dong, 1991). Since the Newtonian cortical shell-liquid model requires only two parameters, and yet, it can satisfactorily model the behaviours of cells for large deformation, the Newtonian cortical shell-liquid model is a better candidate for the finite element analysis of the two-cell system.

3.7 One-dimensional Tape-Peeling Models for Cell-Cell Detachment

A mathematical model for cell detachment has been previously developed by Ward (1995). Wards presented a theoretical framework which demonstrated the relationships between ligand density and the corresponding detachment dynamics. Figure 3.10 shows a graphical representation of Ward's model.
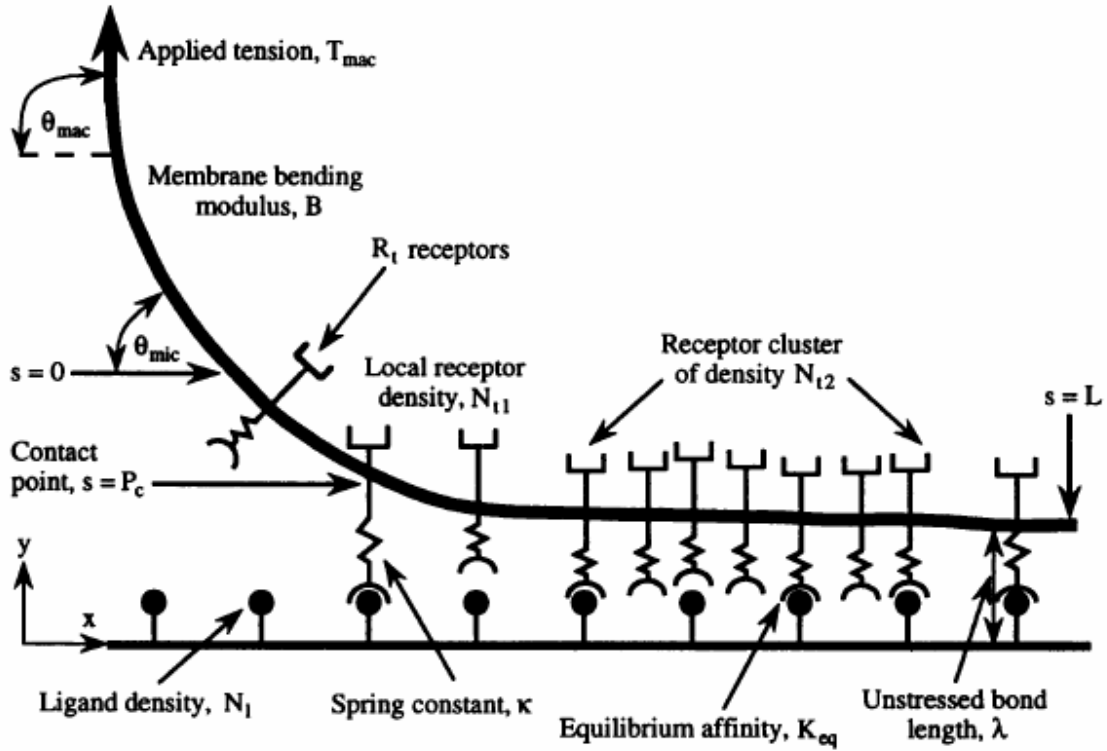
Figure 3.10 – Geometry of the One-dimensional Tape-peeling Model (from Ward, 1995)

Ward suggested that there is a critical tension which determines whether peeling detachment will occur along the membrane. If the applied tension is above the critical tension, the peeling velocity will be positive and cell detachment will occur. Whereas tensions below the critical tension will cause the velocity to be negative, and cell spreading will result (Ward, 1994). The critical tension can be calculated by:

$$T_{crit} = \frac{N_1 k_b \Theta}{1 - \cos(\theta_{mac})} \ln(1 + \frac{R_t K_{eq}}{A_{cell}}) \quad ,$$

(3.6)

Where N_1 is the ligand density of the cell, $k_b \Theta$ is the thermal energy, θ_{mac} is the contact angle, R_t is the receptor number, K_{eq} is the receptor-ligand affinity, and A_{cell} is the cell area. Comparing his numerical analysis with experimental results, Ward found that increasing the

density of ligands and the strength of molecular bonds at the cell-cell interface reduces the peeling velocity (Ward, 1994).

3.8 Viscoelastic Mechanical Models for the Tethers

A viscoelastic mechanical model of tethers has also been previously developed by Schmitz (2008) using the Kelvin body, as illustrated in Figure 3.11.
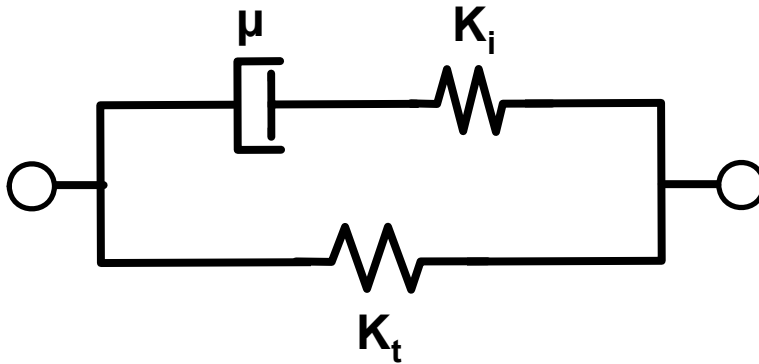
Figure 3.11 – Kelvin Viscoelastic Body

Schmitz used the forces calculated from his model and compared it to rupture forces measured in his AFM experiments (Schmitz, 2008). In Schmitz's model, the tether force is calculated using viscoelastic parameters obtained from Evans' experiments (Evans, 2005) and Equation 3.7, which is derived from the differential equation for a Kelvin body.

$$F_{Kelvin}(z) = k_t \times z + \mu \times v - \mu \times v \times e^{\frac{-k_i \times z}{\mu \times v}} \, , \tag{3.7}$$

where *F(z)* is the force under the boundary condition of a constant pulling velocity, k_i is the stiffness coefficient of the spring in series, μ is the damping coefficient of the dashpot in series, and k_t is the stiffness coefficient of the spring in parallel with the dashpot. The parameter z and v correspond to the position and retracting velocity respectively. In a real tether, k_i would represent the membrane bending rigidity, and k_t is the tether stiffness. Using

34

the above equation, Schmitz also tested the AFM experimental results with the Maxwell and Kelvin-Voigt bodies. The forces are calculated by:

$$F_{Maxwell}(z) = \lim_{k_t \to 0} F_{Kelvin}(z) = \mu \times v - \mu \times v \times e^{\frac{-k_i \times z}{\mu \times v}}$$

(3.8)

$$F_{Voigt}(z) = \lim_{k_i \to \infty} F_{Kelvin}(z) = k_t \times z + \mu \times v$$

(3.9)

By comparing these three models, he found that the Kelvin body best represents the mechanical behaviour of a tether. Not only does the Kelvin model fit the experimental force-time curve better, the model also works well when the tether is under static load, which will behave as a spring (Schmitz, 2008). By means of fitting his model into the experimental curves, Schmitz was able to find the viscoelastic parameters associated with tethers for the integrin VLA-4, summarized in Table 3.2 below.

Table 3.2 – Tether Properties for Integrin VLA-4

Parameter	Symbol	Integrin VLA-4
Tether Stiffness	k_t	1.6 µN/m
Membrane Rigidity	k_i	260 µN/m
Viscosity	μ	5.9 µN-s/m

3.9 Viscoplastic Mechanical Models for the Tethers

A viscoplastic mechanical model was previously introduced by Evans (1976). Rather than studying the elasticity of the plasma membrane as in previous literature, Evans tried to characterize the plasticity of plasma membrane through studying the plastic flow in the membrane, as illustrated in Figure 3.12 (Evans, 1976).
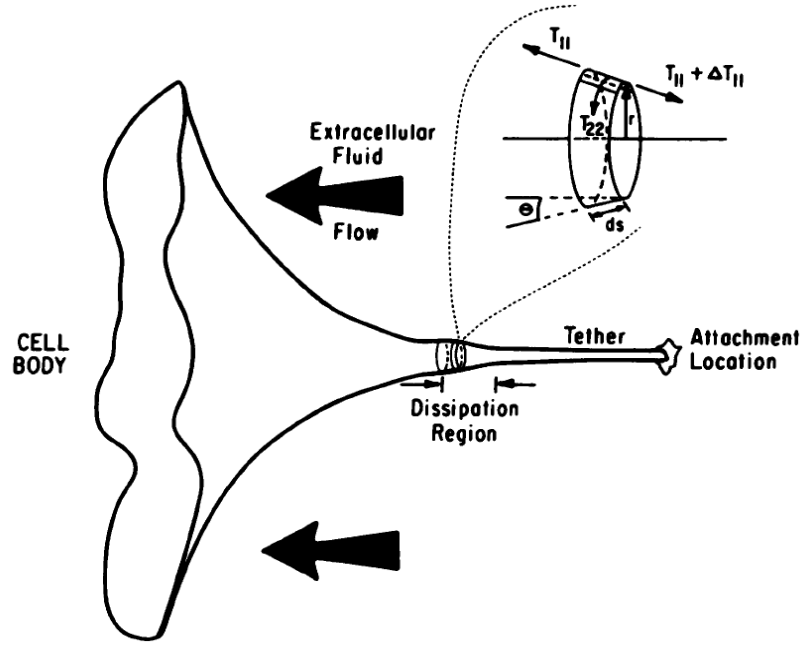
Figure 3.12 – Schematic Illustration of Plastic Flow in Tether (from Evans, 1976)

In his study, he derived a mathematical relationship for membrane tensions and the rate of deformation, as shown in Equation 3.10.

$$2\eta_p\left(\frac{\partial v}{\partial x}\right) = \begin{cases} 0 & ; F < 0 \\ (T_{11}/2) - (T_{22}/2) - T_o & ; F \geq 0 \end{cases},$$

$$(3.10)$$

where η_p is the membrane viscosity, $\partial v / \partial x$ is the rate of deformation, T_{11} and T_{22} are the membrane tension of the tether in the axial and circumferential direction. T_o is the yield shear. The yield function, denoted by F can be determined by Equation 3.11. When the yield function F < 0, the membrane will behave as a rigid solid. When $F \geq 0$, membrane will undergo plastic deformation and flow into the tether.

$$F = 1 - \frac{T_o}{\left| \dfrac{T_{11}}{2} - \dfrac{T_{22}}{2} \right|}$$

$$(3.11)$$

36

The equations of equilibrium for the tangential and circumferential tensions are given by Equations 3.12 and Equation 3.13. As such, the force *Fs* in the tether could be approximated by Equation 3.14, where *r* is the local radius and θ is the angle between the meridian and the tether axis.

$$\left(\frac{T_{11}}{R_1}\right) + \left(\frac{T_{22}}{R_1}\right) = 0$$

(3.12)

$$\left(\frac{d}{ds}\right)(rT_{11}) - T_{22}\left(\frac{dr}{ds}\right) = 0$$

(3.13)

$$F_s = 2\pi \times r \times \cos\theta \times T_{11}$$

(3.14)

The tether mechanical models in more recent literature are found to comply with Evan's viscoplastic tether models, such as the model proposed by Hochmuth (1996). Hochmoth studied the relationship between velocity and force of tethers extracted from neuronal growth cones. In Hochmuth's model, the tether force, F_s, is given by:

$$F_s = f_o + 2\pi \cdot \eta_{eff} \cdot V_t \quad ,$$

(3.15)

where f_o is the constant force term relating surface tension, tether radius, and membrane bending rigidity, η_{eff} is the effective viscosity, and V_t is the velocity of the tether.

3.10 Mathematical Model for Interfacial and Surface Tension

In living organisms, cell interfaces experience interfacial and surface tensions. To date, no one has been able to accurately measure the membrane tensions of living cells. However, these tensions are known to be derived by the contraction of the plasma membrane, the interaction of microfilaments and microtubules inside the cytoskeleton, and cell-cell

adhesions. Interfacial tensions can be calculated using the following equation (Brodland, 2000):

$$\gamma_{AB} = F_{MF}^{A} + F_{MF}^{B} + F_{Mem}^{A} + F_{Mem}^{B} - F_{Adh}^{AB} \; , \tag{3.16}$$

where γ_{AB} is the interfacial tension at the boundary between cells A and B, F_{MF}^{A} is the micro-filament force, F_{Mem}^{A} is the contraction of the membrane, and the F_{Adh}^{AB} are the adhesion force at the cell-cell interface. The subscripts A, B, and AB correspond to the cell(s) that are associated with that force. It can be noted that the cell-cell adhesion force decreases interfacial tension because it tries to increase the length of the junction. Figure 3.13 shows the layout of forces associated with interfacial tension (Brodland, 2000).
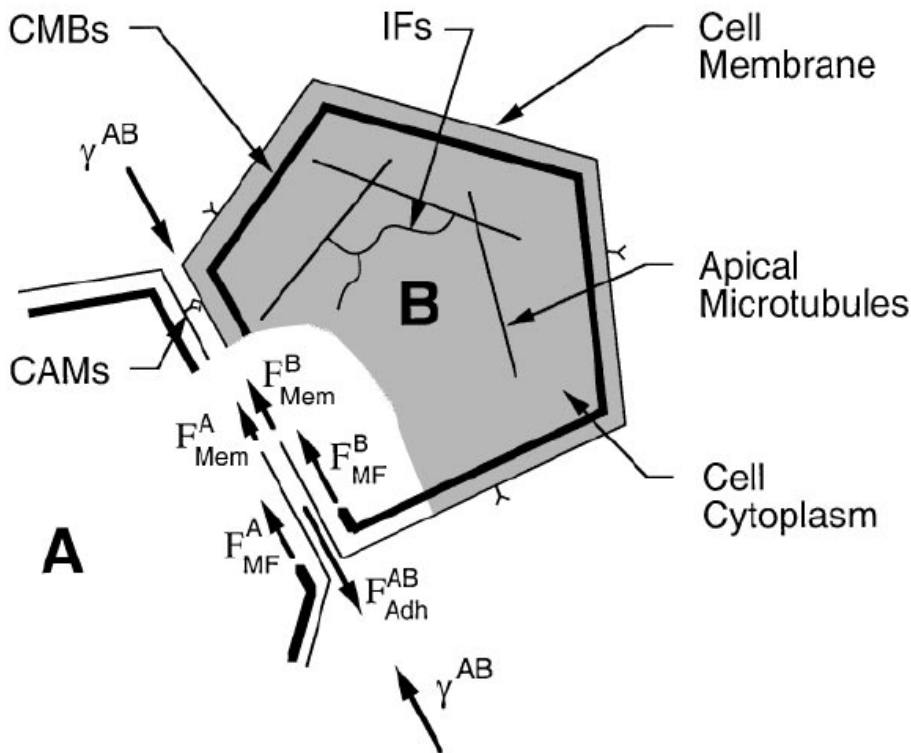
Figure 3.13 – Interfacial Tensions along the Cell-Cell Interface (Brodland, 2000)

Similarly, the surface tension γ_{AM} between cell A and the medium M can be calculated using the following equation (Brodland, 2000):

$$\gamma_{AM} = F_{MF}^{A} + F_{Mem}^{A} - F_{Adh}^{AM} \ ,$$

(3.17)

where F_{Adh}^{AM} is the force associated with the energy at the cell-medium boundary.

3.11 Lifetime Model for the Dissociation of Molecular Bonds

As mentioned previously, both adhesive strength and the probability for bond formation between the two cell surfaces depend on the contact duration of the two cells. Bell (1978) proposed a model to calculate the rate of bond formation for two cells stuck to each other for a period of time. The change in the total number of bonds at the cell-cell interface dN_b/dt is given by:

$$\frac{dN_b}{dt} = k_{+}(N_1 - N_b)N_2 - k_{-}N_b e^{\frac{\gamma f}{kTN_b}} \ ,$$

(3.18)

where k_{+} and k_{-} are the forward and reverse rate constants respectively, N_1 and N_2 are the number of receptors on cell 1 and cell 2 respectively, N_b is the number of bound receptors between the cells, γ is an adjustment factor accounts for the structure of solid and its imperfection, f is the applied force on the bond, K is Boltzmann Constant, and T is the temperature. Previous experiments show that the reverse-rate constant k_{-} ranges from 3 x 10^{-5} sec^{-1} to 6 x 10^{3} sec^{-1} (Bell, 1978).Using the lifetime model, Bell calculated the mean time for breaking a single antibody-hapten bond when subjected to a pulling force. The resulting Force-Lifetime curve is shown in Figure 3.14.
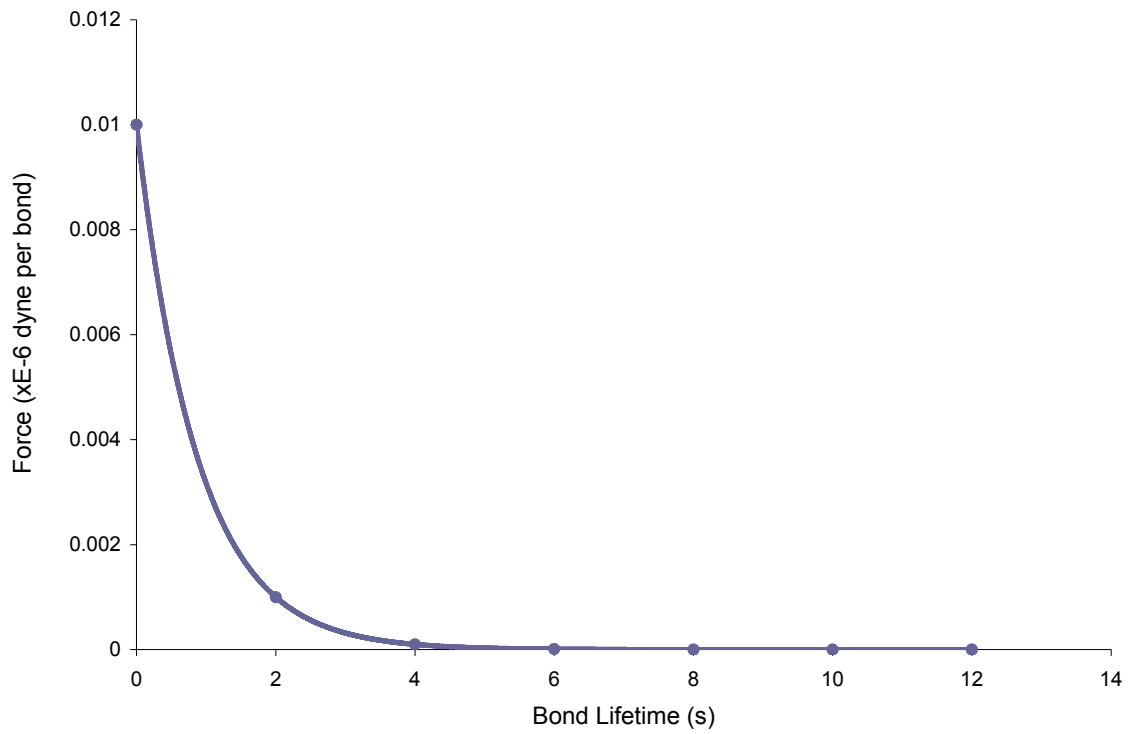
Figure 3.14 – Force versus Lifetime Curve for Antibody-Hapten Bonds (After Bell)

Chapter 4 Finite Element Model

This chapter outlines the construction of the finite element model, with special attention to the bonds and tethers that form between the cells. The model is designed to address the scientific questions that were posed in the Introduction. Earlier chapters stated that some cell components exhibit viscoelastic behaviours and have time-dependent mechanical properties. These features are modeled using an interative, non-linear finite element program.

4.1 Physical Components in the Model

The finite element (FE) model consists of three basic elements: Area2D elements, which are the building blocks of the cell's cytoplasm; actin cortex elements, which model the actin cortex of the cell; and InterfaceTruss elements, which represent the molecular attachments between cells. Figure 4.1 shows the composition of the cell.
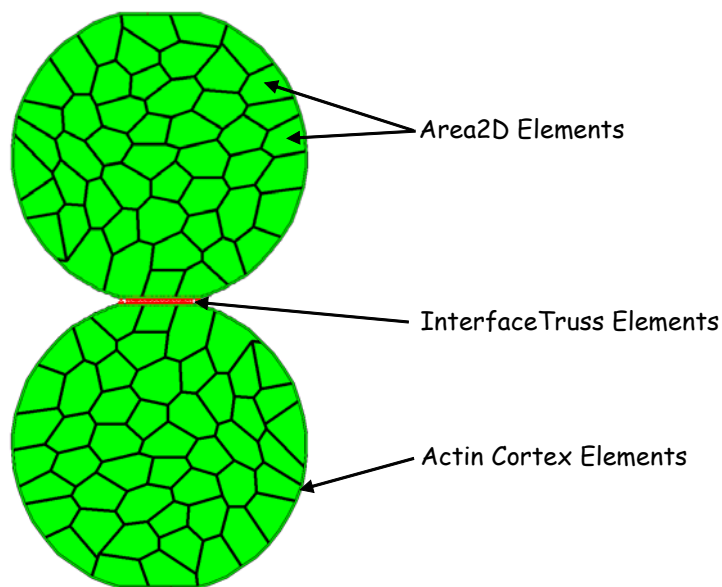
Figure 4.1 – Elements in the Finite Element Model

Along with these elements are a set of boundary conditions that controls the deformations and constraints associated with the adhesion experiments. The mechanical system is deemed

to be symmetric, and only the bottom half of the system is modeled. This approach eliminates instability problems and reduces computer processing time.

4.2 Governing Equations and Constraints

Before going into details of the physical components in the model, it is imperative to understand the basic mathematical principles behind the model. Finite element method relates nodal displacements, velocity, and forces using this equation:

$$f = C\dot{u} + Ku \quad ,$$

(4.1)

where f is a vector of externally applied force and internal surface tension, $\dot{u}$ is a vector of derivative displacement with respect to time, u is the vector of displacement, C is the $n \times n$ damping matrix of the system, and K is the $n \times n$ elastic stiffness matrix of the system. These vectors contain the specific information for each node in both the x- and y- coordinates as shown:

$$\dot{u} = \begin{bmatrix} \dot{u}_{1x} \\ \dot{u}_{1y} \\ \dot{u}_{2x} \\ \dot{u}_{2y} \\ \vdots \\ \dot{u}_{nx} \\ \dot{u}_{ny} \end{bmatrix} \qquad u = \begin{bmatrix} u_{1x} \\ u_{1y} \\ u_{2x} \\ u_{2y} \\ \vdots \\ u_{nx} \\ u_{ny} \end{bmatrix} \qquad f = \begin{bmatrix} f_{1x} \\ f_{1y} \\ f_{2x} \\ f_{2y} \\ \vdots \\ f_{nx} \\ f_{ny} \end{bmatrix}$$

n is the number of nodes in a element. For example, u_{2x} correspond to the displacement of node 2 in the x-direction. Since this study deals with cells that behave as viscous systems, the stiffness matrix K is set to zero. If time intervals Δt are small, and K is set to zero the above equation can be approximated by:

$$f = C\dot{u} \cong C\frac{\Delta u_q}{\Delta t} = \frac{1}{\Delta t}C\Delta u_q = f_q \quad,$$

(4.2)

where Δu_q is the increment displacement vector at incremental time step q, Δt is the incremental time, and f_q is the vector of forces at time step q.

Each area element is subject to a volume constraint, which causes the area within an Area2D element to remain constant throughout the simulation. In addition, boundary conditions were applied to the nodes of specific elements to simulate the relative motion between the cells.

4.3 The Finite Element Program

The computer simulations discussed in this thesis were performed using an existing 2D finite element program developed in Professor Brodland's Biomechanics Lab to which was added a series of cell detachment algorithms (Brodland, 2000). The software is written in the C++ programming language using Visual Microsoft C++ 6.0 application.

The sequence of events in the simulation is illustrated in Figure 4.2. The computer program has been previously applied by Brodland and colleagues to study cell rearrangement in aggregates and fabric evolution (Brodland, 2006). In Brodland's studies, cells are meshed using a class of elements in the FE program called Area2D.
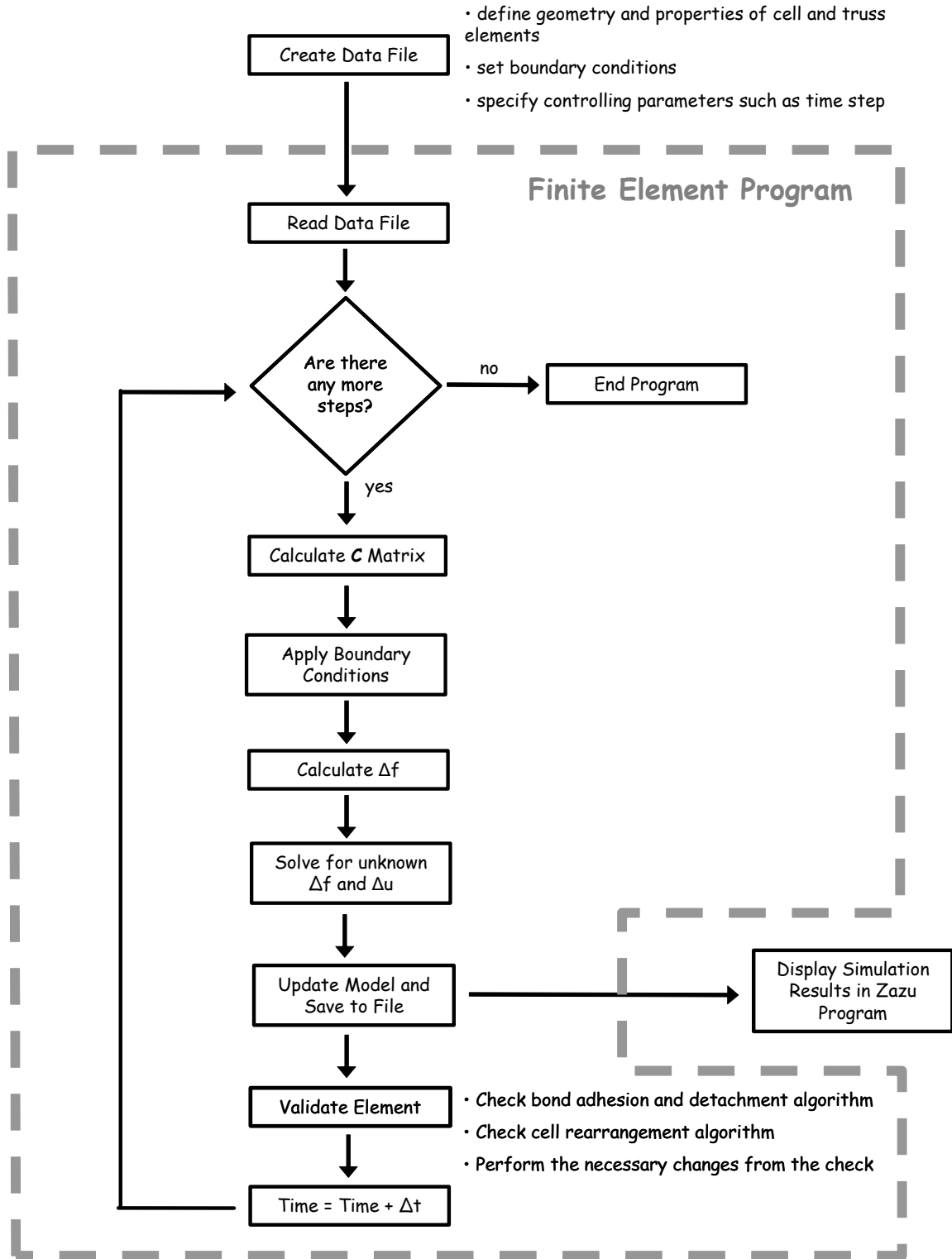
Figure 4.2 – Flowchart of Finite Element Computation Procedure

4.4 Cell-Level Modelling

Each Area2D element follows the cortical shell-liquid core model (Lim, 2006), also known as the μ- γ model. They are made up of nodes and edges, as shown in Figure 4.3. The viscosity of the cytoplasmic structures is represented by μ, whereas the system of forces at the boundary has a constant interfacial tension γ, also known as the tonus. The viscosity μ is represented by two sets of orthogonal dashpot system, each having a damping coefficient η. As shown in the figure below, the dashpots align themselves parallel to the corresponding axis, and connect each node to the imaginary line perpendicular to the dashpots, with a roller support at the end.
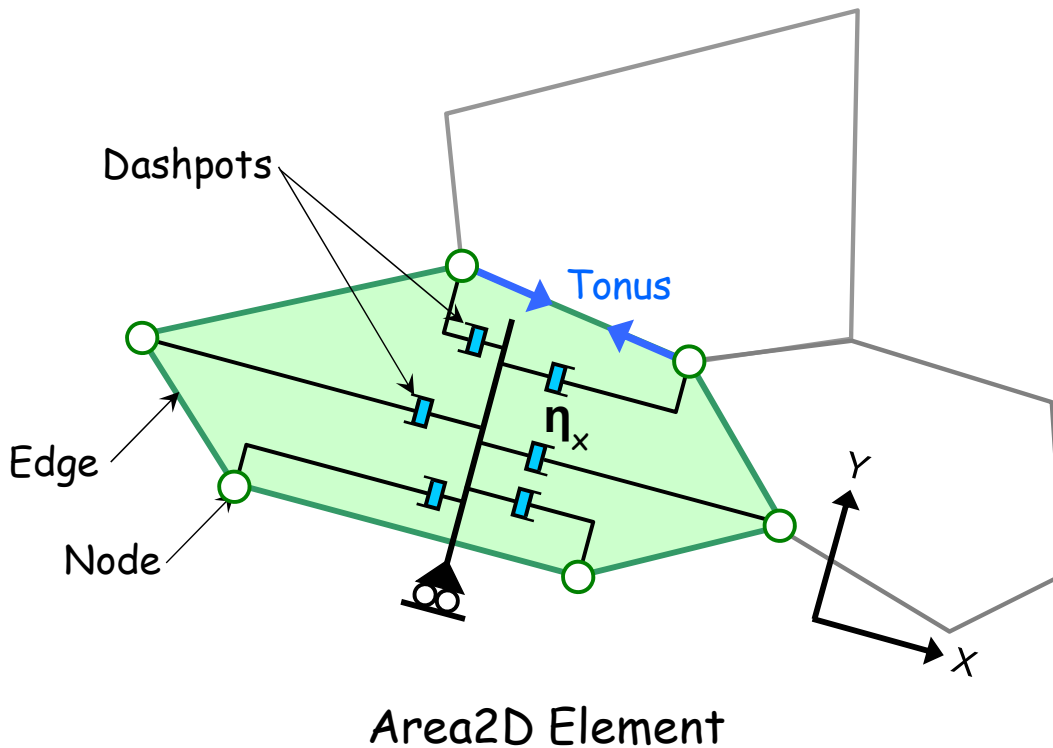
Figure 4.3 – Mechanical Properties of the Area2D Element

These Area2D elements are used to form the overall mesh of the cell. In earlier applications (Brodland, 2006; Brodland, 2003), each Area2D element represents a cell, whereas here, each element represents a portion of the total cell cytoplasm. They best describe the mechanical and structural details of the cell, such as the irregular geometries of the

cytoskeleton structure, the tension along the plasma membrane, and the fluidity behaviour of the cytoplasm. The mesh pattern is constructed using the Voronoi Tessellation technique. The technique first generates forming points randomly in a region, and then edges are formed half way between two points, as shown in Figure 4.4. The resulting edges will become the edges of the polygon which surrounding a forming point.
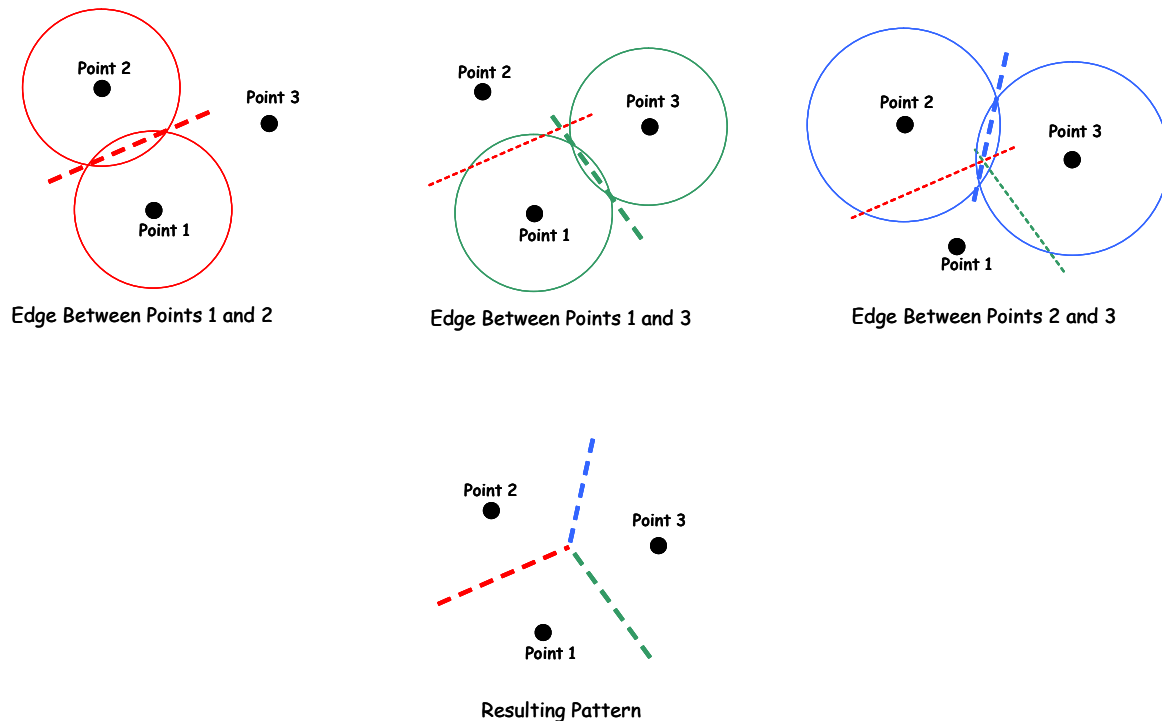
Figure 4.4 – Edge Formation using Voronoi Tessellation

Figures 4.5 and 4.6 show the layout of Area2D elements in the cells using Voronoi Tessellation. These figures are generated by the Zazu graphical program developed in Dr. Brodland's Biomechanics Lab at the University of Waterloo. The Zazu graphical output closely matches Figures 3.4 and 3.5 in Chapter 3. As shown in the figure, the key computational components in the FE model are the Area2D element mesh, a network of truss elements at the cell boundary, and a series of InterfaceTruss elements representing the individual adhesion bonds.

Bond Type
InterfaceTruss Elements

Cell

Cells at Squishing
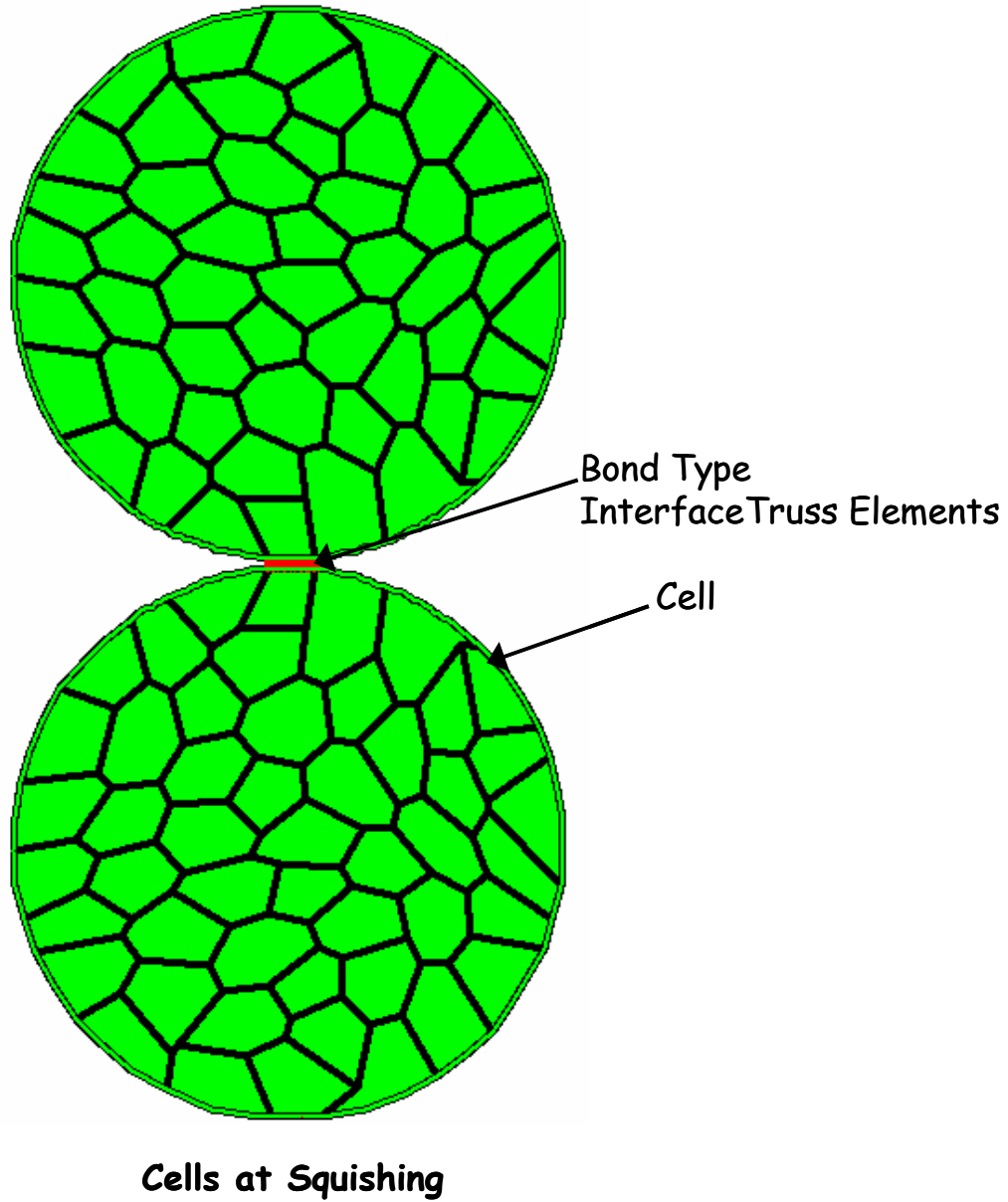
Figure 4.5 – Representation of the Finite Element Model during Squishing

Cells at Separation
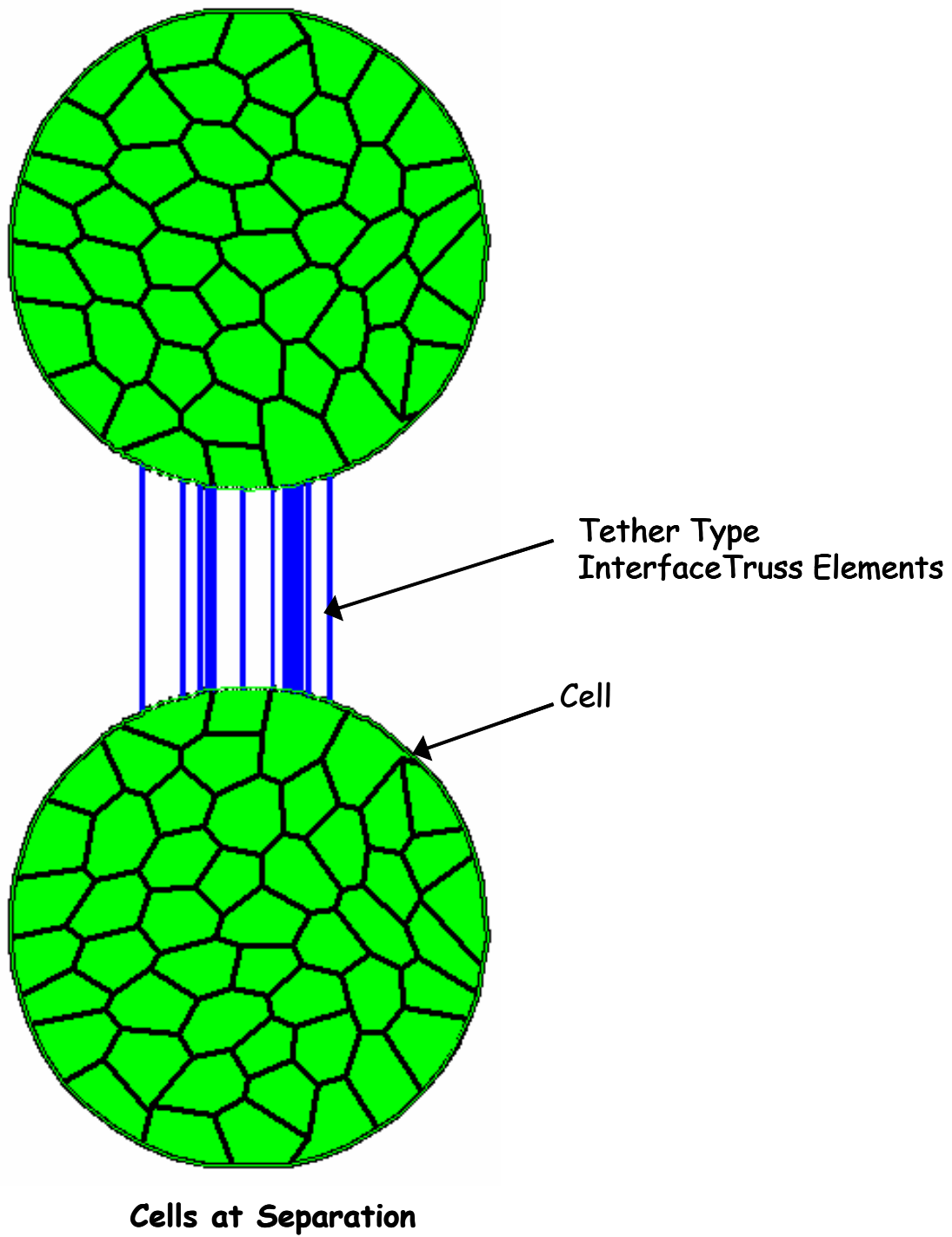
Figure 4.6 – Representation of the Finite Element Model during Pulling

4.5 Cell Boundary and Viscoelastic Truss Elements

As mention in previous chapters, along the boundary of the cell exists a network of micro-filaments bundles called the actin cortex and collectively they give rise to net interfacial and surface tensions. To incorporate both physical components into the FE model, viscoelastic truss elements are used and are set on the cell's entire outer boundary, as shown in Figure 4.7. Each truss element includes an elastic spring, a viscous dashpot, and a tonus force that generate a tension on the cell boundary.
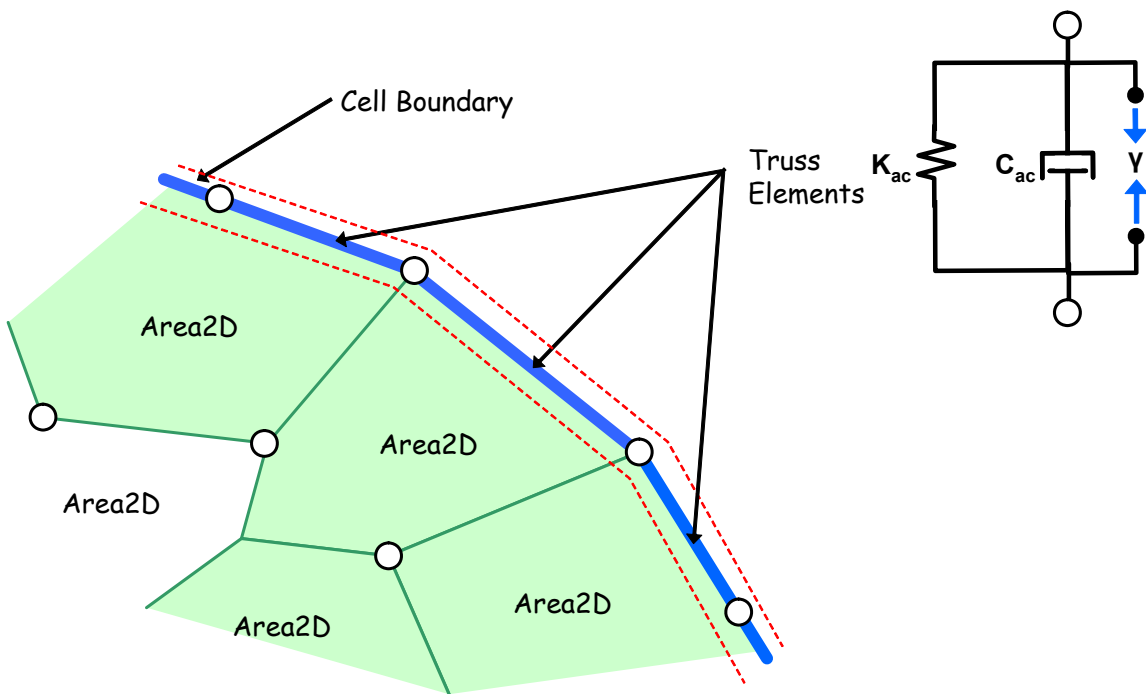
Figure 4.7 – Location and Material Properties of Viscoelastic Truss Elements

In the spring-dashpot-tonus system, all viscoelastic trusses have the same stiffness coefficients K_{ac} and damping coefficients C_{ac}. The relationship between the mechanical properties of each truss element and the resulting force f can be represented by this mathematical equation:

$$f = K_{ac}\varepsilon + C_{ac}\dot{\varepsilon} + \gamma \quad ,$$
(4.3)

where ε and $\dot{\varepsilon}$ are the strain and strain rate respectively, and γ is the interfacial tension along the membrane.

A cell could either experience interfacial tensions at the cell-cell interface γ_{cc}, at the AFM tip contact γ_{cp}, or at the cell-medium interface γ_{cm}, where $\gamma_{cm} > \gamma_{cc}$ in order for cell sorting behaviours to occur (Krieg, 2008). This difference in tension drives the cell to anneal and change its shape until boundary forces are in equilibrium. Therefore, in order to differentiate these tension values, each truss element is assigned one of the three tonus forces, depending on its specific location on the cell boundary.

4.6 Adhesion bonds and InterfaceTruss Elements

As described in Chapter 2, the contacting interfaces are separated by a gap 10-100 nm wide (Ward, 1995). Receptor-ligand bonds are distributed all over this adhesive contact, and in some cases, form clusters of bonds. When two cells are being separated, the bonds will experience a tensile force. As this force becomes larger, the bond may rupture at the binding site or disconnect from the cytoskeleton of the cell body and form tether tubes.
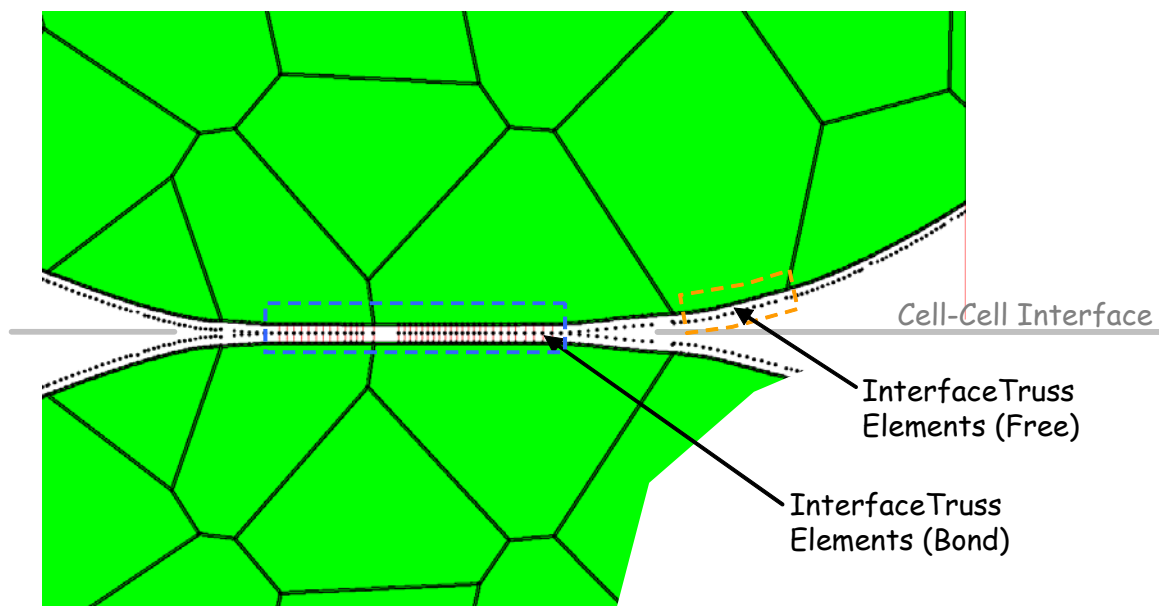
Figure 4.8 – Detailed Close-up View of the Cell-Cell Interface

In this enhanced model, a new element class called the InterfaceTruss was implemented. They represent the individual adhesion molecules associated with the cell-cell interface, as shown in Figure 4.8. Each InterfaceTruss element is classified into one of three categories or types: 1) Bond, which are adhesion molecules that bind to molecules on the other cell; 2) Free, which are adhesion molecules that are free and are not bind to anything; and 3) Tether, which are molecules that have detached from the cytoskeleton but remain connected to the adhesion molecule on the other cell. The InterfaceTruss types are differentiated by colour in the Zazu graphical output program. Table 4.1 provides the color code and a brief description of the three categories.

Table 4.1 – Color Code and Description of InterfaceTruss Element Type

Type	Color	Descriptions
Bond	Red	Adhesion molecule is bound to another molecule on the other cell
Free	White	Adhesion molecule is free and not bound to anything
Tether	Blue	Bonded molecules that are disconnected from the cytoskeleton yet remain attached at the binding site

4.7 Material Properties for Different InterfaceTruss Type

Bond, Free, and Tether type InterfaceTruss elements all have unique material properties. In addition, these elements are based on the Kelvin-Voigt material model. However, they differ in strength and lifetime relationships. The major differences and their specific functions of the three InterfaceTruss element types are described below.

Bond type InterfaceTruss elements resemble those molecules that are still bound with other moelcules. They are very stiff in nature and do not stretch easily, as compared to the viscous cytoplasm and viscoelastic actin cortex. As such, Bond type InterfaceTruss elements are modeled as a very stiff spring, as shown in Figure 4.9. This is accomplished by setting their damping coefficient μ and stiffness coefficient κ in the Kelvin-Voigt material model as zero and 10,000 respectively.

$$\mu = 0$$

$$K = 10,000$$
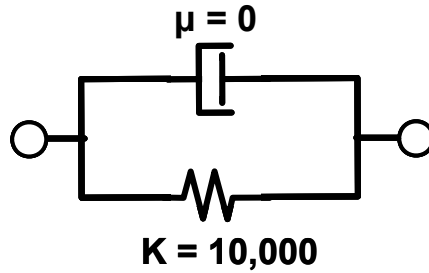
Figure 4.9 – Kelvin-Voigt Model for Bond Type InterfaceTruss Elements

Free type InterfaceTruss elements resemble those molecules that are not bound to other molecules. As shown in Figure 4.10, the damping coefficient μ and stiffness coefficient κ in the Kelvin-Voigt material model are both set to zero. Thus, they will not affect the mechanical properties of the entire two-cell system, and nor will they contribute to the reaction forces associated with the deformation of the cell. However, their existence is important to the formation and destruction of bonds. When the cells approach each other, Free type InterfaceTruss elements will be approaching the cell-cell interface, as shown in Figure 4.8. When an element does contact the interface, that element will change its type from a Free to Bond type element. Subsequently, the rupture of Bond and Tether type elements will cause them to become Free type elements. Rupture of them occurs when their contact duration has exceeded the allowable lifetime assigned to them. Their lifetime curves will be discussed in the next section.

$$\mu = 0$$

$$K = 0$$
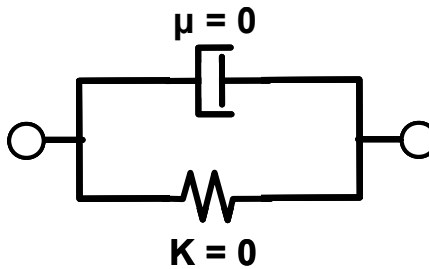
Figure 4.10 – Kelvin-Voigt Model for Free Type InterfaceTruss Elements

Tether type InterfaceTruss elements are those molecules that are detached from the cytoskeleton of the cell body, yet remain attached to the adhesion proteins of the adjacent cell.

As discussed previously, it was found that tethers have viscous properties. However, it is not yet determined whether they behave viscoelastically, or viscoplastically (Evans, 1976).

Therefore, tethers are modeled in two different ways, as shown in Figure 4.11. The first way is to represent these elements as viscoelastic material using the Kelvin-Voigt material model, where both **μ** and **κ** were assigned. The second is to represent them as viscoplastic materials, which also uses the Kelvin-Voigt material model along with a tonus force *T* **(**Evans, 1976). In the latter case, the stiffness coefficient **κ** was set to zero.
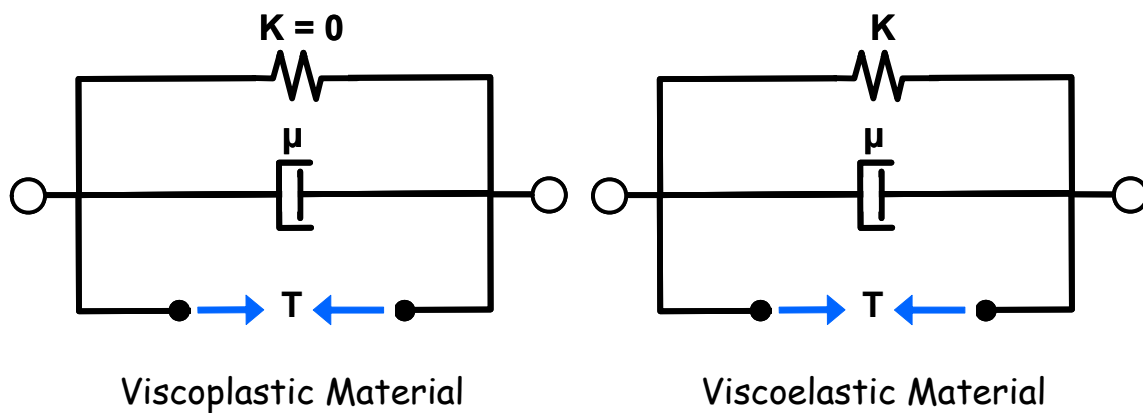
Figure 4.11 – Two Material Models for Membrane Tethers

4.8 Bond Lifetime and Rupture Force Relationships

As discussed previously, the rupture of bonds at the contact depends on the lifetime decay curves and the internal force the bonds are experiencing, as represented by the Bell's Model (Bell, 1978). Here Bell's model was implemented into the cell detachment algorithm using the following equations:

$$\text{Dissociation Rate} = K_{off} \times e^{(\frac{\gamma \times f}{K \times T})}$$

(4.4)

$$\text{Bond Lifetime} = \frac{1}{\text{Dissociation Rate}} \text{ ,}$$

(4.5)

where K_{off} is the reverse-rate constant, γ is an adjustment factor accounts for the structure of solid and its imperfection, f is the applied force on the bond, K is Boltzmann Constant, and T is the temperature. Combining Equations 4.4 and 4.5 yields the relationship between bond lifetime and the applied force. The equations can be further simplified to Equation 4.6, where λ is the relationship between γ, K, and T. Thus, forces in the bonds and tethers can be related to their contact time in lifetime curves. Figure 4.12 shows the force-lifetime curve when λ is 0.002 pN^{-1}, and K_{off} is set to 0.4 and 0.2 sec^{-1}, for applied forces ranging from 100 pN to 600 pN. These values were used for generating the figure, but were not necessarily used in the simulations.

$$\text{Bond Lifetime} = \frac{1}{K_{off} \times e^{\lambda \times f}}$$

(4.6)
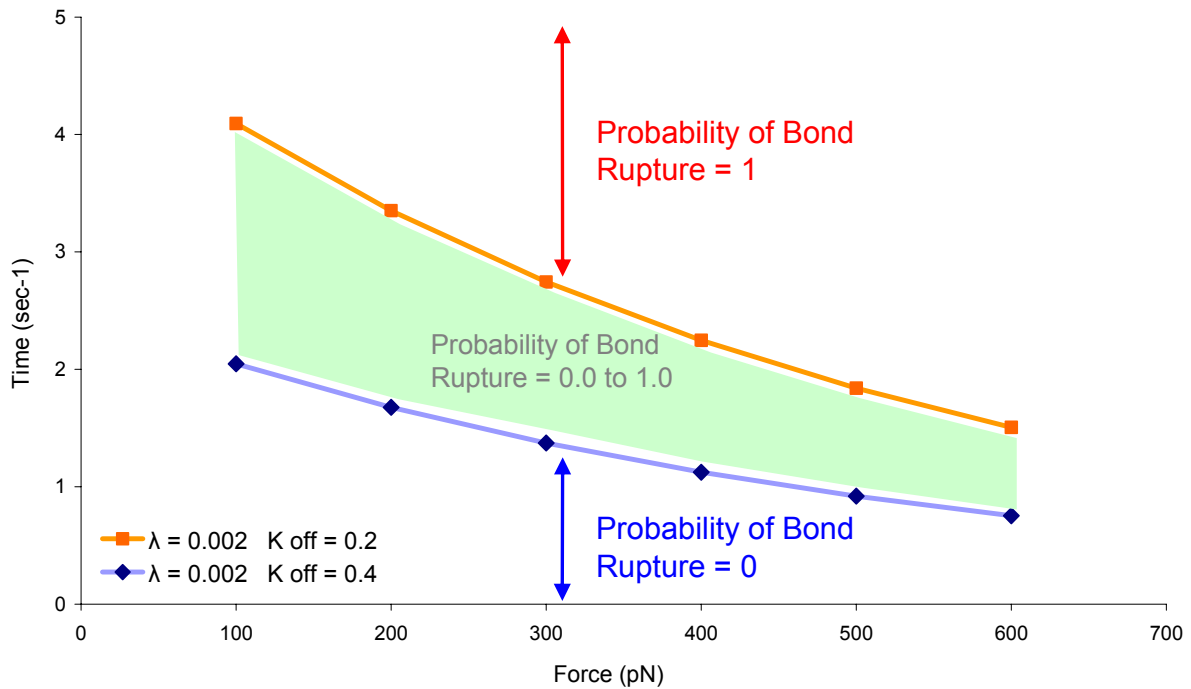
Figure 4.12 – Bond Lifetime versus Tether Force

Each bond is associated with an upper-bound and a lower-bound lifetime curves. For a given force, if the contact time of a bond is below the blue lower-bound curve, the probability of bond rupture would be 0 and the bond will remain attached. If the contact time is above the orange upper-bound curve, the probability of bond rupture would be 1 and the bond will rupture. If the contact time is in between the two curves, the contact duration of the bond will be compared to a randomly generated lifetime, which determines whether or not the bond will rupture. The reason for a probability zone is that detachment of bonds is a stochastic process, rather than a strict comparison between the contact duration and the lifetime threshold (Evans, 1991).

Each Bond type InterfaceTruss elements are associated with four lifetime curves: upper-bound and lower-bound curves for bond dissociation, and upper-bound and lower-bound for tether formation. However, Tether type elements will only have two lifetime curves: upper-bound and lower-bound curves for tether rupture.

Tether forces, or the internal forces in Tether type InterfaceTruss elements, are calculated using the equation below. This assumes a tether to be a viscoelastic tube with a membrane tension.

$$F_{Tether} = \mu\dot{\varepsilon} + \kappa\varepsilon + T_{Tonus} \quad , \tag{4.7}$$

where F_{Tether} is the tension force in the tether, μ is the damping coefficient of the tether element, $\dot{\varepsilon}$ is the strain rate, and T_{Tonus} is the tonus force assigned to the tether.

In contrast, internal forces in the Bond type InterfaceTruss elements are obtained through a system of equations, which are also the boundary conditions that governs the position of the nodes of these elements. These boundary conditions are presented in the following section.

4.9 Model Simplification and Boundary Conditions

During simulations using a two-cell system, the structure of the system often becomes unstable, as shown in one of the earlier simulations in Figure 4.13. During squishing, the elements adjacent to the cell-cell interface will overlap each other, until the cells are complete on top of each other, producing unrealistic results. Also, the difference in surface tension along the cell boundary and the different mesh patterns in the two cells occasionally cause the top cell to slide off the side of the bottom cell, giving unfavourable force-time curves.

Prior to Squishing   During Squishing   After Squishing
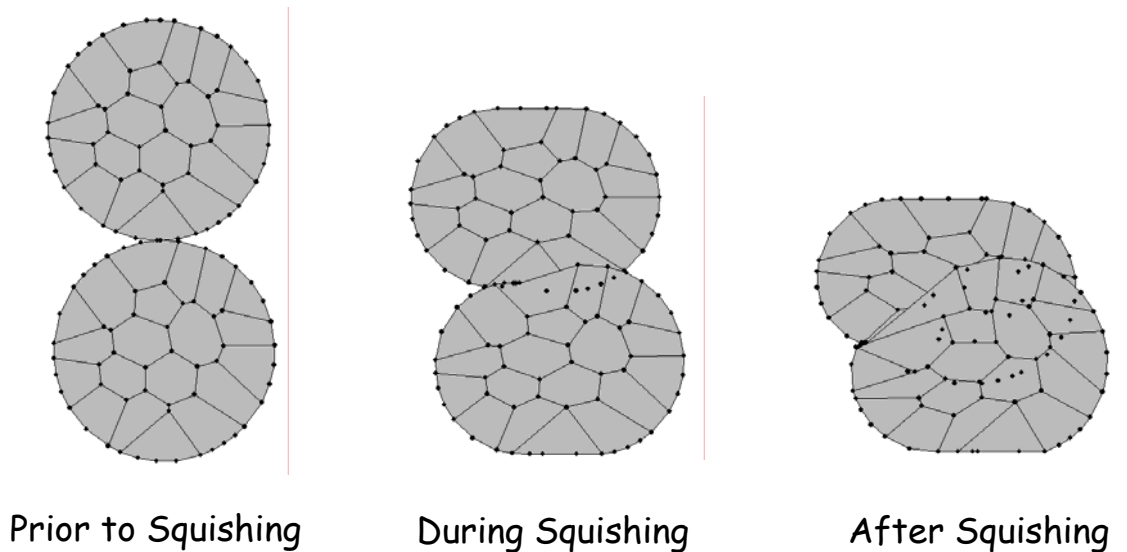
Figure 4.13 – Incorrect geometry from Earlier 2-Cell Simulations

Unless extensive computer codes are written to accommodate all of the possible overlapping scenarios for the cell-cell interface, this problem is expected to occur even with the InterfaceTruss elements implemented for the two-cell modeling. As such, knowing that the structure is axis-symmetric at the cell-cell interface and the cells are approximately the same size, the instability problem was addressed by simplifying the system, modelling only the bottom half of it. This technique not only eliminates unrealistic solutions, it also minimizes the computer processing time.

Since only half of the system is modeled, namely the bottom cell and the associated adhesion molecules, proper boundary conditions must be place at the mirror-line to correctly replicate the behaviour of the entire system. In total, four main boundary conditions are predefined into the model: Top-Face, Bottom-Face, Top-Node, and Bottom-Node conditions. Description of each boundary condition is summarized in Table 4.2.

Table 4.2 – List of Boundary Conditions

Boundary Condition	Associated Nodes	Descriptions
Top – Face	List of nodes at the Cell-cell interface	Set the upper limit for which the y-coordinates of any node cannot go above. The upper limit changes as the nodes in the condition are moving down or up.
Bottom – Face	List of nodes at the very bottom of the cell	Set the lower limit for which the y-coordinates of any node cannot go below. The lower limit remains constant for the entire experiment.
Top – Node	Bottom-Center Node	Set the velocity of a node in the Top-Face condition so as to compress or pull the cell.
Bottom – Node	Top-Center Node	Restrict a bottom node from moving in the y-direction during compression and retraction.

The Top-Face condition consists of all the nodes in contact with the cell-cell interface, whereas the Bottom-Face condition consists of all the nodes at the bottom of the cell. For example, if a Free InteraceTruss element contacts the cell-cell interface and becomes a Bond type element, the upper node of the element will be added to the existing list of Top-Face condition nodes.

At the Bottom-Face, the nodes are allowed to freely move in the horizontal direction, while vertical movements are restricted, resembling a set of rollers located at the bottom of the cell. However, at the Top-face the nodes are allowed to move horizontally, but changes to the

vertical position are based on node condition. Thus, these nodes resemble a set of rollers that are moving upward or downward at a constant rate. Figure 4.14 illustrates the location and function of the four main boundary conditions.
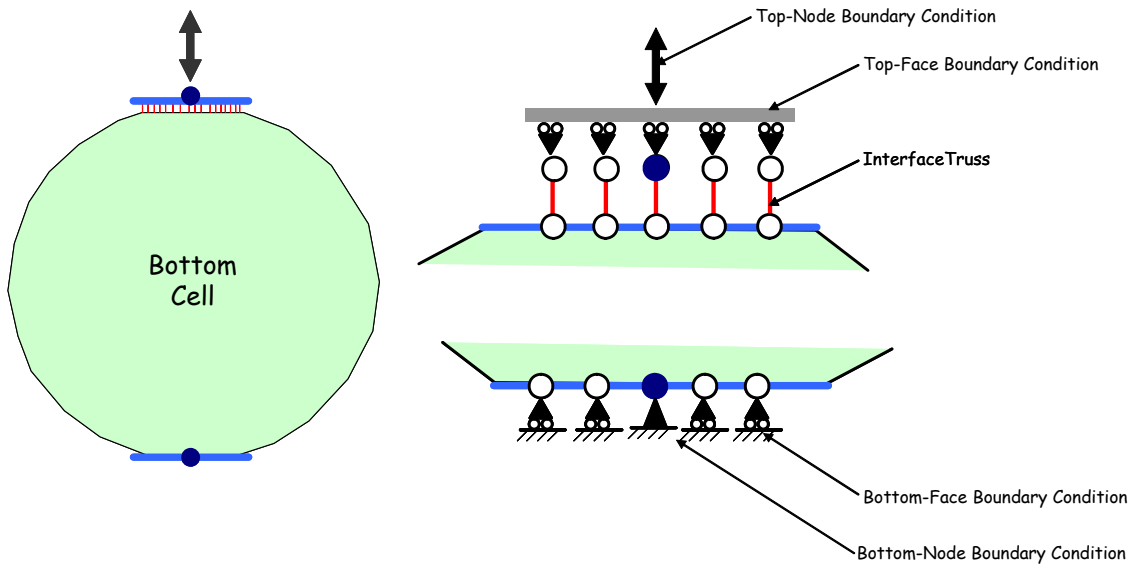
Figure 4.14 – Schematic Representation of Boundary Conditions

For the Top-Node condition, a velocity was assigned in the input file to either compress or pull the cell at a specific speed. Since only half of the system is modeled, it is necessary to divide the predefined the deformation rate by half. For example, if the two-cell system is to be squished at 10 μm per second, the cell-cell interface in the middle would have only moved downward 5 μm in one second. As such, for the half model, the velocity assigned in the Top-Node condition should be 5 μm per second. Subsequently, the interfacial tensions and the mechanical properties of the trusses along the top cell boundary should be divided by two to compensate the exclusion of the top cell in the model.

4.10 Scale Differences between the FE Model and the Experiments

The cells in our model are 200 units in diameter, whereas a typical zebrafish blastoderm cell is 20 μm in diameter. Therefore, a unit length of the program represents 10 μm in the actual

experiment. In addition, a unit time in the program corresponds to 0.1 seconds in the actual experiment.

As such, if the cells are squished at a speed of 5 μm/s for 0.2 seconds in the cell adhesion experiments, the computer program will squish the cells at a speed of at 5 length units per unit time for a period of 2 unit time.

Chapter 5 Results

This chapter presents families of parametric analyses that show how changes to specific cell and tether properties affect the force-time curve. Prior to running simulations for the analysis, a convergence test was conducted on the element size. Once a reasonable mesh size was determined, the parameters that govern the shape of the force-time curves were continually modified, until a set of parameters that closely matches the experimental curves was obtained. Subsequently, by altering these parameters and comparing their force-time curves, the significance of these parameters to how they contribute to the overall mechanical properties of the two-cell system can be observed.

5.1 Details of the Force-Time Curve

Figure 5.1 shows a typical simulated force-time curve. The simulated curve closely resembles the shape of the experimental curve in Figure 5.2. Simulations were run in three separate phases: compression, relaxation, and separation.
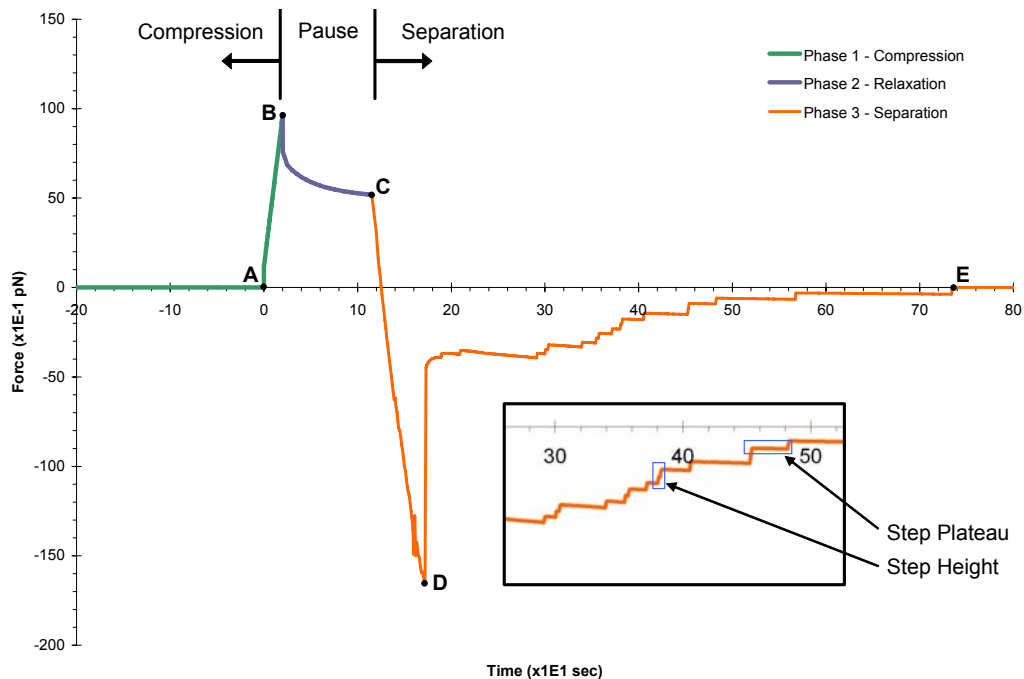
Figure 5.1 – Simulated Force-Time Curve
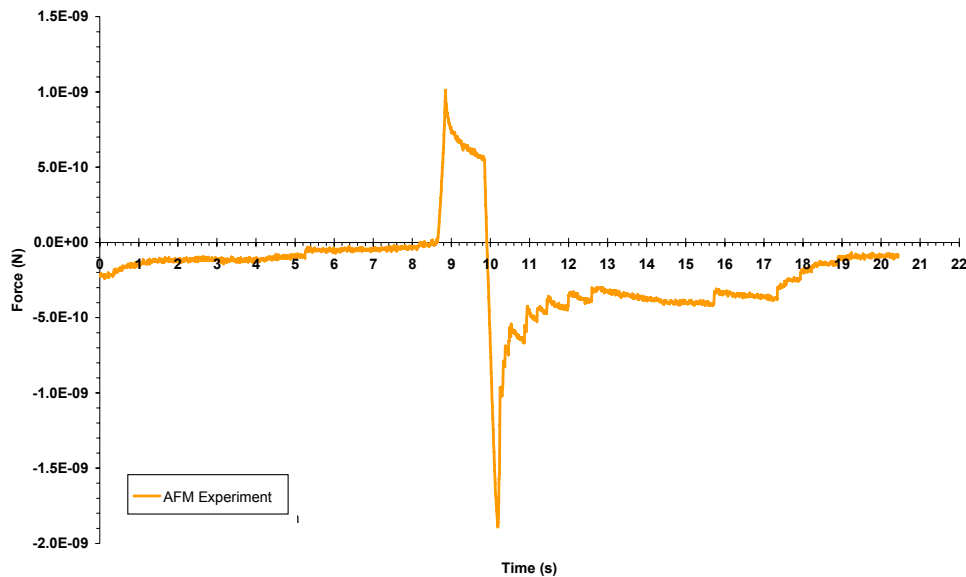
Figure 5.2 – Experimental Force-Time Curve

For this particular simulation, the cells were compressed at a rate of 5 µm/s for 0.2 seconds, relaxed for 1 s, and finally, pulled apart at a rate of 5 µm/s until the cells were separated. These loading conditions were used for the parametric study and in comparing with the experiment curves.

Prior to the compression phase, the cells were not in contact, resulting in a zero force. At the beginning of the compression phase at point A, an initial force F is required to compress the cells, which changes the velocity of the system. This force increases linearly as the cells deform, until the compression phase has completed at point B.

In the relaxation phase, the squished cells are held in position for a pre-defined time period, which allow the cells to anneal and reshape. An initial drop in force was observed, primarily due to changes in the peizo-velocity. During the relaxation phase, the force required to hold the cells slowly decays until it reaches a steady-state force Fss at point C.

In the separation phase, the cells are pulled apart and the applied force decreases and eventually becomes negative. At point D, the de-adhesion peak, all the Interfacetruss bond

elements either break off or become tethers. The reduction in strength of these elements decreases the negative pulling force required to separate the cells. The tethers rupture stochastically creating step patterns in the force-time curve. As shown in the squared box, the steps created by the rupture of tethers are followed by a plateau, until the next rupture event occurs. Ultimately, all the tether elements are ruptured and no force is needed to pull the cells apart at point E.

5.2 Convergence Test on Mesh Size

To verify whether or not these simulations are valid for any mechanical analysis, the number of elements used for the cell was varied. For the convergence test, four simulations were ran using 5, 20, 50, and 100 Area2D elements. The force-time curves are shown in Figure 5.3. As shown in the figure, increasing the number of elements used for the cell, the steady-state force approaches 900 pN. It was observed that using 50 or 100 elements is sufficient to yield convincing results for qualitative analysis. However, using too many elements in the simulations will require large computations. As such, the parametric studies were performed using 50 elements.
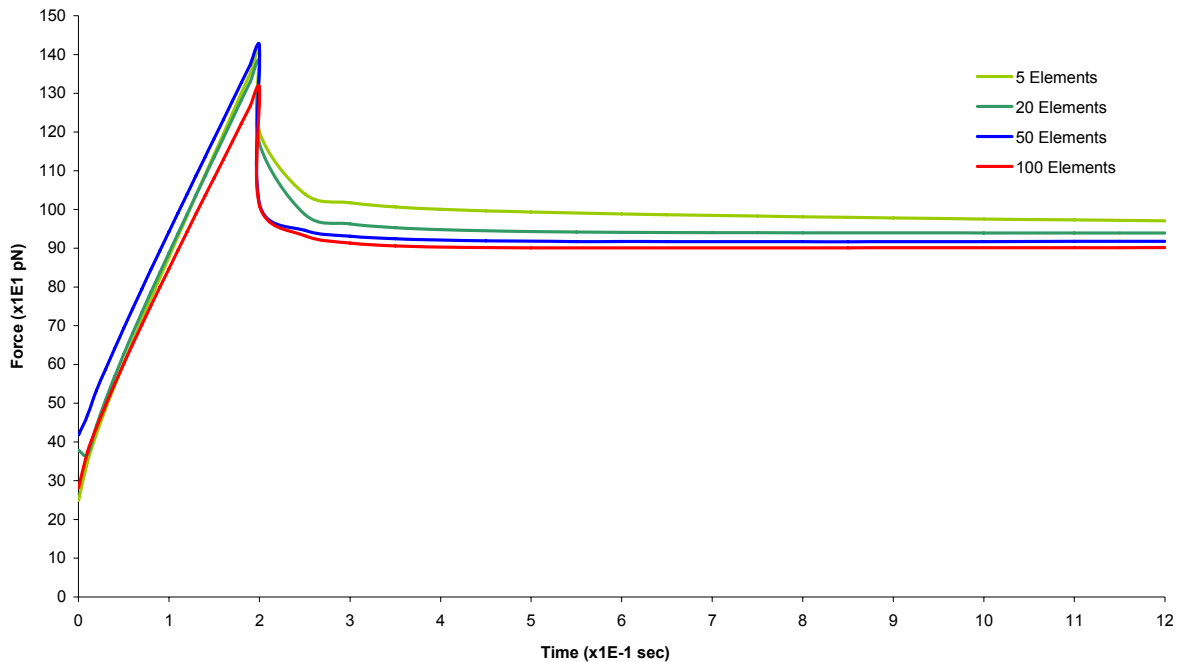
Figure 5.3 – Effects of Mesh Size on Force-Time Curve

5.3 Parametric Study of Force-Time Curves

Force-Time curves generated from the computer program are governed by a set of parameters. In this thesis, interest is shown in the understanding of some of these parameters, which are listed in Table 5.1, with their corresponding symbols and units. These units are used throughout this chapter, and will not be shown in the tables that follow.

Table 5.1 – Governing Parameters in the Finite Element Model

Parameters	Symbol	Units
Cell-Cell Interfacial Tension	γ_{cc}	$10^1 \cdot$ pN
Cell-Medium Surface Tension	γ_{cm}	$10^1 \cdot$ pN
Cell-Plate Interfacial Tension	γ_{cp}	$10^1 \cdot$ pN
Cytoplasmic Viscosity	μ	$10^2 \cdot$ pN-s/μm²
Actin Cortex Stiffness	K_{ac}	$10^1 \cdot$ pN
Actin Cortex Damping Coefficient	C_{ac}	$10^0 \cdot$ pN-s
Tether Stiffness	K_{tether}	$10^2 \cdot$ pN /μm
Tether Damping Coefficient	C_{tether}	$10^0 \cdot$ pN-s
Tether Membrane Tension	T_{tether}	$10^1 \cdot$ pN
Tether Rupture Lifetime	K_{TR}, λ_{TR}	$10^1 \cdot s^{-1}$, $10^1 \cdot pN^{-1}$
Tether Formation Lifetime	K_{TF}, λ_{TF}	$10^1 \cdot s^{-1}$, $10^1 \cdot pN^{-1}$
Bond Rupture Lifetime	K_{BR}, λ_{BR}	$10^1 \cdot s^{-1}$, $10^1 \cdot pN^{-1}$

In the parametric study, each variable in the list is varied while all other variables remain constant. By studying individual variables case by case, the effects of each parameter have on the simulated force-time curves can be observed.

5.3.1 Interfacial Tension at the Cell-Cell Interface

The relationships between interfacial tension and forces were examined first. Four different cases were simulated to observe the effect of interfacial tension γ_{cc} on the force-time curve. Computer simulations were performed to the end of relaxation phase, until the cells were in

total relaxation and the applied force reaches steady-state. The cases are listed in Table 5.2, and the resulting force-time curve is shown in Figure 5.4.

Table 5.2 – Simulations ran for Various Interfacial Tension Values

Case	γ_{cc}	γ_{cm}	γ_{cp}	μ	K_{ac}	C_{ac}
1	**1020**					
2	**1000**	1000	1000	10	1	10
3	**980**					
4	**960**					
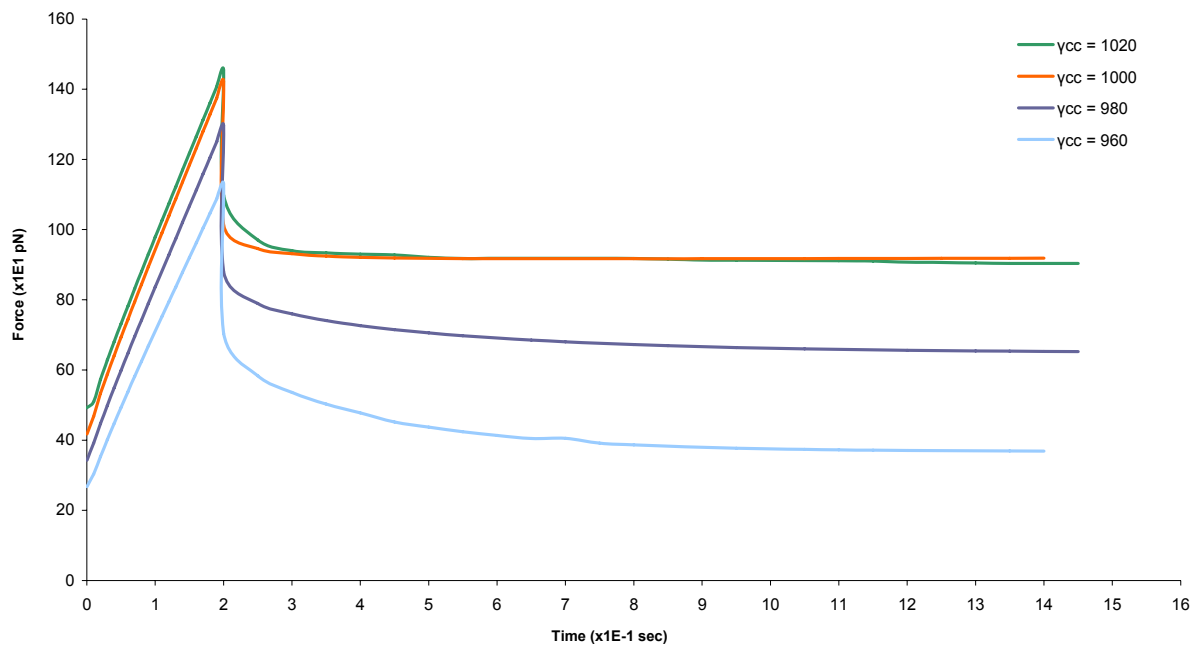
Figure 5.4 – Effects of Interfacial Tension on the Force-Time Curve

As the interfacial tension between the cells increase, the peak force and the steady-state force increases. It was noticed that as γ_{cc} approaches the γ_{cm}, the differences become less dominant. The reason for this is that if γ_{cc} is larger than γ_{cm}, the cells will try to minimize the contact surface. Since initially the contact region was assigned to be small, there will be a limit

where the contact region can no longer shrink, when the maximum allowable steady-state force is reached.

It was also observed that the larger the difference between the interfacial and surface tensions, the longer it takes for the cells to reach the equilibrium steady-state force. This correlation is due to the fact that the difference in interfacial and surface tensions causes the cells to anneal. As this difference increases, the annealing process will take longer to complete.

5.3.2 Surface Tension at Cell-Medium Boundary

Four different cases with varying cell-medium surface tension were simulated, which are summarized in Table 5.3. The resulting force-time curve is shown in Figure 5.5.

Table 5.3 –Simulations for Various Cell-Medium Surface Tension Values

Case	γ_{cc}	γ_{cm}	γ_{cp}	μ	K_{ac}	C_{ac}
1		**1040**				
2		**1020**				
3	1000	**1000**	1000	10	1	10
4		**980**				
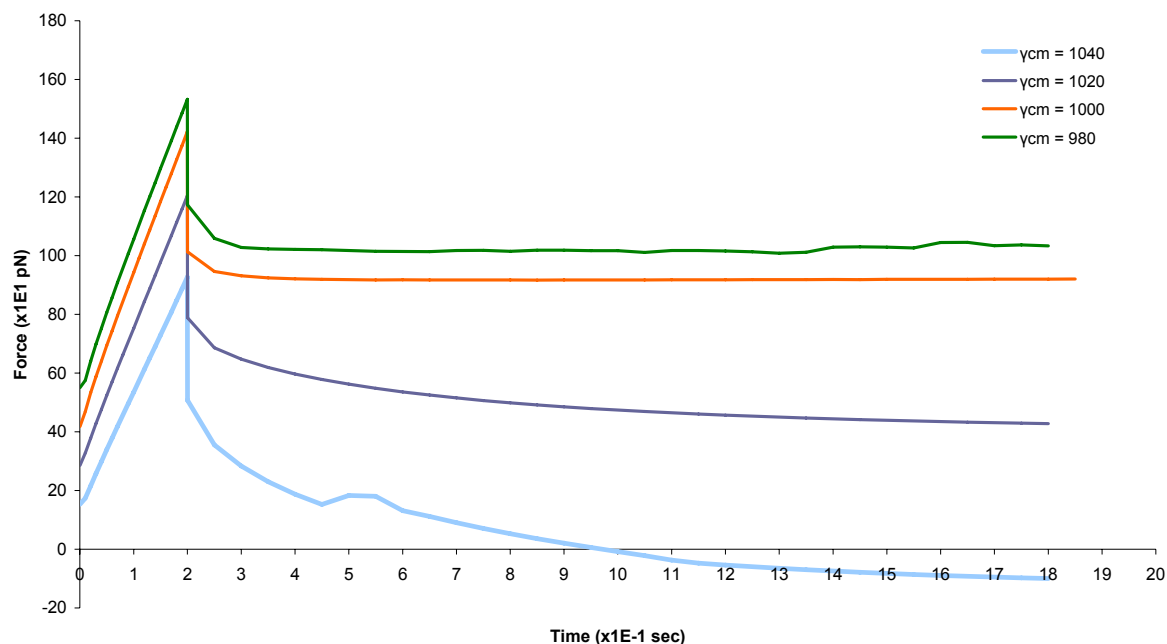
Figure 5.5 – Effects of Cell-Medium Surface Tension on the Force-Time Curve

As shown in Figure 5.5, increasing the cell-medium tension causes the peak force and steady-state force to decrease. Rather than a positive correlation, a negative correlation between cell-medium surface tension γ_{cm} and the forces was observed. However, as the differences between the tensions becomes large, it takes longer for the force to reach equilibrium, as shown in the previous section.

Interestingly, when the cell-medium tension becomes large compared to the interfacial tensions, the steady-state force becomes negative which means that a pulling force is required to hold the cells in that position. This implies that the extent of compression has not yet surpassed the level at which the cells would, if they are allow to anneal freely. Therefore, a negative pulling force is needed to keep the cells from annealing downward. Figure 5.6 shows the resulting height differences between: a) compressed cells; b) cells of high cell-medium tensions without compression but annealed through time; and c) cells of low cell-medium tensions without compression but annealed through time.

- Cells With Compression
- Cells Without Compression
  - γcm = 1040
  - γcc = 1000
- Cells Without Compression
  - γcm = 980
  - γcc = 1000
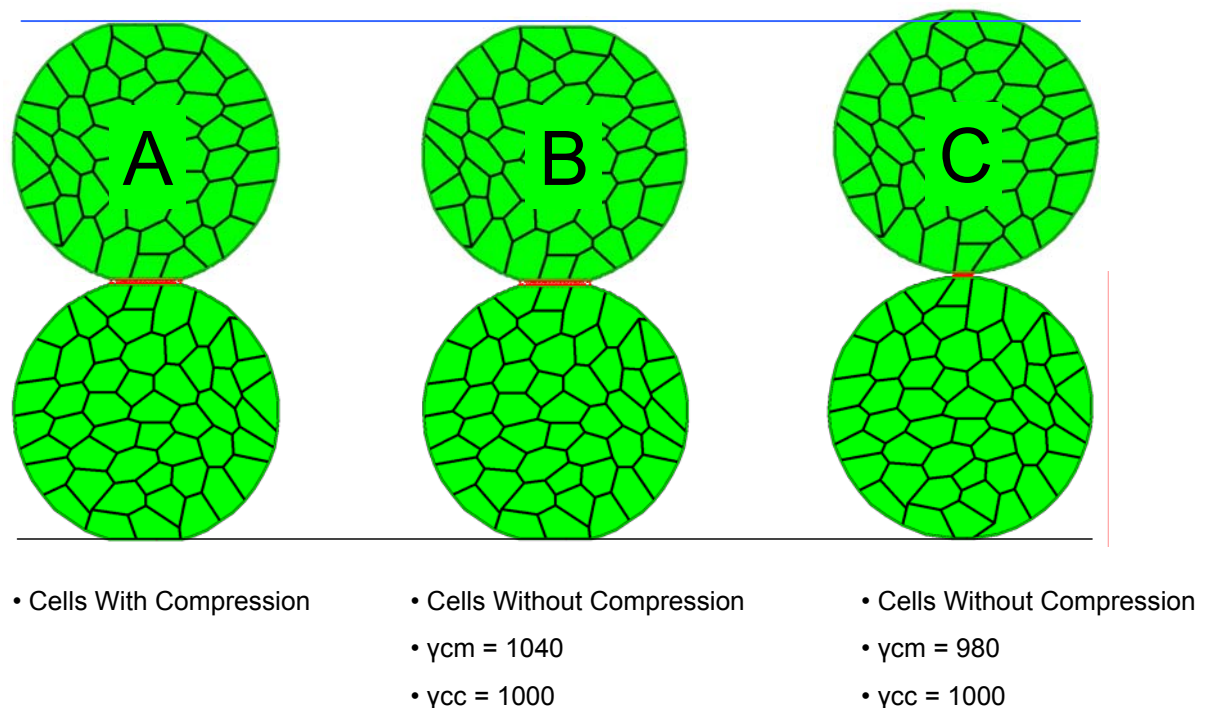
Figure 5.6 – Height Differences of Annealed Cells of varying Cell-Medium Tensions

As shown in cell A, since a displacement of 1 μm was imposed, the cells will remain compressed by 1 μm regardless of the assigned tension along the cell boundaries. However, if no boundary condition were assigned to cells with varied boundary tensions, they would anneal and change heights. In cells B, the cell-medium tensions are high. In order to minimize the energy in the system, the cells have to reduce its cell-medium surface, which lower the overall height of the cells by 1.06 μm, below the blue line. Yet in the simulations, only a downward displacement of 1 μm was imposed. As such, a negative pulling force is necessary to hold the cells at that predefined level. Furthermore, it is shown in cells C that lowering the cell-medium surface tension requires more force to compress the cell system downward.

5.3.3 Interfacial Tension at the Cell-AFM Plate Contact

To observe the relationships between the cell-plate interfacial tension and the resulting peak and steady-state forces F_{ss}, four cases with varying cell-plate tension were ran, as listed in Table 5.4. Figure 5.7 shows the resulting force-time curves.

Table 5.4 – Simulations for Various Cell-Plate Interfacial Tension Values

Case	γ_{cc}	γ_{cm}	γ_{cp}	μ	K_{ac}	C_{ac}
1			**1020**			
2	1000	1000	**1000**	10	1	10
3			**980**			
4			**960**			
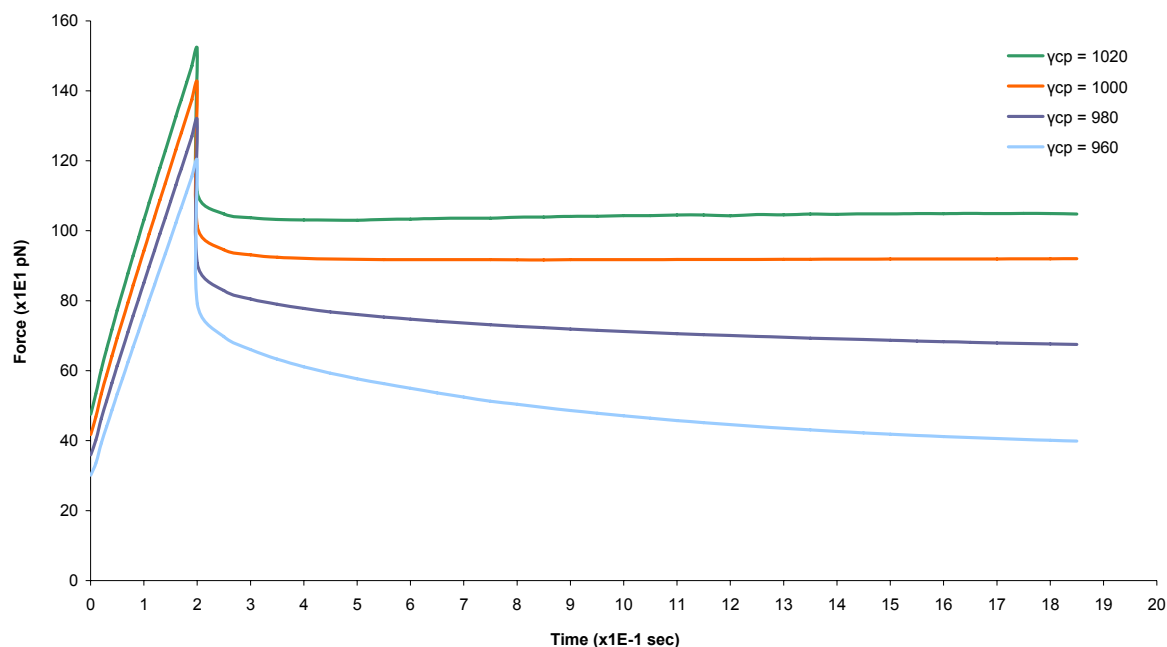
Figure 5.7 – Effects of Cell-Plate Surface Tension on the Force-Time Curve

As in the case of varying cell-cell interfacial tension, increasing the cell-plate surface tension will generate higher peak and steady-state forces. Furthermore, it takes a shorter duration before the cells reaches steady-state, and it can be seen that the slope of the curve in the compression phase increases with increasing cell-plate surface tension.

5.3.4 Cytoplasmic Viscosity

The cytoplasmic viscosity provides the time-dependent behaviour of the cells, and therefore, three different cases with varying viscosity were simulated to observe this relationship. Table 5.5 summarized the three cases. Figure 5.8 shows the resulting force-time curves.

Table 5.5 – Simulations for Various Cytoplasmic Viscosity Values

Case	γ_{cc}	γ_{cm}	γ_{cp}	μ	K_{ac}	C_{ac}
1				**15**		
2	1000	1000	1000	**10**	1	10
3				**5**		
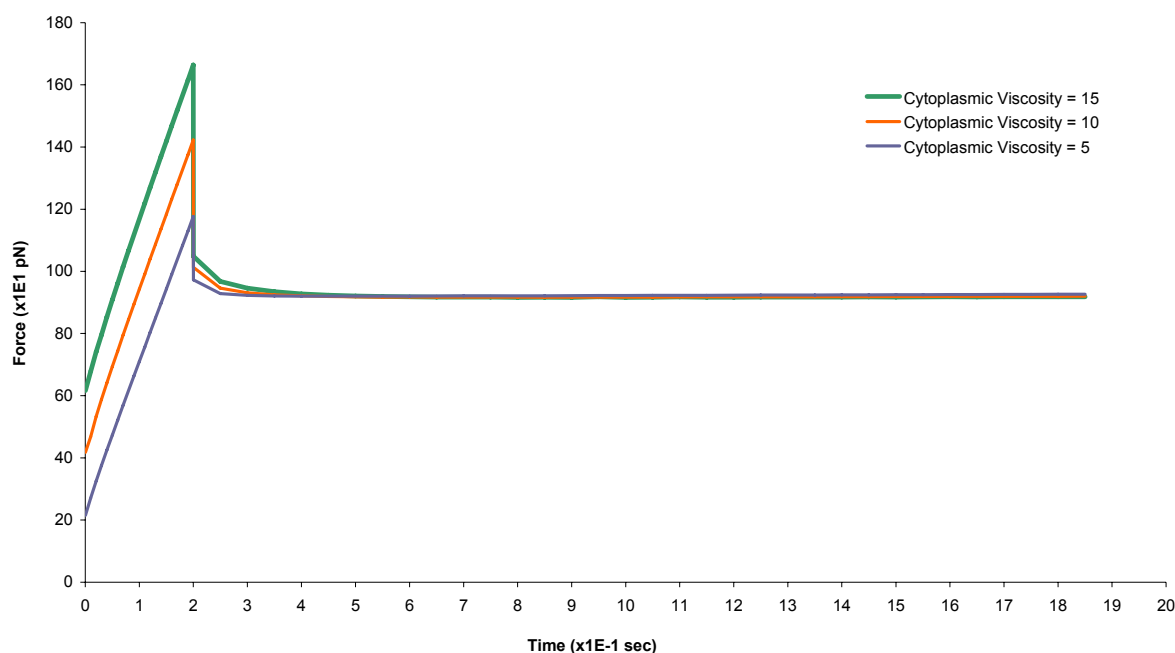
Figure 5.8 – Effects of Cytoplasmic Viscosity on the Force-Time Curve

The curves indicate that as the cytoplasmic viscosity increases, the force contribution from the cytoplasm also increases. In addition, the viscosity increases the peak force at the end of the compression phase. Surprisingly, cytoplasmic viscosity has no effect on the steady-state force when relaxation reaches equilibrium. However, the initial decay in the relaxation phase

shows that a viscous cytoplasm will require more time for the steady-state force to be reached.

5.3.5 Actin Cortex Stiffness

Three different curves were also simulated with varying actin cortex stiffness. The tension parameters γ_{cc}, γ_{cm}, and γ_{cp} are all set to 1000, and the cytoplasmic viscosity is set to 10. Table 5.6 summarized these parameters. Figure 5.9 shows the resulting force-time curves.

Table 5.6 – Simulations for Various Actin Cortex Stiffness Values

Case	γ_{cc}	γ_{cm}	γ_{cp}	μ	K_{ac}	C_{ac}
1					**1000**	
2					**100**	
3	1000	1000	1000	10	**1**	10
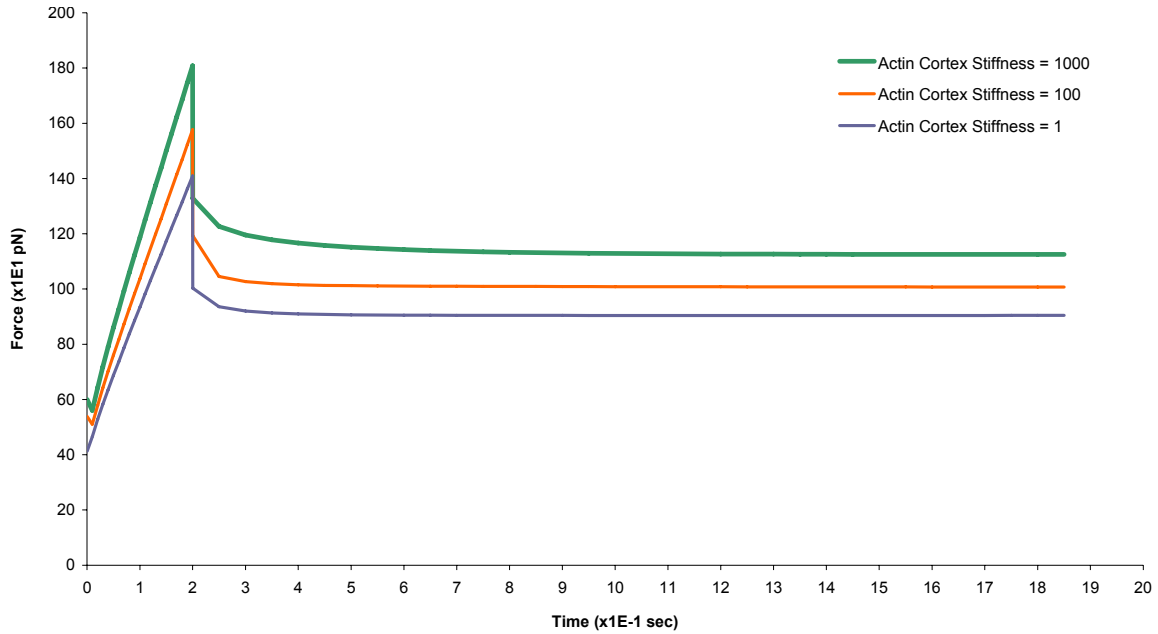
Figure 5.9 – Effects of Actin Cortex Stiffness on the Force-Time Curve

As shown in Figure 5.9, increasing the actin cortex stiffness increases the Young's modulus of the cells, which results in more force required to compress the cells together. Not only does the slope of the compression phase increases, the steady-state force F_{ss} in the relaxation phase also increases due to the change in actin cortex stiffness. In addition, it was observed that the initial jump force F remains unchanged with varying cortex stiffness.

5.3.6 Actin Cortex Damping Coefficient

Since the actin cortex might be of viscoelastic material, three different cases were also simulated with varying actin cortex damping coefficient. Here the actin cortex damping coefficient was varied from 10 to 10,000. Table 5.7 summarized these parameters. Figure 5.10 shows the resulting force-time curves.

Table 5.7 – Simulations for Various Actin Cortex Damping Coefficient Values

Case	γ_{cc}	γ_{cm}	γ_{cp}	μ	K_{ac}	C_{ac}
1						**10000**
2						**1000**
3	1000	1000	1000	10	1	**10**
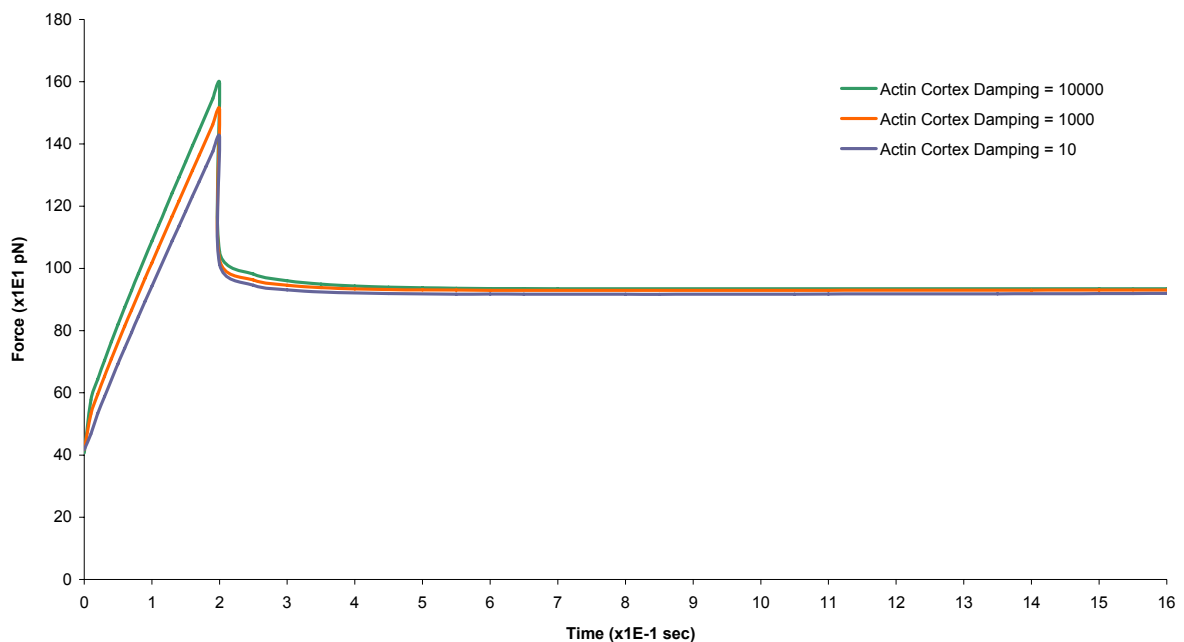
Figure 5.10 – Effects of Actin Cortex Damping Coefficient on the Force-Time Curve

As shown in Figure 5.10, increasing the damping coefficient of the actin cortex causes the peak force to increase slightly. Moreover, very little changes were observed in the steady-state force. This indicates that the damping coefficient of the actin cortex is has little or no effect on the force-time curves.

5.4 Properties of Molecular Attachments

To understand the mechanical properties of bonds and tethers, an analysis was carried out to compare the force-time curves resulted from the two tether models: viscoplastic and viscoelastic. First, a parametric study for tethers and molecular bond is conducted using the viscoplastic model. Secondly, a similar study was carried out using the viscoelastic model. Major differences between the two models are then discussed briefly. Lastly, force-time curves simulated using the FE model are compared with the experimental results. In doing so, the properties of the molecular bonds along the cell-cell interface can be approximated.

Given that bond rupture and tether formation occur during the third phase, the model pre-defined the mechanical properties for the cell, as listed in Table 5.8. These values were chosen by adjusting these parameters in the input file until the resulting force-time curve closely matches experimental results, as shown in Figure 5.11. To imitate the rest of the experimental curve, the separate phase begins 12.0 seconds after the cells were in contact.

Table 5.8 – Pre-defined Values for the Mechanical Properties of the Cells

γ_{cc}	γ_{cm}	γ_{cp}	μ	K_{ac}	C_{ac}
1000	1015	1000	5	10	0.01
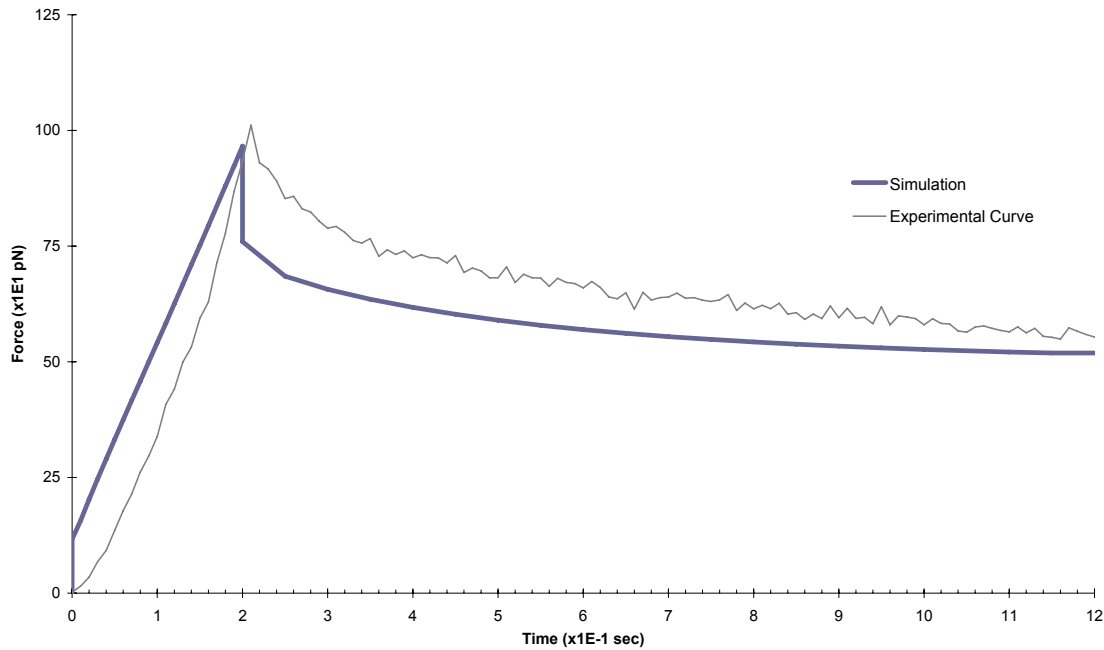
Figure 5.11 – Simulation and Experimental Results from the Compression and Relaxation
Phases

Values were also assigned to the mechanical parameters governing the InterfaceTruss elements, which are listed in Table 5.9. As mentioned previously, bond type InterfaceTruss elements will be very stiff while free type elements represent a molecular connection that no longer exists. As such, the stiffness coefficient *K* for the Bond and Free type elements would

be 100,000 and 0 respectively. However, the tether mechanical properties are subject to change during our parametric studies.

Table 5.9 – Values for the Mechanical Properties of the InterfaceTruss Elements

InterfaceTruss Type	Stiffness K	Damping C	Tension T
Bond	100,000	0	0
Free	0	0	0
Tether	0	0.1	2

5.4.1 Tether Membrane Tension in the Viscoplastic Model

To examine the relationships between tether membrane tension and the resulting force-time curves, three cases with varying tether membrane tension were simulated. The cases are listed in Table 5.10. The resulting force-time curve is shown in Figure 5.12.

Table 5.10 – Simulations for Various Tether Membrane Tension Values (Viscoplastic)

Case	K_{tether}	C_{tether}	T_{tether}
1			**3**
2	0	0.1	**2**
3			**1**
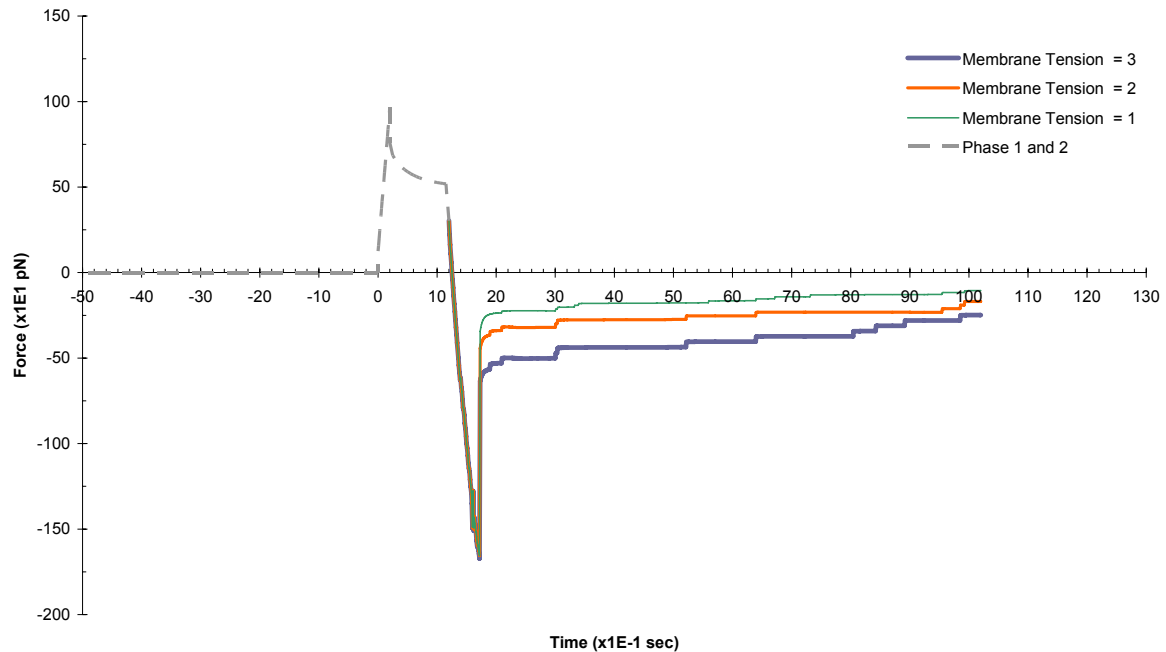
Figure 5.12 – Effects of Viscoplastic Tether Membrane Tension on the Curve

It was observed that increasing the tether membrane tension will increase the negative pulling required to separate the cells. The simulations also showed that this tension in the tether will not influence the curve before the de-adhesion peak, because none of the tethers have been formed yet. In addition, it was found that increasing the tether tension will not have a significant effect on the lifetime of the tether rupture. However, there are noticeable changes in the height of the step-events during tether rupture, where the height of these steps increases with increasing tether membrane tension.

5.4.2 Tether Damping Coefficient in the Viscoplastic Model

Since tethers might exhibit viscous behaviour, a parametric study on tether damping coefficient was conducted. Three simulations with varying tether damping coefficient were performed. The cases are listed in Table 5.11, and the resulting force-time curve is shown in Figure 5.13.

Table 5.11 – Simulations for Various Tether Damping Coefficient Values (Viscoplastic)

Case	K_{tether}	C_{tether}	T_{tether}
1		**0.1**	
2	0	**1**	2
3		**2**	

Figure 5.13 – Effects of Viscoplastic Tether Damping Coefficient on the Curve

As shown in the figure, increasing the tether damping coefficient C_{tether} increases the force required to pull the cells apart. The increase in force is due to the additional viscous parameter that accounts for the strain rate of these tether tubes. However, as the separation phase continues, the tethers gradually relax and cause the pulling force to decay. Subsequently, the differences between the three cases gradually disappear.

5.4.3 Lifetime of Tether Elements in the Viscoplastic Model

As stated in previous chapters, the lifetime of tethers will have a significant influence on the bond dissociation rate. Here, three cases were considered, where the tether rupture coefficient $K_{TR\text{-upper}}$ for the upper bound lifetime curves were varied while the lower bound lifetime curve remained the same. Table 5.12 summarizes the parameters used in the three cases, and Figure 5.14 shows the resulting force-time curves.

Table 5.12 – Simulations for Various Tether Rupture Coefficient Values (Viscoplastic)

Case		1	2	3
Tether Formation	$K_{TF\text{-upper}}$ / $K_{TF\text{-lower}}$		0.045 / 0.055	
	λ_T		0.0015	
Bond Rupture	$K_{BR\text{-upper}}$ / $K_{BR\text{-lower}}$		0.045 / 0.055	
	λ_{BR}		0.0015	
Tether Rupture	$K_{TR\text{-upper}}$ / $K_{TR\text{-lower}}$	**0.001 / 0.05**	**0.0005 / 0.05**	**0.0001 / 0.05**
	λ_{TR}		0.05	
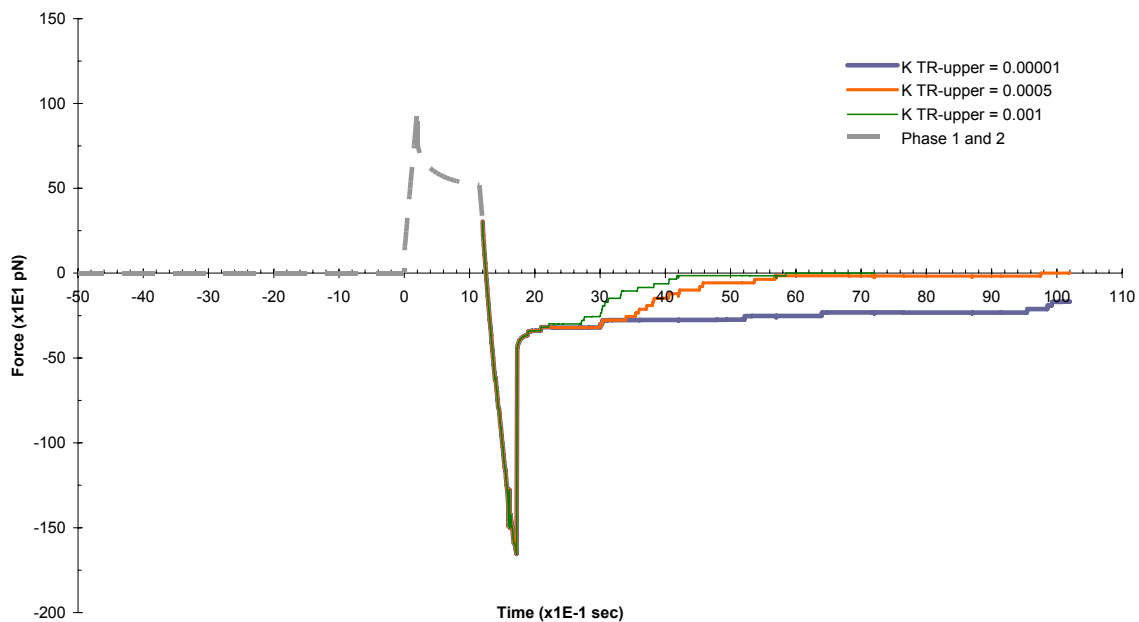
Figure 5.14 – Effects of Viscoplastic Tether Rupture Coefficient on the Curve
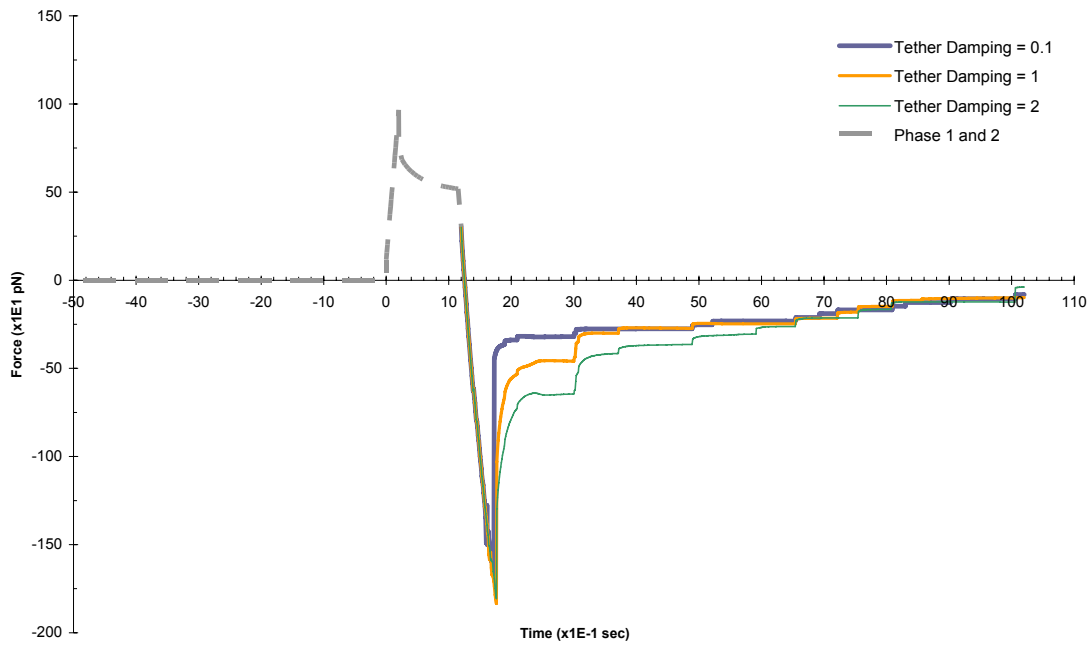
As shown in the figure, as the tether rupture coefficient $K_{TR-upper}$ increases, the step-like events in the curve will occur much faster. Subsequently, total separation, in which all the tethers are ruptured, will happen much sooner. This is because the $K_{TR-upper}$ is inversely-proportion to the lifetime. Therefore, higher $K_{TR-upper}$ will result in lower lifetime for any given force. As such, tethers are more likely to dissociate with high $K_{TR-upper}$. Furthermore, the portion of the force-time curve prior to the de-adhesion peak does not depend on the lifetime of these tethers.

5.4.4 Lifetime of Bond Elements in the Viscoplastic Model

Here the relationships between molecular bond dissociation rates and the force-time curve will be discussed. Since an attached molecular bond could be either coupled to the cytoskeleton or connected to the cell membrane (Evans, 1995), the finite element model incorporates two different sets of lifetime parameters for the bond: those bonds that will become Tether type InterfaceTruss elements; and Free type InterfaceTruss elements. First, three cases with varied tether formation coefficients K_{TF} for were considered. Table 5.13 lists the lifetime. The resulting force-time curves are summarized in Figure 5.15.

Table 5.13 – Simulations for Various Tether Formation Coefficient Values (Viscoplastic)

Case		1	2	3
Tether Formation	$K_{TF-upper}$ / $K_{TF-lower}$	**0.035 / 0.045**	**0.045 / 0.055**	**0.055 / 0.065**
	λ_T		0.0015	
Bond Rupture	$K_{BR-upper}$ / $K_{BR-lower}$		0.045 / 0.055	
	λ_{BR}		0.0015	
Tether Rupture	$K_{TR-upper}$ / $K_{TR-lower}$		0.0005 / 0.05	
	λ_{TR}		0.05	

Figure 5.15 – Effects of Viscoplastic Tether Formation Coefficient on the Curve

The simulated curves show that increasing the tether formation coefficient K_{TF} will generate a smaller de-adhesion peak, because bonds are more likely and quickly to become tethers. Subsequently, rather than being freely detached, more bonds will develop into tethers. As a result, larger applied forces will be required to lengthen the tethers and pull the cells apart. It is also interesting to note that total separation of the cells will occur at a later time because of the increased number of tethers at the cell-cell interface. Contrarily, having a lower K_{TF} will cause a reduction in tether formation, causing bonds dissociate freely. As a result, no force will be needed to pull the cells apart.

Three additional cases with varied bond rupture coefficient for uncoupled bonds to freely detach were also considered. Table 5.14 lists the lifetime, while the resulting fore-time curves are summarized in Figure 5.16.

Table 5.14 – Simulations for Various Bond Rupture Coefficient Values (Viscoplastic)

Case		4	5	6
Tether Formation	$K_{TF\text{-upper}}$ / $K_{TF\text{-lower}}$		0.045 / 0.055	
	λ_T		0.0015	
Bond Rupture	$K_{BR\text{-upper}}$ / $K_{BR\text{-lower}}$	**0.035 / 0.045**	**0.045 / 0.055**	**0.055 / 0.065**
	λ_{BR}		0.0015	
Tether Rupture	$K_{TR\text{-upper}}$ / $K_{TR\text{-lower}}$		0.0005 / 0.05	
	λ_{TR}		0.05	

Figure 5.16 – Effects of Viscoplastic Bond Rupture Coefficient on the Curve

Similar to the tether formation coefficient K_{TF}, increasing the bond rupture coefficients K_{BR} will reduce the de-adhesion peak. However, unlike the previous case, increasing these rates will cause more bonds to become freely detached, reducing the required pulling force after the de-adhesion peak. Furthermore, it was observed that the force-time curves for Cases 3

and 4 in this section are almost identical. This suggests that increasing K_{TF} and reducing K_{BR} have equivalent effects on the number of tethers that will form after the de-adhesion peak.

5.4.5 Tether Membrane Tension in the Viscoelastic Model

In the following sections, the relationships between the mechanical properties in the viscoelastic model and the resulting force-time curves are discussed. First, three cases of varied tether membrane tensions were simulated, which are listed in Table 5.15. The force-time curves are shown in Figure 5.17.

Table 5.15 – Simulations for Various Tether Membrane Tension Values (Viscoelastic)

Case	K_{tether}	C_{tether}	T_{tether}
1			**1**
2	0.025	0.1	**2**
3			**3**
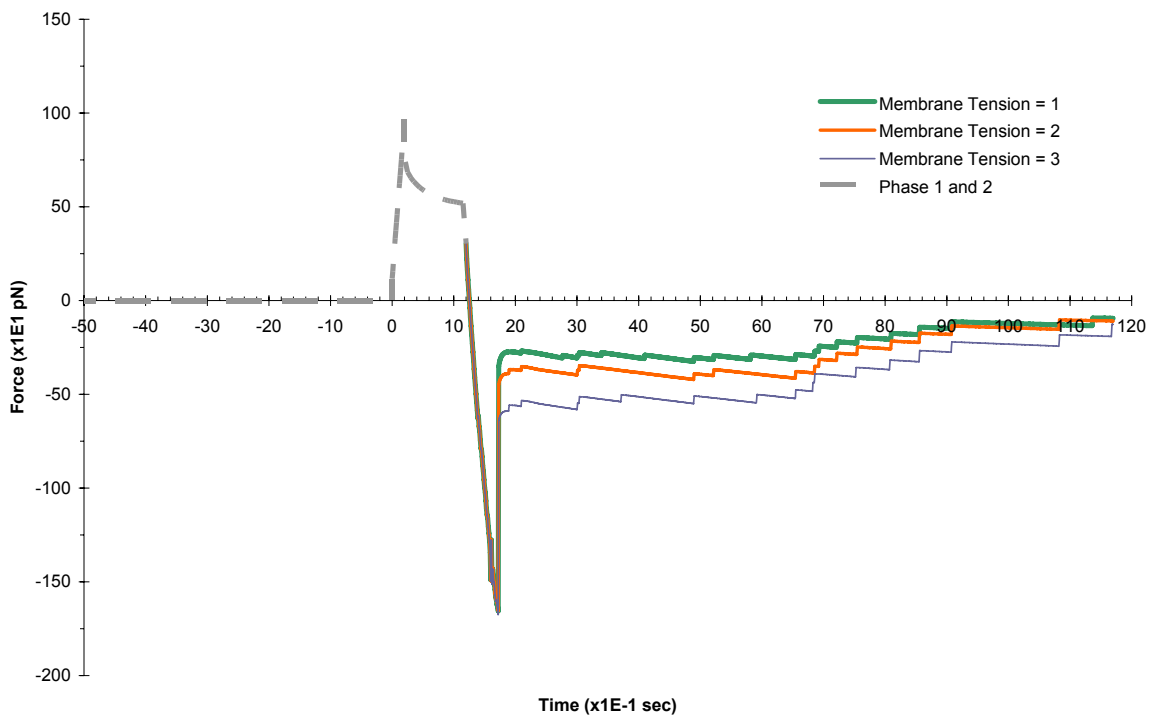
Figure 5.17 – Effects of Viscoelastic Tether Membrane Tension on the Curve

In the viscoelastic model, the step patterns after the de-adhesion peak were also observed, as in the viscoplastic model. However, due to the additional stiffness component of the tether, the flat plateaus observed in the previous model are now sloped. In addition, the steepness of the slopes appear to reduce as more and more tethers rupture. This suggests that the overall stiffness of the system is reduced as the tethers in the cell-cell interface are ruptured.

The figure also indicates that increasing the tether membrane tension parameter will increase the negative pulling force required to separate the cells. Also, any changes in the tension parameter will not have a significant effect on the likelihood of tether rupturing, since the time at which tether breaks remains somewhat constant. Moreover, the slope of the plateaus after each step event does not change with varied tether membrane tensions. Again, the membrane tension does not influence the portion of the force-time curve prior to the de-adhesion peak.

5.4.6 Tether Membrane Stiffness in the Viscoelastic Model

The stiffness of the tethers is another significant parameter that may govern the shape force-time curves. Three different cases with varying stiffness were considered and are listed in Table 5.16. Figure 5.18 shows the resulting force-time curve.

Table 5.16 – Simulations for Various Tether Stiffness Values (Viscoelastic)

Case	K_{tether}	C_{tether}	T_{tether}
1	**0.1**		
2	**0.05**	0.1	2
3	**0.025**		
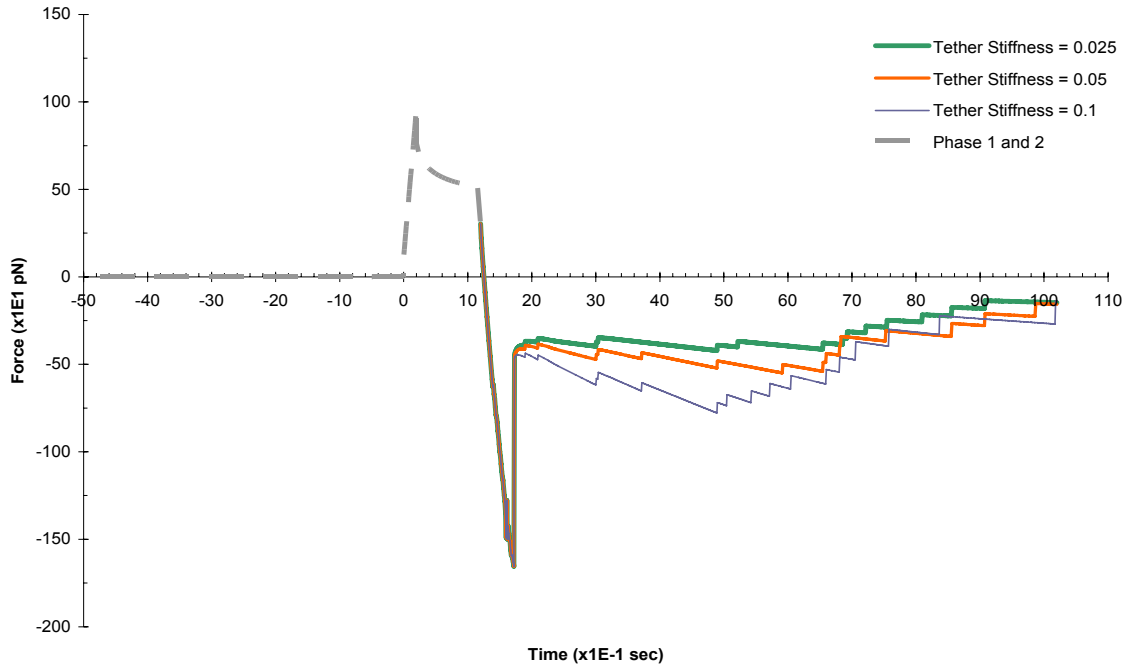
Figure 5.18 – Effects of Viscoelastic Tether Stiffness on the Curve

As shown in the curve, increasing the stiffness coefficient of the tether will increase the required pulling force to separate the cells. This increase also causes the slopes of each plateau to become steeper. Since the steepness of the plateau causes the applied forces to increase at different rates, it also affects the time at which a tether would rupture. Finally, the portion of the force-time curve prior to the de-adhesion peak is independent of the tether stiffness coefficient.

5.4.7 Lifetime of Tether Elements in the Viscoelastic Model

To examine the relationships between tether lifetime in the viscoelastic model and the force-time curve, three different cases were set up, with varying tether rupture coefficients. Table 5.17 summarized these parameters, and Figure 5.19 shows the resulting force-time curves.

Table 5.17 – Simulations for Various Tether Rupture Coefficient Values (Viscoelastic)

Case		1	2	3
Tether Formation	$K_{TF\text{-upper}}$ / $K_{TF\text{-lower}}$		0.045 / 0.055	
	λ_T		0.0015	
Bond Rupture	$K_{BR\text{-upper}}$ / $K_{BR\text{-lower}}$		0.045 / 0.055	
	λ_{BR}		0.0015	
Tether Rupture	$K_{TR\text{-upper}}$ / $K_{TR\text{-lower}}$	**0.00015 / 0.05**	**0.0003 / 0.05**	**0.0006 / 0.05**
	λ_{TR}		0.05	
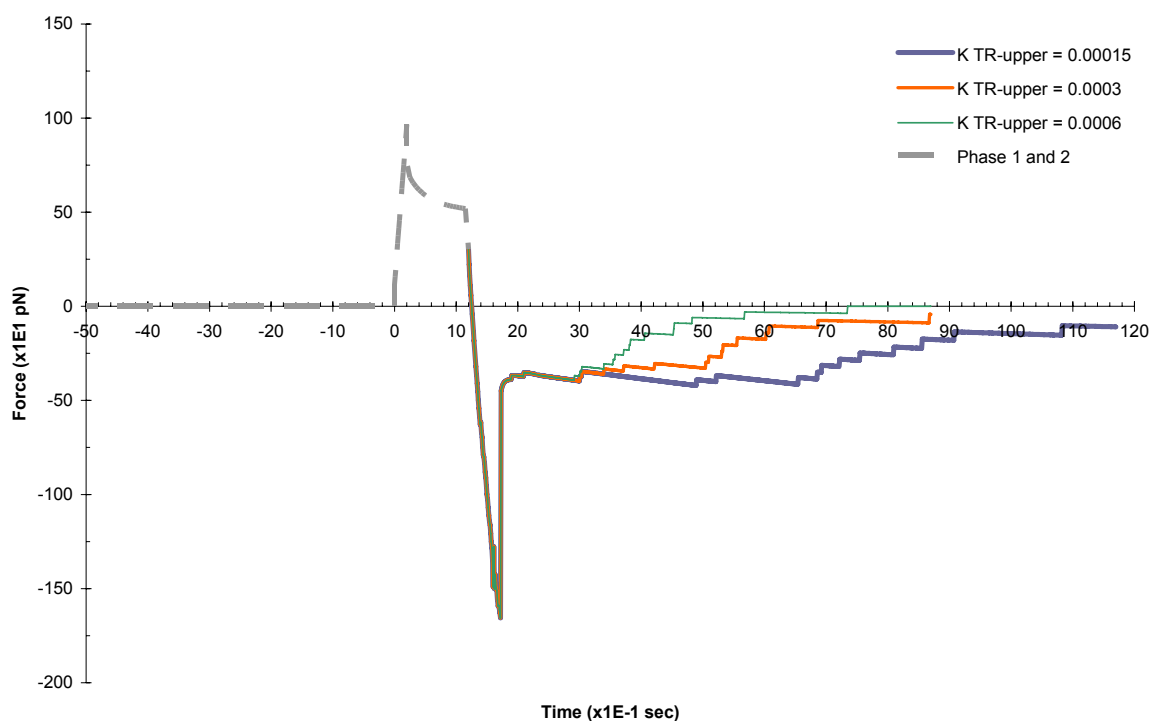
Figure 5.19 – Effects of Viscoelastic Tether Rupture Coefficient on the Curve

As indicated by the curves, increasing the tether rupture coefficient $K_{TR\text{-upper}}$ will cause the tethers to rupture at a faster rate, because the likelihood of a tether rupture has increased. This also suggests that lower $K_{TR\text{-upper}}$ will take a longer pulling time for total separation. Moreover, it was observed that the slope of the plateau reached zero much sooner with high

$K_{TR\text{-}upper}$, which means that the steepness of the plateaus depends directly on the number of remaining tethers and their stiffness, rather than contact time of the tethers or the extent of separation.

5.4.8 Lifetime of Bond Elements in the Viscoelastic Model

The correlation between bond lifetime and the force-time curve are examined here. As usual, three cases with varying bond rupture coefficients for bond dissociation were considered, and are listed in Table 5.18. Figure 5.20 shows the resulting force-time curve.

Table 5.18 – Simulations for Various Bond Rupture Coefficient Values (Viscoelastic)

Case		1	2	3
Tether Formation	$K_{TF\text{-}upper}$ / $K_{TF\text{-}lower}$		0.045 / 0.055	
	λ_T		0.0015	
Bond Rupture	$K_{BR\text{-}upper}$ / $K_{BR\text{-}lower}$	**0.035 / 0.045**	**0.045 / 0.055**	**0.055 / 0.065**
	λ_{BR}		0.0015	
Tether Rupture	$K_{TR\text{-}upper}$ / $K_{TR\text{-}lower}$		0.00015 / 0.05	
	λ_{TR}		0.05	

Figure 5.20 – Effects of Viscoelastic Bond Rupture Coefficient on the Curve

As shown in the curve, as the bond rupture coefficient K_{BR} decreases, it becomes less likely for the bonds to freely detach, and the majority of the bonds will want to become tethers instead. As a result, the de-adhesion peak will increase negatively, and require greater applied forces to elongate the tethers and separate the cells apart. Again, due to the number of tethers initially formed right after the de-adhesion peak, the lower K_{BR} curves have greater slopes in their plateau at the beginning. However, in time, more tethers are ruptured and eventually minimize the difference in slope between the three curves.

5.5 Comparison between the Viscoplastic and Viscoelastic Models

A typical experimental curve received from Michael Krieg (personal communication) was compared with force-time curves generated using the two mechanical models, as shown in Figure 5.21. The experimental curve was scaled by a factor of 10^{11} in the force y-axis, and a

factor of 10 in the time x-axis, to account for the fact that each time unit corresponds to 0.1 seconds.
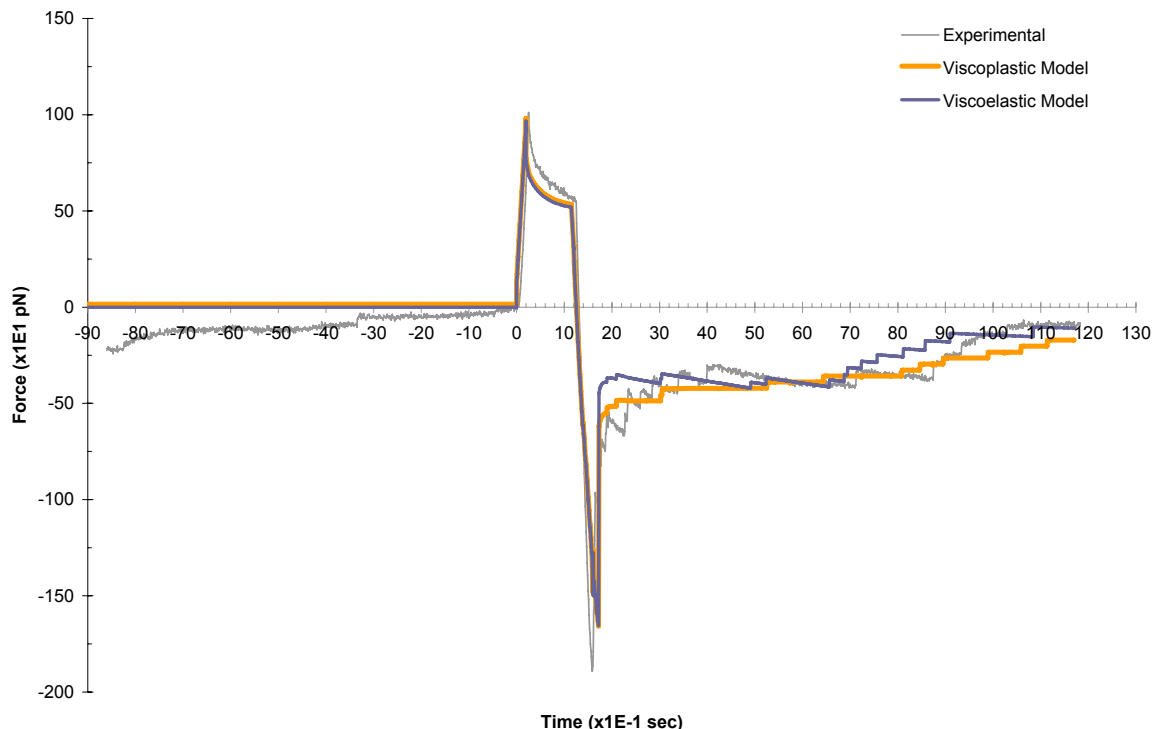
Figure 5.21 – Viscoplastic and Viscoelastic Model Comparsion

The major difference between the two proposed models is the slope of the plateaus after each step event. Since the viscoelastic model comprises of an additional spring, the negative pulling force will increase gradually after tether rupture events. However, since this force depends on the elongation that the tethers are experiencing, the height of the steps is no longer constant and increases slightly through time.

As shown in the purple experimental curve, the negative pulling force increases after each rupture event. This indicates that the tethers might have a stiffness component to them which increases the force required to separate the cells. However, the spring constant in the model will cause the pulling force in the simulation to become large if the tethers remain in contact. The viscoplastic model allows the pulling force to continue to decrease regardless of tether

rupture events. Furthermore, it can generate the somewhat constant rupture forces as observed in the experiments.

5.6 Computer Simulation and Experimental Results Matching

The parametric studies discussed earlier were able to identify the parameters that affect the shape of the force-time curves. Here, the parameters were modified to match three of the experimental curves from the AFM cell adhesion tests. Table 5.19 lists the estimated parameters for Experimental Curve A. The corresponding simulation and experimental curves are shown in Figure 5.22.

Table 5.19 – Parameter Estimations for Experimental Curve A

Parameters	Symbol	Value	Units
Cell-Medium Surface Tension	γ_{cm}	1015	$10^1 \cdot$ pN
Cell-Cell Interfacial Tension	γ_{cc}	1000	$10^1 \cdot$ pN
Cell-Plate Interfacial Tension	γ_{cp}	1000	$10^1 \cdot$ pN
Cytoplasmic Viscosity	μ	5	$10^2 \cdot$ pN-s/μm²
Actin Cortex Stiffness	K_{ac}	1	$10^1 \cdot$ pN
Actin Cortex Damping Coefficient	C_{ac}	10	$10^0 \cdot$ pN-s
Tether Stiffness	K_{tether}	0.025	$10^2 \cdot$ pN /μm
Tether Damping Coefficient	C_{tether}	0.1	$10^0 \cdot$ pN-s
Tether Membrane Tension	T_{tether}	2	$10^1 \cdot$ pN
Tether Rupture Lifetime	K_{TR}	0.00015 – 0.05	$10^1 \cdot$ s^{-1}
	λ_{TR}	0.05	$10^1 \cdot$ pN^{-1}
Tether Formation Lifetime	K_{TF}	0.045 – 0.055	$10^1 \cdot$ s^{-1}
	λ_{TF}	0.0015	$10^1 \cdot$ pN^{-1}
Bond Rupture Lifetime	K_{BR}	0.045 – 0.055	$10^1 \cdot$ s^{-1}
	λ_{BR}	0.0015	$10^1 \cdot$ pN^{-1}
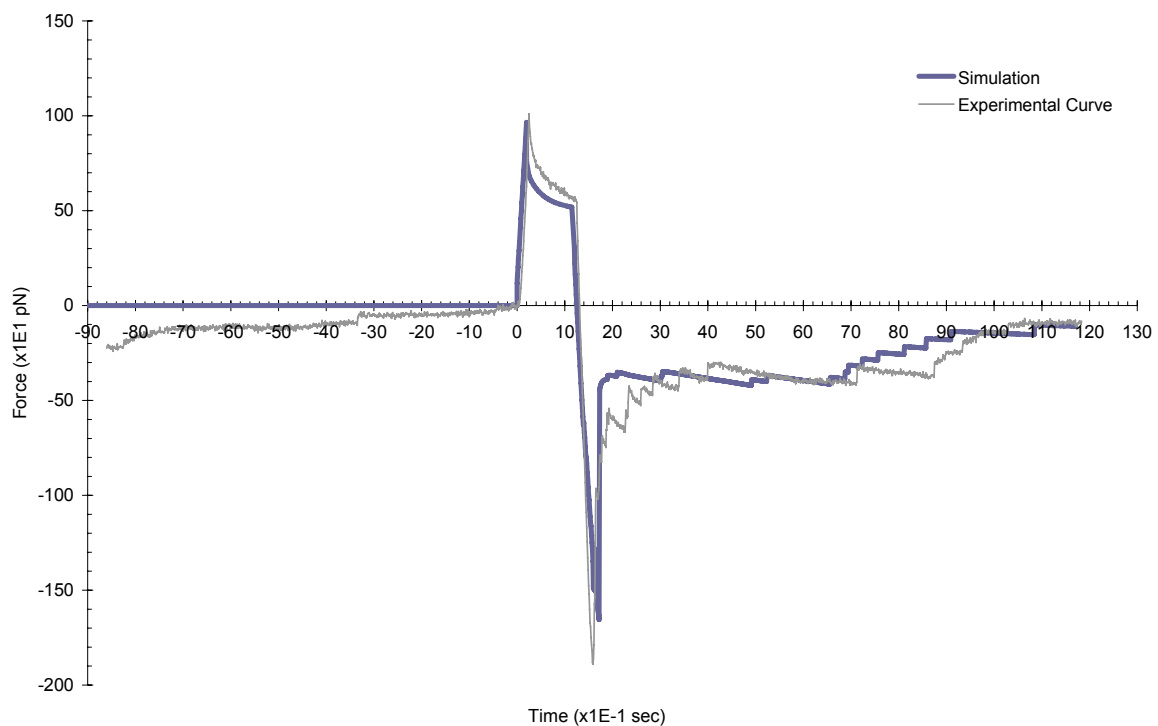
Figure 5.22 – Simulation Matching for Curve A

The simulation from the estimated parameters closely matched the forces at the end of the compression and relaxation phases, as well as the de-adhesion peak force during the separation phase. However, there is an observable difference between the slope of the step plateaus shortly after the de-adhesion peak, which may be due to an unknown factor that was not incorporated into the finite element model.

A set of parameters were also estimated for Experimental Curve B, which are shown in Table 5.20. For this experiment, the cells are squished at a rate of 5 μm/s for 0.2 seconds, relaxed for one second, and finally pulled apart at a rate of 5 μm/s until the cells are separated. Figure 5.23 shows the resulting computer simulation.

Table 5.20 – Parameter Estimations for Experimental Curve B

Parameters	Symbol	Value	Units
Cell-Medium Surface Tension	γ_{cm}	1015	$10^1 \cdot$ pN
Cell-Cell Interfacial Tension	γ_{cc}	1003	$10^1 \cdot$ pN
Cell-Plate Interfacial Tension	γ_{cp}	1003	$10^1 \cdot$ pN
Cytoplasmic Viscosity	μ	5	$10^2 \cdot$ pN-s/μm²
Actin Cortex Stiffness	K_{ac}	1	$10^1 \cdot$ pN
Actin Cortex Damping Coefficient	C_{ac}	10	$10^0 \cdot$ pN-s
Tether Stiffness	K_{tether}	0.01	$10^2 \cdot$ pN /μm
Tether Damping Coefficient	C_{tether}	0.1	$10^0 \cdot$ pN-s
Tether Membrane Tension	T_{tether}	2.5	$10^1 \cdot$ pN
Tether Rupture Lifetime	K_{TR}	0.00015 – 0.05	$10^1 \cdot s^{-1}$
	λ_{TR}	0.05	$10^1 \cdot pN^{-1}$
Tether Formation Lifetime	K_{TF}	0.06 – 0.07	$10^1 \cdot s^{-1}$
	λ_{TF}	0.0015	$10^1 \cdot pN^{-1}$
Bond Rupture Lifetime	K_{BR}	0.06 – 0.07	$10^1 \cdot s^{-1}$
	λ_{BR}	0.0015	$10^1 \cdot pN^{-1}$
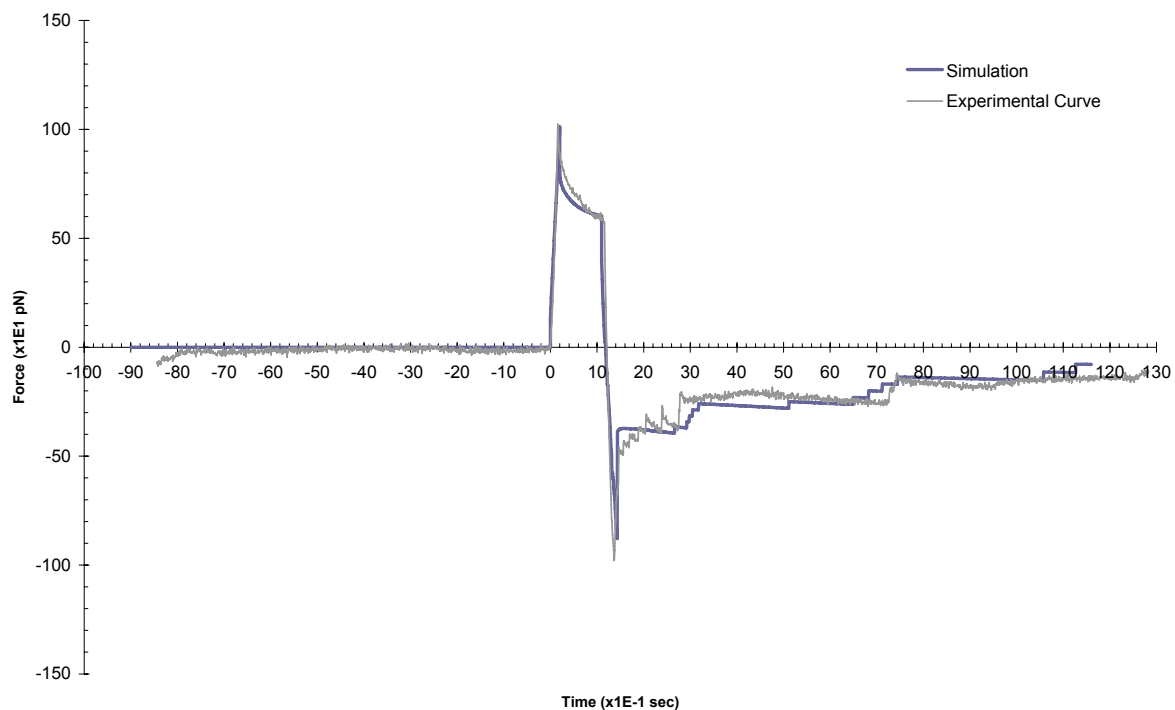
Figure 5.23 – Simulation Matching for Curve B

Experimentals Curve A and B are very similar in the compression and relaxation phases. As such, the cyotplasmic viscosity and the interfacical tensions were only adjusted slightly to accommodate the small differences between Curve A and B. Yet, the de-adhesion peak for Curve B is much is much higher than the one in Curve A. Therefore, the lifetime parameters were adjusted to reduce the lifetime of adhesion bonds. By doing so, the simulated curve achieved the de-adhesion peak value as in the experiment.

A third set of parameters were estimated for Experimental Curve C, which are shown in Table 5.21. Experiment C is very different than the previous two in that the relaxation phase is much longer in duration. The cells are squished at a rate of 5 µm/s for 0.2 seconds, relaxed for 60 seconds, and finally, pulled apart at a rate of 5 µm/s until the cells are separated. Figure 5.24 shows the resulting computer simulation.

Table 5.21 – Parameter Estimations for Experimental Curve C

Parameters	Symbol	Value	Units
Cell-Medium Surface Tension	γ_{cm}	1045	$10^1 \cdot$ pN
Cell-Cell Interfacial Tension	γ_{cc}	1000	$10^1 \cdot$ pN
Cell-Plate Interfacial Tension	γ_{cp}	1000	$10^1 \cdot$ pN
Cytoplasmic Viscosity	μ	1.5	$10^3 \cdot$ pN-s/µm²
Actin Cortex Stiffness	K_{ac}	0.1	$10^1 \cdot$ pN
Actin Cortex Damping Coefficient	C_{ac}	1	$10^1 \cdot$ pN-s
Tether Stiffness	K_{tether}	0.025	$10^2 \cdot$ pN /µm
Tether Damping Coefficient	C_{tether}	0.1	$10^0 \cdot$ pN-s
Tether Membrane Tension	T_{tether}	7	$10^1 \cdot$ pN
Tether Rupture Lifetime	K_{TR}	0.00015 – 0.0165	$10^1 \cdot s^{-1}$
	λ_{TR}	0.05	$10^1 \cdot pN^{-1}$
Tether Formation Lifetime	K_{TF}	0.0165 – 0.0166	$10^1 \cdot s^{-1}$
	λ_{TF}	0.00005	$10^1 \cdot pN^{-1}$
Bond Rupture Lifetime	K_{BR}	0.0165 – 0.0166	$10^1 \cdot s^{-1}$
	λ_{BR}	0.00005	$10^1 \cdot pN^{-1}$
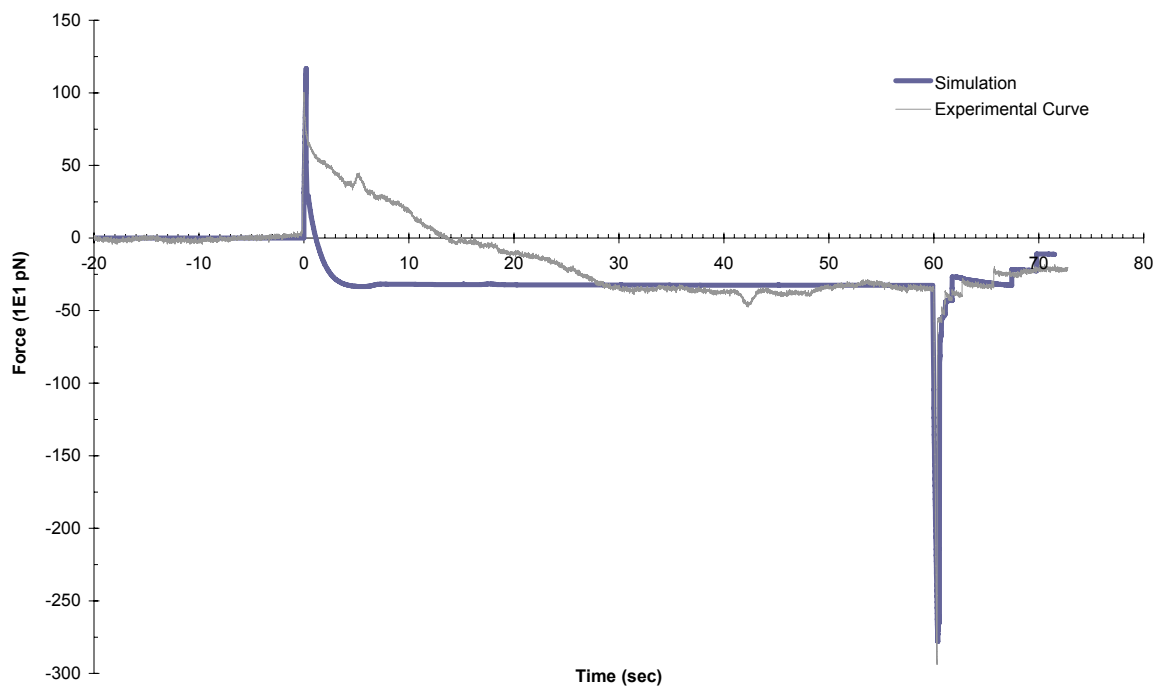
Figure 5.24 – Simulation Matching for Curve C

As shown in the figure, the model was able to capture the peak force, steady-state force, and the de-adhesion peak as in the actual experiment. However, it was unable to imitate the much longer decay during the relaxation phase of the real experiment. The difference in the decay may be due to stochastic events or an unknown factor that associates with the reshaping of the cell during relaxation.

This chapter has presented a brief parametric analysis on the factors that affect the shape of the force-time curve. The computer simulation was able to generate and explain the distinctive details observed in the experimental curves by varying the control parameters. Furthermore, after several trials of approximating the cell properties for three different experiment curves, the results shows that the finite element model is valid for cell-adhesion analyses, as well as an effective tool for future investigations.

Chapter 6 Conclusions and Future Work

Enhancement to the existing 2D finite element computer program enabled the modelling of the cell-cell interface, including the detachment of adhesion molecules between two cells. The finite element model was able to explain significant details in the force-time curves obtained from cell adhesion experiments. This is an important result because without the simulations the effects of specific cell parameters could not be determined.

In particular, this study has identified how each of the following parameters affects the force-time curve:

- Cell-Cell Interfacial Tension
- Cell-Plate Interfacial Tension
- Cell-Medium Surface Tension
- Cytoplasmic Viscosity
- Actin Cortex Stiffness and Damping Coefficient
- Tether Stiffness and Damping Coefficient
- Tether Membrane Tension
- Rupture Coefficients of Tethers
- Rupture Coefficients of Adhesion Bonds

This study has also shown that it is practical to match finite element simulations to actual experimental data. By doing so, we can estimate the values of specific mechanical properties in the cells and their tethers.

Future work might include further validation of the finite element model by comparing the simulations with more experimental data. Ideally, the model would be further enhanced to include tether fusing and clustering. A 3D version of the code would have the potential to allow the numerical values of the cell parameters to be determined quantitatively.

References

Alberts, B., K. Roberts, J. Lewis, M. Raff, and D. Bray. *Molecular Biology of the Cell.* 2nd Ed. New Yok: Garland Publishing, Inc., 1989

Bell, G. "Models for the Specific Adhesion of Cells to Cells – A theoretical framework for adhesion mediated by reversible bonds between cell surface molecules." *Science* 200 (1978): 618-627

Brodland, G. W., D. Chen, and J. Veldhuis. "A Cell-based Constitutive Model for Embryonic Epithelia and Other Planar Aggregates of Biological Cells." *International Journal of Plasticity* 22 (2006): 965-995

Brodland, G. W. "New Information from Cell Aggregate Compression Tests and Its Implications for Theories of Cell Sorting." *Biorheology* 40 (2003): 273-277

Brodland, G. W. "The Differential Interfacial Tension Hypothesis (DITH): A Comprehensive Theory for the Self-Rearrangement of Embryonic Cells and Tissues." *ASME Journal of Biomechanical Engineering* 124 (2002): 188-197

Brodland, G. W., and H. Chen. "The Mechanics of Cell Sorting and Envelopment." *Journal of Biomechanics* 33 (2000): 845-851

Brodland, G. W., and D. W. Shu. "Are Intercellular Membrane Forces Important to Amphibian Neurulation?" *Dynamical Phenomena at Interfaces* (1991): 237-245

Cuvelier, D., I. Derenyi, P. Bassereau, and P. Nassoy. "Coalescence of Membrane Tethers: Experiments, Theory, and Applications." *Biophysical Journal* 88 (2005): 2714-2726

Dai, J., and M. Sheetz. "Membrane Tether Formation from Blebbing Cells." *Biophysical Journal* 77 (1999): 3363-3370

Dai, J., M. Sheetz, X. Wan, and C. Morris. "Membrane Tension in Swelling and Shrinking Molluscan Neurons." *The Journal of Neuroscience* (1998): 6681-6692

Dong, C., R. Skalak, and K. Sung. "Cytoplasmic Rheology of Passive Neutrophils." *Biorheology* 28 (1991): 557-567

Engel, A., H. Janovjak, D. Fotiadis, A. Kedrov, D. Cisnero, and D. J. Mueller. "Single-Molecule Microscopy and Force Spectroscopy of Membrane Proteins." *Single Molecules and Nanotechnology. Springer Series in Biophysics* 12, (2008): 279-306

Evans, E., V. Heinrich, A. Leung, and K. Kinoshita. "Nano– to microscale dynamics of P-Selectin Detachment of P-selectin Detachment from Leukocyte interfaces. I. Membrane Separation from Cytoskeleton." *Biophysical Journal* 88 (2005): 2288-2298

Evans, E. "Chapter 15 – Physical Actions in Biological Adhesion." *Handbook of Biological Physics* 1, (1995): 725-752

Evans, E., D. Berk, and A. Leung. "Detachment of Agglutinin-bonded Red Blood Cells." *Biophysical Journal* (1991): 838-848

Evans, E., and R. Hochmuth. "Membrane Viscoplastic Flow." *Biophysical Journal* 16 (1976): 13-26

Heinrich, V., A. Leung, and E. Evans. "Nano- to Microscale Dynamics of P-Selectin Detachment from Leukocyte Interfaces. II. Tether Flow Terminated by P-Selectin Dissociation from Psgl-1." *Biophysical Journal* 88 (2005): 2299-2308

Hibbeler, R. C. *Statics and Mechanics of Materials*. New Jersey: Prentice Hall, 1995

Hochmuth, R., J. Shao, J. Dai, and M. Sheetz. "Deformation and Flow of Membrane into Tethers Extracted from Neuronal Growth Cones." *Biophysical Journal* 20 (1996): 358-369

Krieg, M., Y. Arboleda-Estudillo, P.H. Puech, J. Kafer, F. Graner, D.J. Mueller, and C.P. Heisenberg. "Tensile Forces Govern Germ-layer Organization in Zebrafish." *Nature Cell Biology*, (2008): 429-436

Lim, C. T., E. H. Zhou, and S. T. Quek. "Mechanical Models for Living Cells – A Review." *Journal of Biomechanics* (2006): 195-216

Mueller, D. J., A. Engel, U. Matthey, P. Dimroth, and K. Suda. "Observing Membrane Protein Diffusion at Subnanometer Resolution." *Journal of Molecular Biology* 327 (2003): 925-930

Ohmori, T., and Y. Maeda. "Implications of Differential Chemotaxis and Cohesiveness for Cell Sorting in the Development of Dictyostelium Discoideum." *Development Growth and Differentiation* (1986): 169-175

Puech, P. H., K. Pool, D. Knebel, and D. J. Mueller. "A New Technical Approach to Quantify Cell-cell Adhesion Forces by AFM." *Ultramicroscopy* (2006): 637-644

Puech, P. H., A. Taubenberger, F. Ulrich, M. Krieg, D.J. Mueller, and C.P. Heisnberg. "Measuring Cell Sdhesion Forces of Primary Gastrulating Cells from Zebrafish Using Atomic Force Microscopy." *Journal of Cell Science* 118 (2005): 4199-4206

Raucher, D., and M. Sheetz. "Characteristics of a Membrane Reservoir Buffering Membrane Tension." *Biophysical Journal* 77 (1999): 1992-2002

Rieu, J., A. Upadhyaya, J. Glazier, N. Ouchi, and Y. Sawada. "Diffusion and Deformations of Single Hydra Cells in Cellular Aggregates." *Biophysical Journal* 79 (2000): 1903-1914

Rouslahti, E., and B. Obrink. "Common Principle in Cell Adhesions." *Experimental Cell Research* 227 (1996): 1-11

Schmitz, J., M. Benoit, and K. Gottschalk. "The Viscoelasticity of Membrane Tethers and Its Importance for Cell Adhesion." *Biophysical Journal* 95 (2008): 1448-1459

Sun, M., J. S. Graham, B. Hegedus, F. Marga, Y. Zhang, G. Forgacs, and M. Granbois. "Multiple Membrane Tethers Probed by Atomic Force Microscopy." *Biophysical Journal* 89 (2005): 4320-4329

Swaminathan, R., S. Bicknese, N. Periasamy, and A.S. Verkman. "Cytoplasmic Viscosity Near the Cell Plasma Membrane: Translational Difusion of a Small Floursent Solute Measured by Total internal Reflection-Flouresence Photobleaching Recovery." *Biophysical Journal* 71 (1996): 1140-1151

Taubenberger, A., D. Cisneros, J. Friedrichs, P. H. Puech, D. J. Mueller, and C. Franz. "Revealing Early Steps of α2β1 Integrin-mediated Adhesion to Collagen Tyoe I by Using Single-Cell Force Spectroscopy." *Molecular Biology of the Cell* 18 (2007): 1634-1644

Ward, M., M. Dembo, and D. Hammer. "Kinetics of Cell Detachment: Effect of Ligand Density." *Annals of Biomedical Engineering* 23 (1995): 322-331

Ward, M., M. Dembo, and D. Hammer. "Kinetics of Cell Detachment: Peeling of Discrete Receptor Clusters." *Biophyscial Journal* 67 (1994): 2522-2534

Zhu, C., G. Bao, and N. Wang. "Cell Mechanics: Mechanical Response, Cell Adhesion, and Molecular Deformation." *Annual Review of Biomedical Engineering* (2002): 189-226